

Limits of Localized Control in Extended Nonlinear Systems

A Thesis
Presented to
The Academic Faculty

by

Andreas Handel

In Partial Fulfillment
of the Requirements for the Degree
Doctor of Philosophy

School of Physics
Georgia Institute of Technology
June 2004

Limits of Localized Control in Extended Nonlinear Systems

Approved by:

Professor Roman O. Grigoriev, Advisor

Professor Michael F. Schatz

Professor Predrag Cvitanović

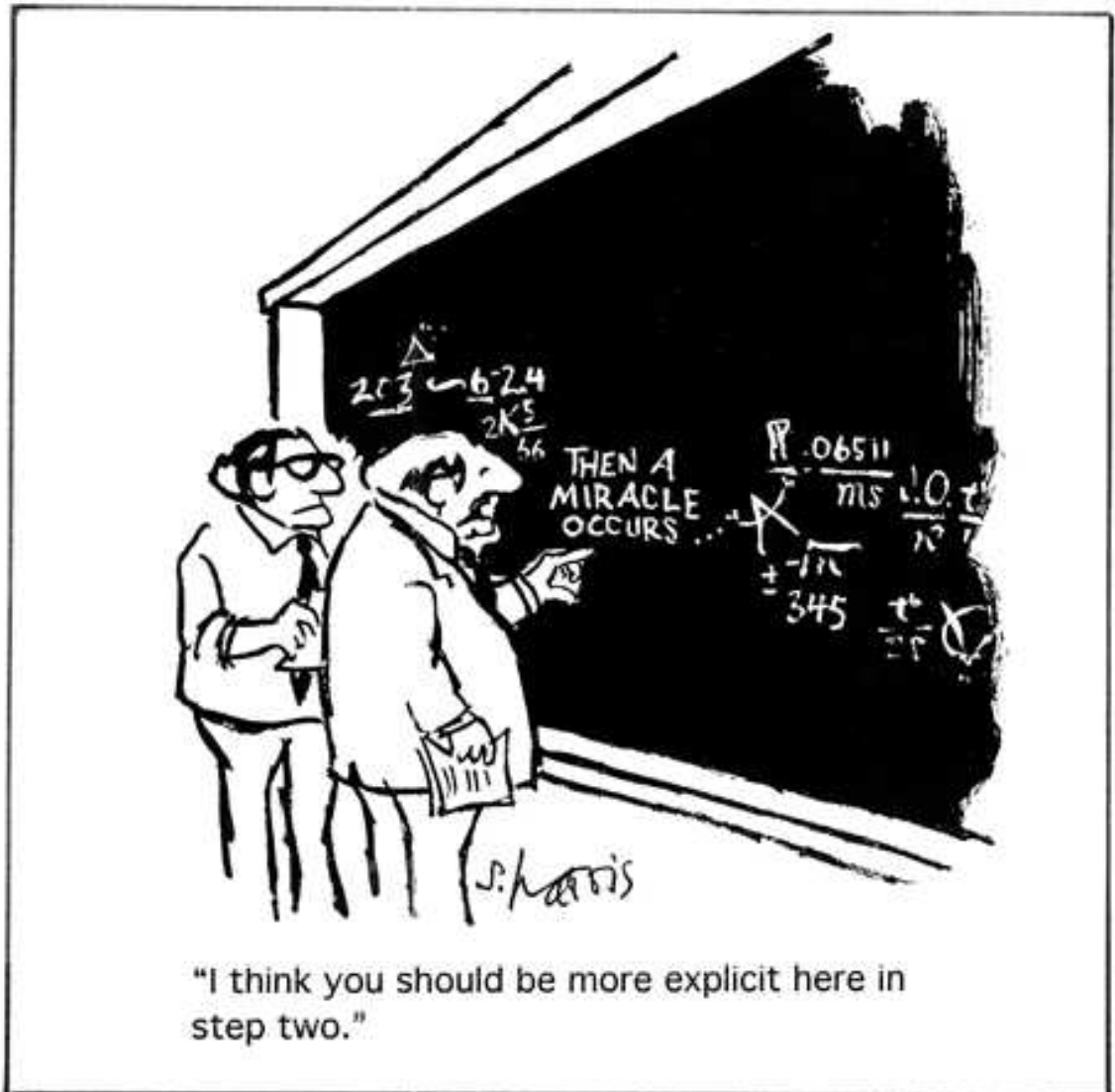
Professor Kurt Wiesenfeld

Professor Peter J. Mucha
(School of Mathematics)

Date Approved: 24th June 2004

DEDICATION

To my parents, who gave me the freedom to venture out into the world and to pursue weird stuff for a living.



ACKNOWLEDGEMENTS

Taking the first steps in the world of science and research seems a bit like learning how to walk. Progress is unpredictable, nonlinear and often not as fast as one would wish for. Fortunately for me, from my first baby steps in life to my most recent baby steps in research, I received support from many people. In fact there are so many of them that if I tried to mention them all, it could easily fill a document of length comparable to this thesis. I therefore restrict myself to thanking those people that have directly influenced the creation of this thesis.

There is of course first and foremost my advisor, Roman Grigoriev, who introduced me to the interesting topics that I have enjoyed working on for the last several years and that are presented in this thesis. He supervised my first baby steps toward independent research and made sure I didn't stumble too much. And in the instances where I fell on my metaphorical, research-unexperienced nose, he helped me to get up and keep going.

Next, I want to mention the members of my thesis committee. Not only for their willingness to serve on the committee, but also for the many other contributions they made throughout my graduate studies.

Predrag Cvitanović taught me a multitude of useful material in the courses I took with him. Furthermore, as chair of the Center for Nonlinear Science, he did (and still does) a great job in providing a stimulating and pleasant work environment with lots of speakers, seminars and of course cookies as well as the biannual picnics.

From Peter Mucha I learned a great deal about numerical methods, some of which I was able to use repeatedly. Though not explicitly mentioned, a significant amount of the tools that I learned from him found their way into this thesis. He was furthermore a very stimulating collaborator and simply a great guy to talk to.

Mike Schatz not only provided me with the essentials of his lab – like printer, couch, fridge and microwave – he was also a great person to interact with, through our joint

research project as well as other interesting discussions inside and outside of science.

Kurt Wiesenfeld influenced my decision to pursue my PhD at Georgia Tech in the first place. After several weeks as an exchange student, I talked to him to learn more about his research and the work of others at Tech's School of Physics - with the result that I decided to extend my stay and pursue a PhD. During these years, he has been a great teacher, mentor and source of excellent advice.

Among my fellow graduate students, there are several I want to specifically mention. With Kapil and John I spent many nights studying and many weekends exploring Atlanta and surroundings. While John left for Duke, Kapil continued to work next door and we had many great discussions on all topics imaginable – and I'm sure also a few unimaginable. Next to Roman, he was the person who helped me the most to step over the small road blocks that tend to clutter the road of scientific progress.

I got to know Denis when I moved into the office next to his lab. He was always fun to talk to and a source of wisdom on topics as varied as physics, cars, girls and world politics. And as a reliable consumer of my coffee, he often provided the excuse for me to brew a few cups – and drink most of it myself.

In the later years of my graduate life, I got to know Matt, who turned out to be a very pleasant and interesting travel companion and who – through multiple discussions at conferences and other instances – helped me understand many things stochastic and noisy.

Ed unfortunately moved to my office only very recently. Sharing the office with him was a pleasure. He was a good source of information, as well as a good source of distraction if my brain needed a break. I hope our online chess games will continue.

Finally, I want to acknowledge the whole CNS troupe as well as the people at the School of Physics. The fellow graduate students, the PostDocs, the Professors and the staff all contributed to the pleasant work environment that I got to experience during my years as PhD student at Georgia Tech/CNS.

The one person outside of the School of Physics that I want to mention is my wife Melanie. She supported me, especially during the final months while I was working long nights and weekends to get everything done. She made sure I was well nourished and dressed

– things that one can easily forget in light of the looming deadline.

And finally, an all encompassing thanks goes to the O.E.O.T.D. [103] for provision and guidance throughout my life.

TABLE OF CONTENTS

DEDICATION	iii
ACKNOWLEDGEMENTS	iv
LIST OF FIGURES	ix
ABSTRACT	xiv
CHAPTER I — INTRODUCTION	1
1.1 Motivation	1
1.2 Outline	6
1.3 Systems under study	8
CHAPTER II — CONTROL IN DYNAMICAL SYSTEMS	9
2.1 Chaos control methods	9
2.2 Control theory methods	12
CHAPTER III — NONNORMALITY AND TRANSIENT GROWTH 19	
3.1 Overview of nonnormality	19
3.2 The limitations of linear stability analysis	23
3.3 Characterization of nonnormality and transient growth	28
3.4 Two toy models	35
CHAPTER IV — LOCALIZED CONTROL OF EXTENDED SYS- TEMS	41
4.1 Control at one boundary	41
4.2 Control at both boundaries	50
4.3 Control at multiple locations	53
4.4 Control and nonnormality	60
CHAPTER V — TRANSIENT GROWTH IN THE CONTROLLED SYSTEM	66
5.1 Scaling of the transient growth - method I	66
5.2 Scaling of the transient growth - method II	73
5.3 Scaling of the transient growth - the sensing case	78

CHAPTER VI —	BREAKDOWN OF CONTROL	84
6.1	Linear breakdown scenarios	84
6.2	Nonlinear breakdown scenarios	87
CHAPTER VII —	CONCLUSIONS AND OUTLOOK	100
APPENDIX A —	ALTERNATIVE COMPUTATION OF THE FEED- BACK GAIN SCALING	103
APPENDIX B —	COMPUTATION OF TRANSIENT GROWTH IN THE CASE OF LOCALIZED SENSING	108
REFERENCES	110

LIST OF FIGURES

Figure 1	The evolution of the state $\phi(x, t) = 0$, perturbed by a random initial disturbance with magnitude $\sigma = 10^{-5}$, in the Kuramoto-Sivashinsky equation (3) with periodic boundary conditions. At this system size, $l = 55$, the state $\phi(x, t) = 0$ is unstable and the system evolves chaotically.	4
Figure 2	The evolution of the state $\phi(x, t) = 0$, perturbed by a random initial disturbance (same as in Fig. 1) in the Kuramoto-Sivashinsky equation with localized control applied at the four points marked with circles. At this system size, $l = 55$, the disturbance transiently grows by more than an order of magnitude before exponential decay to the target state $\phi(x, t) = 0$ sets in.	5
Figure 3	The evolution of a random initial disturbance (same as in Fig. 1) in the Kuramoto-Sivashinsky equation for a slightly larger system size, $l = 60$. Here the transient growth of the disturbance is strong enough to lead to control breakdown. The state will grow until the nonlinearities become important, triggering a nonlinear instability and permanent departure from the target state $\phi(x, t) = 0$	6
Figure 4	Monotone decay for a normal system. The initial state is $\Phi(0) = d_1(0)e_1 - d_2(0)e_2$. Since the amplitude of each eigenvector decays at a rate $\lambda_k < 0$ and the eigenvectors are orthogonal, the magnitude of the state $\Phi(t) = d_1(t)e_1 - d_2(t)e_2$ also decays monotonically with time. The semi-circle highlights the difference in magnitude between the $\Phi(0)$ and $\Phi(t)$	25
Figure 5	Transient growth for a nonnormal system. The initial state is $\Phi(0) = d_1(0)e_1 - d_2(0)e_2$. The amplitude of each eigenvector decays at a rate $\lambda_k < 0$, but since the eigenvectors are not orthogonal, initial cancellations are partly reduced. This leads to transient growth in the state $\Phi(t) = d_1(t)e_1 - d_2(t)e_2$ before exponential decay asymptotically dominates. The semi-circle highlights the difference in magnitude between the $\Phi(0)$ and $\Phi(t)$	26
Figure 6	Largest expansion coefficient $g = \max_k c_k $ as a function of system size l for the controlled GL equation. The different g are computed through (24) with a $\Phi(0)$ normalized to unit magnitude. We choose $\Phi(0)$ to be the largest adjoint eigenfunction (g_1), the disturbance that leads to maximum transient growth (g_2) and a random state (g_3). For comparison, we also plot the maximal transient growth in the system as given by $\max_{t, \Phi(0)} [\Phi(t)/\Phi(0)]$, determined from numerical simulation (NUM).	30
Figure 7	$\ e^{Mt}\ _2$ for the controlled GL equation. Also shown is the maximum transient amplification γ and the corresponding time t_m at which the maximum is reached. Note the logarithmic scale in the time direction to better resolve the fast transient growth.	31

Figure 8	Amplification factor γ given by (25) and direct numerical simulation (SIM) with random initial disturbances as described in the text for the case of the controlled GL equation.	32
Figure 9	Amplification factor γ_c given by (30) and direct numerical simulation (SIM) with continuous noise as described in the text for the case of the controlled GL equation.	34
Figure 10	Norm of adjoint eigenfunctions $\ e'_i\ $, given by (39) and amplification factor γ and γ_c given by (45) and (46) for several choices of the eigenvalue ration ω	37
Figure 11	Eigenvalues λ_n versus wavenumber n for the SH equation ($\epsilon = 0.5$). For this system size ($l = 22$), $a = 5$ and $b = 9$. The lines marked by q_a and q_b are the limits of the continuous wavenumber band for which $\lambda(q) > 0$. . .	44
Figure 12	Gain function $k(x)$ for the three equations under study. The system size is $l = 10$, the new eigenvalues are $\lambda'_a = \dots = \lambda'_b = -1$, the parameter in the SH equation is chosen as $\epsilon = 0.5$	46
Figure 13	Maximal feedback gain $\max_x k(x)$ and analytical result (TH) as given by (77) as a function of the system size l for (a) the KS equation, (b) the SH equation ($\epsilon = 0.75$). The control schemes are PP control with $\Lambda = -0.1$ and $\Lambda = -1$ and LQR control, where the λ'_k are found to lie between -1 and -0.1	49
Figure 14	Maximal feedback gain $\max_x k(x)$ and analytical result (TH) as given by (89) as a function of the system size l for the GL equation with control at both boundaries. The control schemes are PP control with $\Lambda = -0.1$ and $\Lambda = -1$ and LQR control, where the λ'_k are found to lie between -1 and -0.1	52
Figure 15	Maximal feedback gain $\max_x k_1(x)$ and analytical result (TH) as given by (108) as a function of the system size l for the GL equation with six controllers placed according to (91). The control schemes are PP control with $\Lambda = -0.1$ and $\Lambda = -1$ and LQR control, where the λ'_k are found to lie between -1 and -0.1	57
Figure 16	Gain function $k_{15}(x)$ for the three equations under study with LQR control and 30 controllers, $l = 90$. The dotted straight lines indicate positions of the controllers, the solid straight line the location of controller 15.	58
Figure 17	Gain function $k_{15}(x)$ for the three equations under study with LQR control and 30 controllers, $l = 180$. The dotted straight lines indicate positions of the controllers, the solid straight line the location of controller 15.	59
Figure 18	The wave number and corresponding eigenvalues for the linearized GL equation with one controller located at the right boundary and LQR control, $l = 20$. Shown are the eigenvalues for the uncontrolled (square) and controlled (diamond) system.	60

Figure 19	First four eigenfunctions of the GL equation with one controller at the right boundary for $l = 20$. Further closely aligned eigenfunctions exist for this value of l but are not shown. The control is computed using LQR.	61
Figure 20	Nonnormality as defined by γ for PP control at the right boundary of the GL equation with all eigenvalues equal to -2.5 and with eigenvalues linearly spaced in the interval $[-1, -4]$	62
Figure 21	First four eigenfunctions of the SH equation with one controller at the right boundary for $l = 20$. The control is computed using LQR.	63
Figure 22	The sums of the inner products as defined by (110) as a function of l for the three different equations and eight controllers. The feedback gain is computed using LQR.	64
Figure 23	The time at which the maximum in transient amplification is achieved (a) as a function of $ \Lambda $ for $l = 20$ ($s = 7$) and (b) as a function of the system size l . The numerical results shown are for the GL equation with control applied at the two boundaries.	68
Figure 24	Matrix exponential $\ e^{Mt}\ $ and $K^{GL}t$ for the GL equation with control at the two boundaries, $l = 25$ ($s = 8$). Shown are plots for eigenvalues $\Lambda = -0.1$ and $\Lambda = -2$	69
Figure 25	Transient amplification γ as a function of system size l for the GL equation with control at the two boundaries with (a) $\Lambda = -0.1$ and (b) $\Lambda = -2$. Squares show the numerical results (NUM) obtained using (25), circles are the numerical results obtained through simulation (SIM) of 100 initial conditions as explained in the text, the line is the theoretical estimate (TH) as given by (124).	70
Figure 26	Transient amplification γ and estimate $K^{EQ}/ \Lambda $ as a function of $ \Lambda $, shown for the GL equation, $l = 25$, with control located at the boundaries. (The somewhat sharp kink in the γ -curve is due to switching between two different numerical routines at that point and of no significance.)	72
Figure 27	Transient amplification γ as a function of l for the case of the KS equation with 6 controllers located inside the domain. For PP control, the eigenvalues λ'_k are distributed evenly between $[-1, -3]$, the LQR control produces eigenvalues λ'_k mostly clustered around one. For the estimate (TH) as given by (124), we choose Λ as the median of the λ'_k	73
Figure 28	Transient amplification of $\ e^{Mt}\ _2$ and $\ e^{M_{st}}\ _2$ as a function of time for the GL equation with control at the right boundary, $l = 15$ and $\Lambda = -0.5$. The double logarithmic scale is used to resolve the quick transient amplification and the slow exponential decay.	74
Figure 29	Maximum transient amplification γ for $\ e^{Mt}\ _2$ and $\ e^{Q_{st}}\ _2$ as a function of l for the GL equation with control at the right boundary, $\Lambda = -1$	75

Figure 30	Transient amplification γ as a function of l for the case of the KS equation with control applied at the right boundary. For PP control, the eigenvalues are $\lambda'_k = \Lambda = -0.1$, the LQR control produces eigenvalues λ'_k mostly clustered around one. The symbols denoted (SIM) are obtained by numerical integration of 100 random initial conditions as explained earlier. The line denotes the estimate (TH) as given by (133).	77
Figure 31	Transient amplification in the GL equation as a function of the system size l for the case of one and two controllers and sensors. For the one-controller case, both sensor and controller are located at the right boundary, for the two-controller case, the locations are both boundaries. The respective case is indicated by the numbers in parentheses. For the pole placement (PP) calculations we took $\Lambda = -0.5$, for LQR control, the λ'_k are in $[-1, -0.1]$. The theoretical value (TH) is given by (147).	80
Figure 32	Transient amplification in the GL equation as a function of the system size l for the case of six collocated controllers and sensors located inside the domain. In the pole placement (PP) calculations we took $\Lambda = -0.5$, for LQR control, the λ'_k are in $[-1, -0.1]$. The theoretical value (TH) is given by (147).	82
Figure 33	Transient amplification in the GL equation as a function of the system size l for the case of four controllers and sensors. Shown is the case of localized sensors and controllers collocated at the same points inside the domain (γ_{col}), the case of sensor pairs in the middle between controller pairs (γ_{diff}) and the case of distributed sensing everywhere in the domain, as discussed in Section 4.3 (γ_{dist}). The control is computed using the LQR scheme. . .	83
Figure 34	The evolution of the linearized Kuramoto-Sivashinsky equation with continuous random noise of magnitude $\sigma = 10^{-5}$ and system size $l = 55$. The nonnormal amplification is strong enough to produce continuous deviations from the target state of such magnitude that control fails to be effective for any practical application.	85
Figure 35	Limit of perturbation strength σ for a given γ such that the resulting perturbed matrix is still stable. The figure shows the scaling for the GL equation with four controllers.	87
Figure 36	The noise level for which localized linear control fails as a function of the transient amplification factor. The system is the GL equation with control at the right boundary and different types of nonlinearities. The plot shows the range $l = [5, 20]$	91
Figure 37	Amplification $\gamma(q)$ for an initial condition of the form $\sin(qx)$. Shown is the GL equation with LQR control applied at the right boundary. . . .	92
Figure 38	Normalized spectrum $F_k[\phi]$ for the linear GL equation driven by random noise. Control is applied at the right boundary, and computed according to the LQR scheme.	94

Figure 39	Normalized spectrum $F_k[\phi]$ for the quadratic term ϕ^2 of the GL equation driven by random noise. Control is applied at the right boundary, and computed according to the LQR scheme.	95
Figure 40	Normalized spectrum $F_k[\phi]$ for the cubic term ϕ^3 of the GL equation driven by random noise. Control is applied at the right boundary, and computed according to the LQR scheme.	96
Figure 41	The noise level for which localized linear control fails for the GL equation with six controllers (LQR) as a function of the transient amplification factor for different types of nonlinearities. The plot shows the range $l = [30, 130]$	97
Figure 42	The noise level for which localized linear control fails for the KS equation with six controllers (LQR) as a function of the transient amplification factor for different types of nonlinearities. The plot shows the range $l = [30, 130]$	98
Figure 43	The noise level for which localized linear control fails for the SH equation with six controllers (LQR) as a function of the transient amplification factor for different types of nonlinearities. The plot shows the range $l = [30, 130]$	99

ABSTRACT

We investigate the limits of localized linear control in spatially extended, nonlinear systems. Spatially extended, nonlinear systems can be found in virtually every field of engineering and science. An important category of such systems are fluid flows. Fluid flows play an important role in many commercial applications, for instance in the chemical, pharmaceutical and food-processing industries. Other important fluid flows include air- or water flows around cars, planes or ships.

In all these systems, it is highly desirable to control the flow of the respective fluid. For instance control of the air flow around an airplane or car leads to better fuel-economy and reduced noise production. Usually, it is impossible to apply control everywhere. Consider an airplane: It would not be feasible to cover the whole body of the plane with control units. Instead, one can place the control units at localized regions, such as points along the edge of the wings, spaced as far apart from each other as possible.

These considerations lead to an important question: For a given system, what is the minimum number of localized controllers that still ensures successful control? Too few controllers will not achieve control, while using too many leads to unnecessary expenses and wastes resources.

To answer this question, we study localized control in a class of model equations. These model equations are good representations of many real fluid flows. Using these equations, we show how one can design localized control that renders the system stable. We study the properties of the control and derive several expressions that allow us to determine the limits of successful control. We show how the number of controllers that are needed for successful control depends on the size and type of the system, as well as the way control is implemented. We find that especially the nonlinearities and the amount of noise present in the system play a crucial role. This analysis allows us to determine under which circumstances a given number of controllers can successfully stabilize a given system.

CHAPTER I

INTRODUCTION

1.1 Motivation

This work is motivated by the wish to better understand how to successfully control extended systems, using a small number of localized controllers. Extended systems are very important and common in virtually every field of engineering and science. Consider for instance a fluid flowing through a pipe. Oil pipelines or pipes that transport water come to mind immediately. It is not uncommon for such pipes to be several feet in diameter and several hundred yards long or even longer. Such a pipe and the fluid flowing through clearly constitute an extended system.

In order to reduce the time it takes for the fluid to reach its destination, one would often like to pump it through the pipe as fast as possible. However, increasing the fluid velocity to high levels is usually problematic. The reason is that as the velocity increases, the fluid flow changes its overall structure. If the fluid velocity is low, the flow is uniform and smooth. In the study of fluids this is called a laminar flow. A good example would be a large river where the water flows slowly and steadily. If one increases the velocity of the fluid flow, it will at some point become turbulent. Think of a fast flowing mountain stream or a river that has been flooded by heavy rain. The turbulent flow has several disadvantages over the laminar one. First, in turbulent flows, whirls and eddies form and the fluid will locally flow ‘backward’, that is, upstream. This leads to an overall reduced flux of fluid through the pipe – exactly the opposite outcome than what was hoped for by increasing the pumping speed. Second, in turbulent flows, local forces around eddies can become very strong. This can be quite damaging to the pipe, leading in the worst case to leaks and breaking of the pipe. If one wants to prevent such accidents from happening, one would need to replace the pipes frequently.

Due to these problems with turbulent flow, one often wants the fluid flow to remain

laminar. Nevertheless, one would still like to increase the pumping speed, to achieve a faster throughput of the fluid. A solution to this problem is to not only increase the pumping speed, but to also apply control to the fluid such that it does not become turbulent and instead remains laminar. Such control could for instance be applied by heating or cooling certain areas of the pipe or by locally injecting or removing fluid to prevent eddy formation. Since it is impossible to control the fluid everywhere inside the pipe, one needs to find ways that allow for control being applied to localized areas. For instance one could have pairs of controllers sitting at opposite sides of the pipe, each pair spaced as far apart along the pipe from the next pair as possible.

This leads to the question stated similarly in the abstract: For a given system, what is the maximum spacing between controllers that still ensures control? Spacing them too far apart will result in failure of control, spacing them closer than necessary wastes resources. Answering this question lies at the heart of our study. Using mathematical equations that are good models of real fluid flow systems, we investigate some of the fundamental issues that arise if one wants to stabilize the laminar state in an extended system using localized control.

Before we introduce the model equations, let us mention a few more areas where extended systems play a major role. We already mentioned large moving objects, such as cars, airplanes or ships. Each produces a fluid flow (air for cars and planes, water for ships) around it. Since they all move at significant speeds, the flow around them is, at least partly, turbulent. This again leads to eddies and whirls where local forces can become large. That is especially true for planes and ships, where these forces can be huge. Reducing the turbulence and therefore these strong local forces would result in considerable savings on material and repairs. Furthermore, reduction of the turbulence would lead to a more streamlined design with reduced fuel consumption.

Other extended systems can be found in many industrial applications, where fluids not only need to be transported through pipes but also need to be stirred, mixed and separated in a very controlled fashion. One such system that might be of special importance in the near future is the fuel-cell, where hydrogen and oxygen flows come together to produce

electricity. Being able to influence these flows will be crucial in maximizing the cell efficiency. The same is true for such mundane applications as food-processing, where one would like to mix ingredients (for instance sugar, water and chemicals) as efficiently as possible to quickly create the end-product (Coca-Cola). Another area, which is in its infancy but is expected to become very important in the near future, is the field of biological systems. Being able to control for instance blood flow through the human body or through the heart by means of localized control could be one of the promising venues to reduce risks of thrombosis, heart attacks and other related health issues.

All these examples show how ubiquitous spatially extended systems are and that the ability to control them is vital. It should also be obvious that it is usually impossible to control specific properties, for example fluid velocity or fluid temperature, everywhere in the system. For most systems one needs to use control that is localized in certain areas, often on parts of the boundaries or other small regions.

To properly control a given system such as the ones just mentioned, one needs to create a detailed model and design the control for this specific model. Unfortunately, most of these systems are too complex to allow for any analytical treatment. Further, the details of each system easily obscure more fundamental, underlying features that might be shared by a large class of systems. To gain insight into such important, generic and fundamental features, one can instead study control in more simplistic mathematical equations. It is well known that the systems we just mentioned are mathematically best described using nonlinear partial differential equations (PDEs). While these equations do not describe any specific system in full detail, they represent good approximations and capture most of the essential features while still being simple enough to allow for analytic treatment. These will therefore be the equations our study is concerned with.

In Fig. 1 we show such a model equation, the Kuramoto-Sivashinsky (KS) equation (3) on a one-dimensional domain with periodic boundary conditions. We plot the time evolution of the equation, starting from a small random initial disturbance of the homogeneous state $\phi(x, t) = 0$. This state, which is a stationary solution of the KS equation, corresponds to the smooth and laminar state one would like to stabilize in many real fluid flows. One

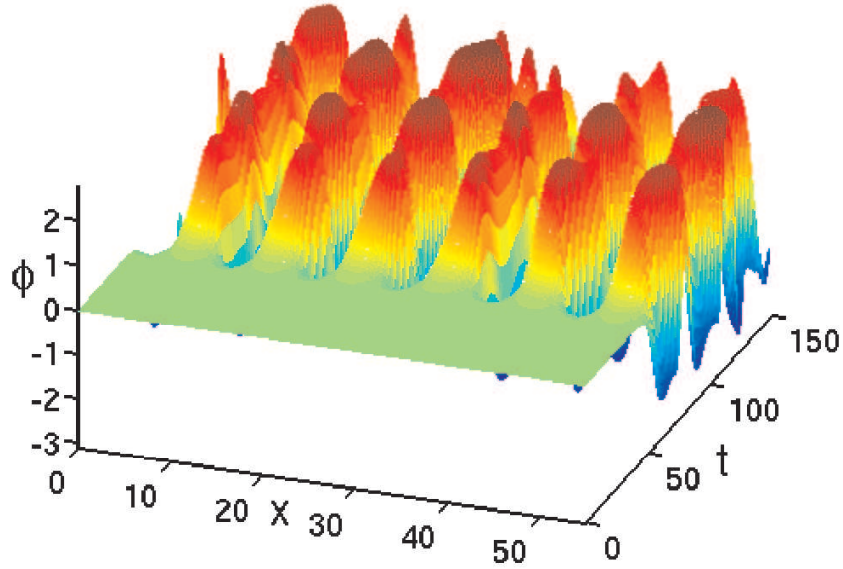


Figure 1: The evolution of the state $\phi(x, t) = 0$, perturbed by a random initial disturbance with magnitude $\sigma = 10^{-5}$, in the Kuramoto-Sivashinsky equation (3) with periodic boundary conditions. At this system size, $l = 55$, the state $\phi(x, t) = 0$ is unstable and the system evolves chaotically.

clearly sees that the state is unstable and that the time evolution of the system is chaotic, corresponding to a turbulent state in the flows mentioned above.

Our objective is to control the model equation such that this unstable homogeneous state becomes stable. We want to achieve this by using localized linear feedback control. Despite the system being nonlinear, we can justify using linear control by the fact that if we are close to the state that we want to stabilize (which in control theory is commonly known as target state), the system can be approximated by a linearized version. Control that renders this linear approximation stable should suffice to stabilize the target state, provided the initial deviation is small. We show such an implementation in Fig. 2, again using the KS equation as an example. We start with the same initial disturbance as before. Control is now applied at the indicated positions. As can be seen in Fig. 2, the control is indeed able to stabilize the target state. One also sees from the figure that, before the system asymptotically approaches the target state, $\phi(x, t)$ experiences significant transient

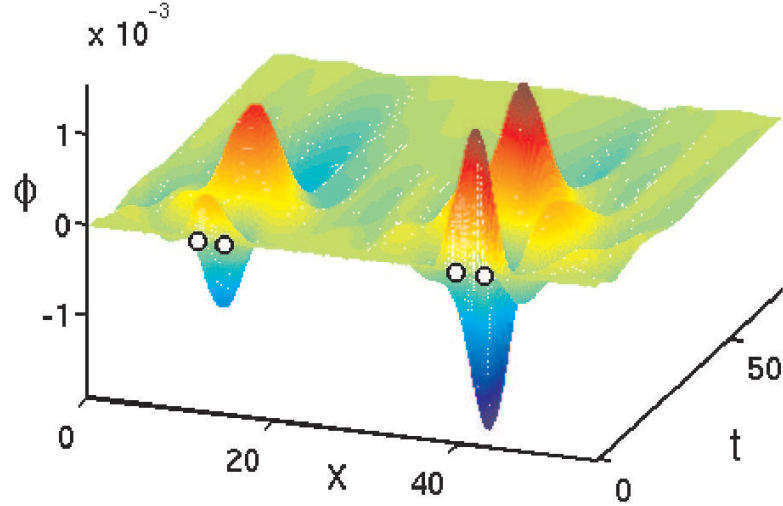


Figure 2: The evolution of the state $\phi(x, t) = 0$, perturbed by a random initial disturbance (same as in Fig. 1) in the Kuramoto-Sivashinsky equation with localized control applied at the four points marked with circles. At this system size, $l = 55$, the disturbance transiently grows by more than an order of magnitude before exponential decay to the target state $\phi(x, t) = 0$ sets in.

growth. In this scenario, that is for the given level of initial noise and the given system size, the transient growth does not prevent the control from succeeding.

However, as is intuitively clear, a fixed number of localized controllers can only stabilize a system up to a certain size. If the distance between controllers becomes too large, the control will eventually fail. This is shown in Fig. 3. The setup is the same as in Fig. 2, but we increased the system size. This leads to a transient growth which eventually reaches $\|\phi(x, t)\| \sim O(1)$. At this point, the linear approximation breaks down and a nonlinear instability sets in, which leads to failure of control. We could have equivalently increased the initial disturbance and kept the system size the same. This would have also led to a deviation of $O(1)$ and failure of control.

The transient growth and the resulting increased sensitivity to noise in locally controlled systems had been observed and studied earlier. It was noted that the transient growth leads to eventual failure of control, and an estimate for the critical amount of noise for a given

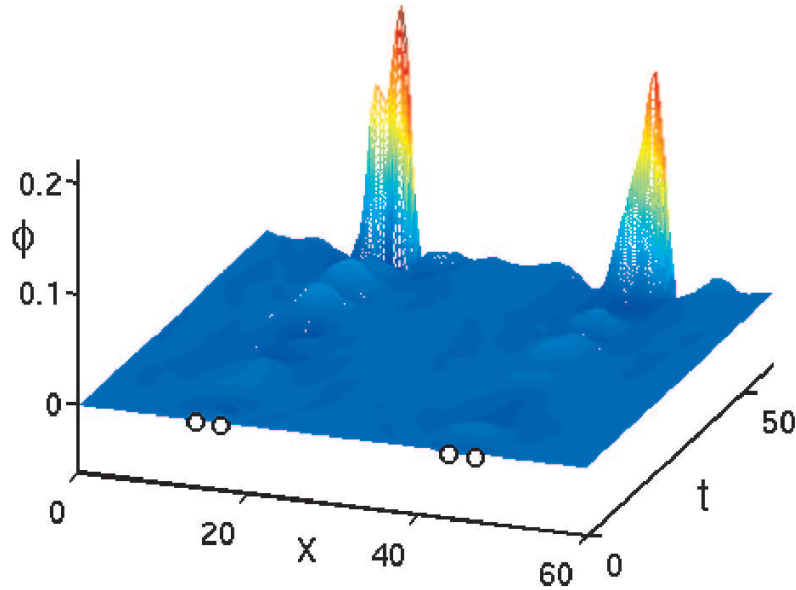


Figure 3: The evolution of a random initial disturbance (same as in Fig. 1) in the Kuramoto-Sivashinsky equation for a slightly larger system size, $l = 60$. Here the transient growth of the disturbance is strong enough to lead to control breakdown. The state will grow until the nonlinearities become important, triggering a nonlinear instability and permanent departure from the target state $\phi(x, t) = 0$.

system size was derived for a nonlinear coupled map lattice [38, 63]. However, the exact mechanism that lead to control failure had not been analyzed and the noise estimates turned out to be valid only for the system under study but not for other systems.

The shortcomings in the explanation of linear control failure motivated the detailed study performed in this work. The question we want to answer is: “What are the limits of localized control?” From what we explained so far, one sees that this question can be split into the two sub-questions: “How does the transient growth and noise amplification arise in locally controlled systems?” and “How much noise can a given controlled system tolerate before control fails?” The present work is an attempt to answer these questions.

1.2 Outline

The outline of this work is as follows. In this Chapter we provide a general motivation, an outline and introduce the class of systems under study. In Chapter 2 we discuss different

control methods. In Section 2.1 we give a short history and background of chaos control as it has been developed mainly in the physics community. This is followed in Section 2.2 by a brief explanation of some key concepts from control theory as it is used in the control engineering community and as we will use it in our work. In Chapter 3 we introduce and describe in detail the phenomenon of nonnormality and how it relates to the transient growth mentioned in the introduction. We start out in Section 3.1 with a general overview. Additionally, we describe some of the recent developments, mainly in the field of fluid dynamics, where nonnormality was found to play an important role. We then set out to explain nonnormality, starting in Section 3.2 with a discussion why standard linear stability theory does not provide enough information to fully describe the dynamics of nonnormal systems. In Section 3.3 we further discuss the phenomenon of transient growth and define some quantities that we utilize later. We end the chapter with Section 3.4, where we use two simple toy systems to illustrate some of the properties introduced in the previous sections. In Chapter 4 we begin with the main part of our work that sets out to answer the questions stated earlier. Section 4.1 describes how to construct feedback gain that stabilizes several one-dimensional systems with one controller placed at the boundary. This is followed in Section 4.2 with a setup that consists of control at both boundaries and Section 4.3 that describes the general case of multiple controllers. For each of these cases, we show that the feedback gain grows exponentially with the system size. In Section 4.4 we provide a qualitative connection between the growing feedback gain and the increase in nonnormality. This is followed by Chapter 5, where we provide in Sections 5.1 and 5.2 two alternative ways to compute the transient growth, and Section 5.3 considers transient growth in a system with localized sensors. Chapter 4 and parts of Chapter 5 are almost identical to our work presented in [64], with only minor modifications. In Chapter 6, we discuss the different scenarios that lead to control breakdown. While Section 6.1 is devoted to linear mechanisms, Section 6.2 is devoted to the investigation of interactions between nonnormality and nonlinearity. For each of these cases, we determine the amount of noise a given system can tolerate before control fails. In the final Chapter 7, we summarize our results, draw conclusions and provide an outlook. Some of the detailed calculations can be found in the

appendices.

1.3 *Systems under study*

The analysis and results presented here apply to a class of systems described by one-dimensional, scalar, nonlinear partial differential equations (PDEs) of the form

$$\partial_t \phi(x, t) = N[\phi(x, t)] \quad (1)$$

where N is a nonlinear differential operator. We assume that the system is written in such a way that the state $\phi(x, t) = 0$ is a steady state solution of the system. This can always be achieved by transformation of coordinates. We further require the linear part L of N to be normal, that is $L^\dagger L = LL^\dagger$. Examples of this class of systems include such model equations as the real Ginzburg-Landau (GL) equation

$$\partial_t \phi = \phi + \partial_x^2 \phi - \phi^3, \quad (2)$$

the Kuramoto-Sivashinsky (KS) equation

$$\partial_t \phi = -\partial_x^2 \phi - \partial_x^4 \phi - \phi \partial_x \phi \quad (3)$$

and the Swift-Hohenberg (SH) equation

$$\partial_t \phi = \epsilon \phi - (1 + \partial_x^2)^2 \phi - \phi^3. \quad (4)$$

These model equations describe the dynamics of generic, spatially extended systems close to several common types of bifurcations and thus are of particular importance. We use these equations as examples throughout our study. However we want to point out that our main results are independent of the exact form of the equation. While there is much that can be said about each of the three equations, none of their specific properties is vital to our study. We will therefore not discuss any of these equations further, instead, we refer to the literature, such as the reviews by Cross and Hohenberg [33] or Aranson and Kramer [3].

CHAPTER II

CONTROL IN DYNAMICAL SYSTEMS

2.1 Chaos control methods

In this section we give a brief overview of some of the developments in chaos control that have taken place over approximately the last 15 years, mostly within the physics community. We want to state at the very beginning that we will not utilize any of the methods that will be described in this section. Instead, we will make use of control theoretical approaches as described in the next section. Nevertheless, it is good to have an overview of the different ideas that exist with regards to control of nonlinear dynamical systems. By explaining some of these methods, we can point out certain shortcomings and motivate our choice of control.

Some of the early studies that tried to control chaos made use of external parametric perturbations, with the goal of changing the unstable chaotic evolution of the system to a regular one [22, 89]. These methods utilized so-called non-feedback control, where the external signal is applied to the dynamical system in a pre-determined way, independent of the state of the system. There have been successful attempts in controlling chaotic systems with non-feedback methods, and it is usually rather easy to implement [120]. A brief overview is given by [49]. However, the method has some serious disadvantages. To compute the necessary perturbation, one needs to know the governing equations of the dynamical system, otherwise one ends up with a trial and error procedure that can sometimes lead to successful control, but not always. Also, it is not possible to use control that will vanish once the system is stabilized. Lastly, the control does not adjust dynamically in response to the system behavior.

Due to these limitations, non-feedback control did not receive as much attention in the physics community as feedback control methods. In the latter approach, a control signal is applied to the dynamical system depending on properties of the system state, hence the term feedback control. One of the advantages of this approach is the fact that one does not

need to know the exact equations of the system but can use experimentally available data to construct the feedback. Another reason feedback control is very appealing is because often one can design it such that, once the system has reached the target state, the control signal goes to zero. A disadvantage of this approach is that the system has to be constantly monitored and the control signal needs to be continuously adjusted.

The first form of feedback control in the context of chaotic systems was suggested in a 1990 paper by Ott, Grebogi and Yorke [98] and became known as the OGY control method. Their idea uses the deviation of the system state from a chosen target state to determine a feedback signal, which is usually applied to a parameter of the system. The goal is to direct the state onto the selected target state, often an unstable periodic orbit. Since its original introduction, the OGY method has been applied and extended in several ways, see for instance [7, 76, 77, 69, 95]. A problem with the OGY method is that it is usually only applicable to low-dimensional systems. Since OGY uses the Poincaré section and the invariant manifolds for finding the unstable periodic orbits and determining the control, it usually prohibits treatment of high dimensional, spatially extended systems. In such systems it is also in general impossible, or at the least highly impractical, to globally change a system parameter. For instance globally changing the Reynolds number in a large fluid system is usually not feasible.

Another feedback control idea was proposed by Pyragas [104]. In this approach, the difference between the current state and a delayed state is used to determine the strength of the feedback signal. The control is usually applied to the state of the system. As with the OGY approach, this method has seen continued variations and improvement, see for instance [113, 82, 105, 112, 106]. The Pyragas method can, in principle, be applied to extended systems if the entire domain of a given system is accessible to control. In its simplest form, the feedback control is applied uniformly over the whole spatial domain. An alternative is to spatially vary the feedback signal. Applicability of this method has been shown in several theoretical and numerical studies [12, 13, 19, 48, 88] as well as several experimental investigations [18, 83, 15, 91, 68]. However, this approach also faces difficulties when applied to extended systems, since for most of these systems, application of control

over the whole spatial domain is impossible.

The impracticality of spatially extended control was soon realized and localized control was studied. Several authors were able to use localized control to stabilize systems of relatively large spatial extent [6, 2, 119, 50]. However, in all the systems these authors studied, a large gradient or flow term was present, which propagated the control signal through the system. Not surprisingly, if the control was applied at the source of the flow, it swept through the system and achieved control. The obvious disadvantage to these control approaches is the fact that they only work for gradient or flow systems, and even there only in narrow parameter ranges. Their general usefulness is therefore rather limited. A more general idea of applying localized feedback control to an extended system described by a PDE was considered by Gang and Kaifen [51]. They suggested applying control at certain localized sites, a method termed pinning control. Further study in that direction, with some variations in the type of control, has been performed by several authors [52, 6, 63, 99, 100]. The control used in these studies is closest in concept to the one we will study. A significant difference between those studies and ours is the way the feedback is computed. Additionally, our main focus is not on using a certain method to control a system, but rather to study the limits of control.

While there exist control approaches in addition to the ones we mentioned, most of them are minor modifications of the ideas just outlined or are approaches that only work for a very specific system and are therefore not worth mentioning here. For more details on chaos control approaches, mostly developed by the physics community, we point to the review by Boccaletti *et al* [20] and references therein.

Most of the control schemes just mentioned perform quite well for the system they were developed for. Further, some analysis has been done to explain how and why they work. Still, there is no consistent general theory on how to design control for a given system. This makes it hard to transfer control approaches from one problem to another. Instead, each time the control has to be ‘cooked up’ again, according to some more or less ingenious idea on how to control a given system. There are no readily available standard recipes that describe how well a certain control performs, to which other systems it can be

extended, when it fails, etc. On the other hand, there is the well developed engineering field of control theory, in which over the years extensive and powerful mathematical models and tools have been developed, allowing rather general treatment and analysis of a broad range of problems. Control theory allows for a more rigorous, systematic approach toward control implementations. Also, quite often using control theoretical approaches to compute a certain feedback control leads to superior results when compared to the more physically motivated approaches. For instance in [63], it was shown how a certain type of control theoretical method, produces superior results compared to an earlier suggested control method [52]. Further, using the control theoretical approach provided significant additional insight compared to the simplistic and ad-hoc ‘physics approach’ toward control. The latter still produces important contributions, for instance in the context of ‘self-control’ between coupled systems, i.e., synchronization [102]. Nevertheless, most of the new and important developments with regards to control of spatially extended chaotic systems come from the control engineering community. While historically the focus in control theory has been on low dimensional, linear systems, nowadays the emphasis is increasingly on high-dimensional, spatially extended, nonlinear systems. Application of the general and powerful tools of control theory has led to significant advances in the ability to control those system [31, 16]. Since we will utilize some of these control theoretical techniques, we will briefly review a few of the ideas in the next section.

2.2 Control theory methods

Control theory is a very broad and mature field of study with many different areas of active research. We have by no means the space or the knowledge to give a comprehensive overview of the whole field. Instead we only discuss the small part of control theory we utilize in this work, in a rather condensed form. For more in depth information, we refer to some of the textbooks describing different aspects of control theory, for instance [36, 34, 96, 57, 101].

Historically, control theory was developed to treat low-dimensional systems. In recent decades, focus has shifted to higher dimensional, extended systems. Application of control theoretic methods to extended systems has recently gained a lot of attention, mostly because

of their practical importance. Foremost among the systems studied are fluid systems. These are almost always extended, and control almost always has to be localized, for instance at the boundaries. Control of several physically important fluid systems has been studied, for instance Raleigh-Bénard convection [115, 97], plane Poiseuille flow [79], flow past a cylinder [86] and thin film flows [60]. It was shown that utilizing control theoretic methods can greatly enhance stability. Other studies applied control to amplitude equations that can be good approximations for certain extended fluid systems [33]. For instance in [4, 5] control of the Kuramoto-Sivashinsky equation was studied while [87, 85] studied the Ginzburg-Landau equation. Several other approaches are mentioned in a recent review [90]. Since these extended systems, specifically the PDEs just mentioned, are the systems we set out to study, we only explain control theory approaches that are applicable to these types of systems. All the methods presented are relatively new, compared with the overall history of control theory and are therefore often referred to as ‘modern control’.

While there is work that deals with control of continuous and infinite dimensional systems, such as PDEs given by (1), these studies for the most part deal with the general possibility and existence of control only [84], without giving specific results on how to compute it. This results in very limited practical applicability.

Significant analytical progress can be made and more control theoretical tools can be used if one instead approximates the continuous and infinite dimensional PDE by a discrete, finite dimensional system. In addition, numerical analysis usually also requires systems that are discrete and finite-dimensional. There are different possibilities to approximate a PDE by a finite, discrete system. Often, a first step is to convert the PDE into an infinite set of ordinary differential equations (ODEs). This can be done by a modal expansion using Fourier modes or other basis functions. Next, if the system is such that it can be separated in slow and fast modes, one can most often ignore the equations corresponding to the fast, strongly damped dynamics. Performing a Galerkin truncation of the infinite set of ODEs then results in a discrete, finite-dimensional approximation. Another method is to perform an invariant manifold reduction, which can result in a better approximation of the infinite dimensional system [32, 31]. For all the systems studied in this work, we can obtain a

discrete form by means of a modal expansion. Additionally, we will show later that for our analysis, we can restrict ourselves to a finite-dimensional space.

Despite the fact that nonlinear control has received increased attention in recent years, the majority of theoretical results exist for linear control theory. Throughout our investigation, we will exclusively use linear control. This is justified since our goal is to stabilize a given target state subject to small initial disturbances or small background noise. Therefore the linear approximation should be valid. We do not concern ourselves with the problem of controlling a system that is already in a fully turbulent state. This, so called global control of nonlinear systems, is a different issue under active study [31]. Since we utilize linear control, we additionally need to linearize the original nonlinear system around the target state.

Performing these three steps, discretizing, reducing the system to a finite dimensional system and linearizing around the target state, we transform a system given by (1) into one described by an equation of the form

$$\dot{\Phi} = A\Phi. \quad (5)$$

A denotes the discrete, finite dimensional linear evolution operator, and the corresponding discrete function describing the state is denoted by Φ . In the following we will almost exclusively work with this representation. Since for that case, linear operators like A are represented by matrices and the functions they act on are represented by vectors, we interchangeably use the terms ‘linear evolution operator’ or ‘evolution matrix’ for quantities like A and we refer to quantities like Φ as ‘vector’, ‘function’ or ‘mode’.

Now that the system is brought to the linear, discrete form (5), one can add the control term to the system to obtain

$$\dot{\Phi} = A\Phi + Bu. \quad (6)$$

This representation of the system is known as state-space representation. It is the most common starting point for control design using modern control approaches for high-dimensional systems. In this representation, the matrix B describes the location and shape of the so-called actuators (the physical control units). For a system of N equations and r independent

controllers, the dimensionality of B is $N \times r$. The r -dimensional vector u represents the r control signals that will be applied to the system. For linear feedback control, u is chosen according to

$$u = -K\Phi \quad (7)$$

where the matrix K is $r \times N$. This matrix is the so-called feedback gain matrix and needs to be chosen such that in the evolution equation

$$\dot{\Phi} = A\Phi - BK\Phi = M\Phi \quad (8)$$

of the controlled system, the matrix M is linearly stable, i.e., the real part of all eigenvalues is negative.

For a given system, there usually exist strong constraints with respect to the number, location and shape of the actuators. The objective is often to use few localized control units, as such a setup is relatively easy to implement. For instance in a fluid flow system, one might want to have the control units placed at the boundaries of the system. The one quantity that allows for a significant amount of freedom when designing the linear feedback control is the feedback gain matrix K . While there are many different possible choices for K , in modern control theory three main approaches are used to determine it. Each of these approaches has many variations, we only discuss the simplest cases. The historically oldest approach is called the pole placement (PP) method. Here, one specifies the eigenvalues of the evolution matrix M and then calculates (sometimes analytically, as we will be doing later in Chapter 4, but usually numerically) a gain matrix K that achieves this. This approach ensures that M has the chosen, negative eigenvalues and is therefore stable.

The second control method – and its many variations – is known as optimal control, often also called the H_2 or Linear Quadratic Regulator (LQR) method. Here, one starts out by specifying a quadratic, energy-like functional called the cost function. In its simplest form, this functional is given by

$$J = \int_0^\infty (\Phi^\dagger V \Phi + u^\dagger Y u) dt. \quad (9)$$

The first term under the integral represents the generalized energy of the deviations from the target state, the second term is a measure of the control effort. The matrices V and Y

can be chosen to assign different weights to specific state variables Φ_n or specific controllers u_m . One chooses these matrices to best represent the physical problem under study. For problems where all the discretized variables are of equal importance – which is the case for translationally invariant PDEs – one can simply choose the matrices to be a multiple of the identity matrix $V = vI$ and $Y = yI$. The scalar factors now determine the importance of either minimizing the deviation from the target state (large v) or reducing the control effort (large y). The control $u = -Kx$ is now found by minimizing J , subject to the dynamical constraint (6). The solution found for K is unique and is referred to as ‘optimal’, in the sense that it minimizes the given functional. The derivation of the solution to this problem can be found in most textbooks on modern control, see for instance [34, 96]. We therefore just state the result. One finds

$$K = -B^\dagger Y^{-1} X \quad (10)$$

where X is the solution of the so called algebraic Riccati equation

$$A^\dagger X + XA - XBY^{-1}B^\dagger X + V = 0. \quad (11)$$

While it is usually not possible to solve this equation analytically, standard numerical routines exist. For some of the numerics in our work, we will make use of the LQR method along with the PP method. We want to point out that we only showed a very simple form of the functional J . There are more difficult cases, in which for instance the integral goes over a finite time or where the control needs to ensure a minimum final state when some disturbances are present. Again, for more details we refer to the literature mentioned above.

Finally, while we do not utilize this method, we want to briefly mention the so-called ‘robust’ or H_∞ control method. The name stems from the fact that the method is designed to be robust toward disturbances and uncertainties in the controlled system. One again starts out by specifying a functional similar to (9), however this time one includes external disturbances. Again, we only show a very simple case, for which the functional is given by

$$J = \lim_{T \rightarrow \infty} \frac{1}{T} \int_0^T (\Phi^\dagger V \Phi + u^\dagger Y u - w^\dagger S w) dt. \quad (12)$$

Here w are external disturbances added to (6) and S is their weight matrix. One now finds the gain matrix by simultaneously minimizing J with respect to u and maximizing it with

respect to w , subject to the dynamical constraint (6). This leads to a control that is less optimal – in the sense defined above – than the LQR control, but with improved robustness properties toward external disturbances w [17, 85]. One can find solutions to this problem by iteratively solving several matrix equations similar to (11). The resulting solutions are non-unique. Since the equations one obtains are complicated and not very insightful, and since we will not make use of the H_∞ method in this work, we do not show them here. Details can be found in [35] or in many standard textbooks, for instance [101, 57]. We want to point out that while H_∞ control allows for control design with specified robustness toward external disturbances, there might not always exist a solution. That is, one might find that for a given system, control with a specified robustness does not exist. This is important to realize in light of the fact that, as we will show, control becomes more and more susceptible to very small amounts of noise for growing system size and a fixed number of controllers. H_∞ control might potentially perform best in that limit. However, at some point it becomes simply impossible to construct such a controller for a given noise robustness specification.

This very brief description of some of the control theoretical state space methods is sufficient for the purpose of this work. There are many variants of the control schemes we just presented. One can distinguish between continuous and discrete dynamical systems and control, one can define infinite and more complicated finite time horizon problems, as well as a large number of other variations, depending on the problem under study. Further the linear control ideas have recently been extended to nonlinear control schemes [31]. Again, for further details we refer to the control theory literature.

As mentioned in Section 2.1, one of the advantages of the approaches presented here is the fact that they usually lead to better results when compared to more physically straightforward control ideas. Furthermore as one might already guess from the little presented here, the framework of control theory is much more general, allowing for any number of controllers and – as we will discuss in Section 5.3 – sensors. The control units can have almost any physical shape and can be placed at any location inside or at the boundaries of the system. All this is described in the appropriate space by the matrix B . It is therefore possible to cast many different problems into the mathematical formulation outlined here.

This allows for a much better analytical treatment and therefore a much more systematic approach toward analysis and improvement of control [21], compared with the often ingenious but rather ‘ad hoc’ methods of control used by most of the physics community. Because of these advantages, we will exclusively use the control theory approach.

Finally we want to point out one more result that was obtained utilizing the methods and framework of control theory, because it is important to the motivation of our study. In [62, 59], Grigoriev showed that the required number of localized controllers needed to stabilize an arbitrarily large system in the absence of noise only depends on the symmetry of the system and target state, and not on its size. However, this is not true for noisy systems. In these systems, the amount of tolerable noise decreases with increasing system size, eventually leading to breakdown of control. As it turns out – and had been noted earlier [38] – the strong sensitivity toward noise for large systems stems from the fact that the underlying linearized evolution operator becomes strongly nonnormal as the system increases. This nonnormality is a crucial element and we will therefore explain it in great detail in the next chapter.

CHAPTER III

NONNORMALITY AND TRANSIENT GROWTH

3.1 Overview of nonnormality

We refer to a dynamical system as nonnormal if its linearized evolution operator is nonnormal. A nonnormal operator M is a linear operator for which $MM^\dagger \neq M^\dagger M$ or, equivalently, the eigenfunctions of M are not orthogonal. While nonnormal operators have been studied for quite some time [55] and some of their peculiar properties had been realized [94], their importance in physical systems has only been appreciated and studied in the last few decades.

It was found that the nonnormality of an evolution operator can have a profound influence on the time evolution of the corresponding dynamical system. As we explain in detail in Section 3.2, for nonnormal systems, linear stability becomes a poor predictor of short term dynamics. Systems that are linearly stable might experience significant transient growth before eventual decay. One might argue that transient growth is of minor importance when trying to determine the long-term behavior of a dynamical system. Traditionally, this was in fact the prevailing view, relatively little attention has been given to transient dynamics. However, in recent years the realization began to emerge that a significant number of physically interesting and important systems are nonnormal and that this nonnormality and the connected transient growth can be vital in understanding the global and long-term dynamics of these systems.

An area where nonnormality was found to play a crucial role is fluid dynamics. In fluid systems, the underlying equations, most notably the Navier-Stokes equations, are nonlinear PDEs, usually defined on extended spatial domains [28, 92]. It is well known that for certain parameter ranges, many fluid systems are turbulent. While fully developed turbulence is still an unsolved problem and remains an area of active research [114], likely to pose a challenging problem for some time to come, great progress has been made in recent years in

understanding the transition to turbulence in certain systems. Most notably systems with strong mean flow have posed a longstanding problem due to the fact that the base flow for certain geometries is linearly stable but experimentally it is nevertheless found to become turbulent. It has been known for some time that linear stability analysis is inadequate in describing the transition to turbulence [78]. The discrepancy between linear analysis and experiment was usually attributed to nonlinear effects.

Lately, focus shifted from the nonlinear effects to the linearized equations themselves. In several recent contributions, it has been shown that for fluid systems with a strong mean flow, the underlying linearized evolution operators, usually some form of the Orr-Sommerfeld and Squire operators, can be strongly nonnormal [107]. Aside from a few studies in the 80s, for instance [40], the main investigation of nonnormality and turbulence transition started in the 90s. Some of the work can be found in [25, 41, 117, 54, 108, 47, 8] and more recently in [1, 110, 37]. In the last few years, further significant advances in analytical [29], numerical [93] and experimental [72] studies seem to close in on a full explanation of turbulence transition, at least in geometrically simple flows. Recent and rather comprehensive reviews that discuss this line of research can be found in the articles by Grossmann [67] and Rempfer [109], and especially the book by Schmid and Henningson [111] and references therein.

In all these investigations, the nonnormality of the underlying linear evolution operator was shown to play a significant role in the transition to turbulence by means of its ability to amplify small amounts of noise. In fact, while in some work the interaction between the nonnormality and the nonlinearity of the system was emphasized [118], other authors suggested that the specifics of nonlinearity might be of rather little importance [9]. The debate on this issue is still continuing and the question will likely have to be answered for every specific system. Nevertheless it is now generally acknowledged that nonnormality plays a crucial role in the transition to turbulence.

The study of nonnormality has not only improved the understanding of transition to turbulence for certain fluid flows. Other areas of research where nonnormality was found to play an important role are for instance plasmas [26, 45, 110] and liquid films [14, 61, 53].

Another field where nonnormality has been studied extensively in recent years is the area of numerical analysis. There, nonnormality is often described by the concept of pseudospectra analysis, which has been introduced in its current form by Trefethen (for a history on pseudospectra, see [116]). The pseudospectra approach generalizes eigenvalue analysis to include so-called pseudo-eigenvalues. Several theorems exist linking those pseudo-eigenvalues to the nonnormality of an operator [108, 116]. Unfortunately, to evaluate most of the results obtained using the pseudospectra approach, one almost always needs to resort to numerical methods. Another disadvantage is the fact that the study of the pseudospectrum alone does not provide information about the eigenvectors, which might lead to an incomplete description of the problem. Nevertheless this approach has been shown to provide useful insights in the study of nonnormal operators. Since we will not make use of this approach in our work, we do not discuss it in detail. For more information on pseudospectra and nonnormality, we refer to the extensive 'Pseudospectra Gateway' webpage maintained by Embree and Trefethen [39].

The importance of nonnormality for the problem of turbulence transition has very recently been noted by some researchers in the control theory community. It was realized that some of the control theoretic ideas and concepts are very closely related to the idea of nonnormality. Specifically the use of the state space description, transfer norms and input-output analysis, all common concepts in control theory, have proven to be useful tools for the study of nonnormality. For a line of research that uses these control theoretic ideas to further explain nonnormal effects in the transition to turbulence, see for instance [80, 81, 10].

While understanding transition to turbulence is of great interest, the ability to control this transition is probably of greater practical significance. Some studies considered non-normal effects in recently devised control schemes. To our knowledge the first such control scheme that accounted for nonnormality was considered in [43]. This study did not use control theoretic ideas for the computation of the feedback, instead a simple trial and error approach was used to determine the optimal feedback. Some recent control theoretical approaches that take into account nonnormality are developed mostly by the group of Bewley

and collaborators [17, 16, 86, 73]. This line of research has only emerged in the last few years and is a very young and active field of study. A unifying aspect in the control studies just mentioned is that the uncontrolled fluid system is nonnormal, due to a large mean flow. As we will show in detail, another class of systems that shows strong nonnormality are systems which start out as normal but unstable. In these normal systems, nonnormality arises as a result of localized feedback control. The fact that control introduces nonnormality was pointed out in [38] and very recently in [87, 85]. Our work is related to these studies while viewing the problem from a different angle. Most importantly, we will derive several analytical expressions that show explicitly how nonnormality arises and how it leads to control breakdown, something not found in other works so far.

While we later discuss the details of localized control and nonnormality, we want to already mention a fact that might otherwise not be clear. From what has been said so far and will be discussed later, one could assume that the reason we encounter nonnormality is completely due to the fact that we utilize localized control. This assumption is not entirely correct. It is true – as we will see in detail later – that the localization is an important ingredient for nonnormality. However, some of the studies we mentioned in Section 2.1 utilized localized control that did not lead to nonnormality. In these studies, the control happened to be chosen (simply on physical grounds, without any knowledge of the nonnormality issue) such that the controlled system remained normal. This choice of control had the disadvantage that it required a fairly close spacing of localized controllers in order to stabilize the system. In contrast, as shown in [63], using a control scheme like LQR allows significant reduction of controller density. But this comes at a price. The control renders the linear evolution operator nonnormal, and for a fixed number of controllers, this nonnormality grows with increasing system size. This in turn leads to the possibility of transient amplification and to a decrease in the amount of noise the system can tolerate before control fails. We therefore find ourselves in almost a ‘catch-22’ [70] situation: while modern control theoretic techniques allow for a smaller density of controllers for a given system size, the fact that these control techniques render the evolution operator nonnormal (which helps them to perform better) inherently leads to their eventual

breakdown through transient growth of minute disturbances. While control schemes like H_∞ are able to minimize the amount of transient growth and produce a more robust control, they will still eventually fail for large enough systems, or it is simply impossible to design a controller with a certain robustness toward noise. Nevertheless, the control theoretic approaches usually significantly outperform the more simplistic approaches mentioned in Section 2.1 and we will therefore only study those methods and their limitations.

3.2 *The limitations of linear stability analysis*

After giving an overview of research related to nonnormality, we will now provide a more detailed explanation of the phenomenon. We first show the shortcomings of standard linear stability analysis in that context. Linear stability analysis is a simple yet powerful tool that has been used with great success in almost every area of physics. Even after the increasing realization several decades ago that for most systems, nonlinear effects are important, linear stability analysis still proved to be useful. For instance, in Rayleigh-Bénard convection, linear stability analysis accurately predicts the critical Rayleigh number at which the instability of the spatially homogeneous state sets in [28]. However, as mentioned in Section 3.1, there are systems where the predictions of linear stability analysis do not agree with the experimental findings. We will explain why this is not primarily a nonlinear effect as has usually been speculated. Rather, in certain circumstances, linear stability analysis is not a useful tool to predict the dynamics of the system, regardless of nonlinear effects.

We start the analysis with the dynamical system (8), given by

$$\dot{\Phi}(t) = M\Phi(t). \quad (13)$$

We will later show specific examples of M for the systems and the control we study. For now, M is simply an unspecified linear evolution operator, represented by a matrix. If M has a complete set of N eigenvalues and eigenvectors $\{\lambda_k, e_k\}$, we can write any state of the system as

$$\Phi(t) = \sum_{k=1}^N d_k(t) e_k. \quad (14)$$

For notational convenience, we will from now on assume the eigenvalues and eigenvectors of

the system to be real valued. We make this assumption throughout the work unless specifically mentioned otherwise. The generalization to complex quantities is straightforward and does not change the analysis and results presented.

Substituting (14) into (13) and taking the inner product with respect to a set of functions e'_k that have the property $(e'_k, e_n) = \delta_{kn}$, one obtains

$$\dot{d}_k(t) = \lambda_k d_k(t), \quad k = 1, \dots, N. \quad (15)$$

The solution to these equations is

$$d_k(t) = e^{\lambda_k t} c_k \quad (16)$$

with the notation $d_k(0) = c_k$. Substituting (16) into (14), the state of the system can be written as

$$\Phi(t) = \sum_{k=1}^N c_k e^{\lambda_k t} e_k. \quad (17)$$

For any $\lambda_k > 0$, the amplitude of the associated eigenfunction e_k grows exponentially, which leads to unbounded growth in $\Phi(t)$. The state is called linearly unstable or often simply unstable. If on the other hand all $\lambda_k < 0$, the amplitudes of all eigenfunctions e_k decay exponentially and therefore any initial state

$$\Phi(0) = \sum_{k=1}^N c_k e_k \quad (18)$$

will also decay to zero. These are the classical results of linear stability analysis. For the remainder of this section, we assume that all $\lambda_k < 0$ such that we have a linearly stable system. We now want to investigate more carefully the behavior of $\Phi(t)$, specifically its change in magnitude over time. An important quantity to consider when describing the magnitude of the state Φ is its norm

$$\|\Phi\|_2 = \sqrt{(\Phi^\dagger, \Phi)}. \quad (19)$$

In the physical context one often considers $\|\Phi\|_2^2$ instead, which represents a generalized energy. Throughout this work we will exclusively use the 2-norm, for vectors as well as for matrices. We therefore often do not specifically indicate it.

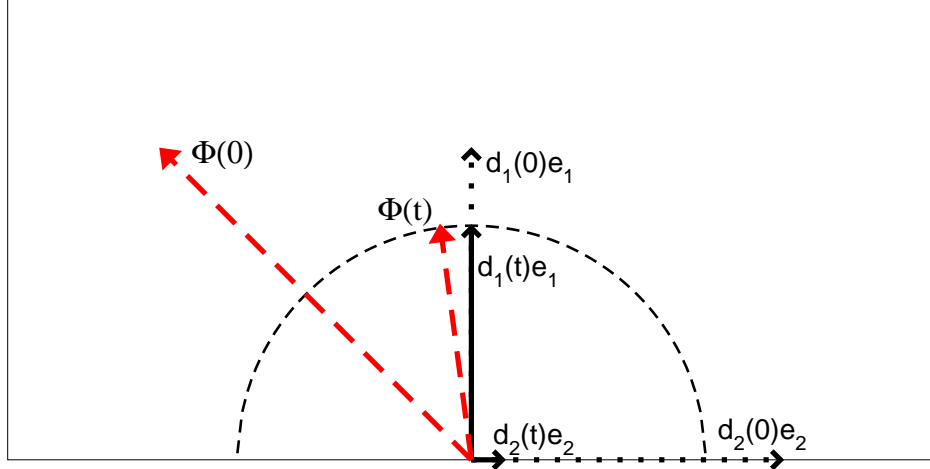


Figure 4: Monotone decay for a normal system. The initial state is $\Phi(0) = d_1(0)e_1 - d_2(0)e_2$. Since the amplitude of each eigenvector decays at a rate $\lambda_k < 0$ and the eigenvectors are orthogonal, the magnitude of the state $\Phi(t) = d_1(t)e_1 - d_2(t)e_2$ also decays monotonically with time. The semi-circle highlights the difference in magnitude between the $\Phi(0)$ and $\Phi(t)$.

Using (17) we find for the generalized energy

$$\|\Phi(t)\|^2 = \sum_{k,n=1}^N c_k c_n e^{(\lambda_k + \lambda_n)t} (e_k^\dagger, e_n). \quad (20)$$

As a measure of change in the magnitude of $\Phi(t)$, a further quantity of interest is the derivative of (20), given by

$$\frac{d}{dt} \|\Phi\|^2 = \sum_{k,n=1}^N 2\lambda_k c_k c_n e^{(\lambda_k + \lambda_n)t} (e_k, e_n). \quad (21)$$

Now let us discuss the behavior of (20) and (21) for the case where the operator M is normal. For this to be the case, M has to satisfy $M^\dagger M = M M^\dagger$. Many physically important operators are normal, such as Hermitian and Unitary ones. If M is a normal operator, its eigenfunctions e_k are orthogonal, $(e_k^\dagger, e_n) = \delta_{kn}$. For a normal operator, any initial state $\Phi(0)$ of unit magnitude, given by (18), has coefficients $|c_k| \leq 1$, owing to the fact that all e_k are orthogonal. Further, (20) and (21) simplify to

$$\|\Phi(t)\|^2 = \sum_{k=1}^N c_k^2 e^{2\lambda_k t} \quad (22)$$

and

$$\frac{d}{dt} \|\Phi\|^2 = \sum_{k=1}^N 2\lambda_k c_k^2 e^{2\lambda_k t}. \quad (23)$$

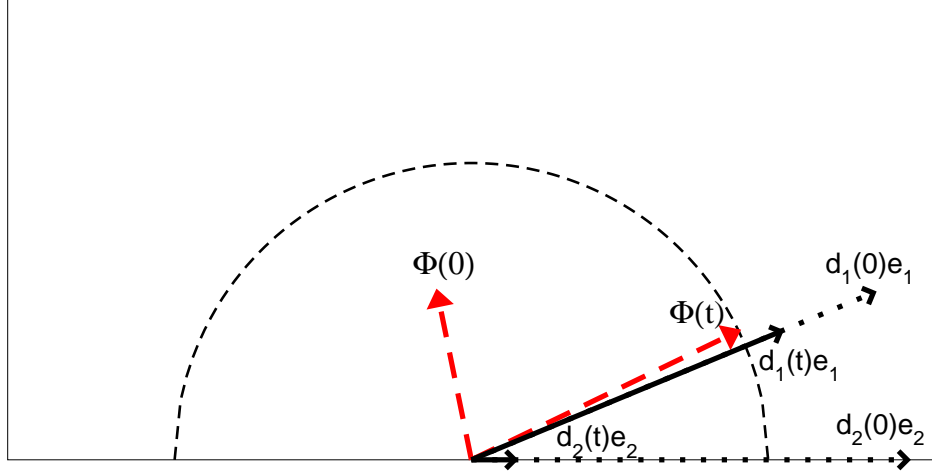


Figure 5: Transient growth for a nonnormal system. The initial state is $\Phi(0) = d_1(0)e_1 - d_2(0)e_2$. The amplitude of each eigenvector decays at a rate $\lambda_k < 0$, but since the eigenvectors are not orthogonal, initial cancellations are partly reduced. This leads to transient growth in the state $\Phi(t) = d_1(t)e_1 - d_2(t)e_2$ before exponential decay asymptotically dominates. The semi-circle highlights the difference in magnitude between the $\Phi(0)$ and $\Phi(t)$.

These expressions show that if all $\lambda_k < 0$, the energy change of the system is always negative and the norm of the state decays monotonically from some initial state to zero. Fig. 4 shows this very well known result for a two-dimensional system. Assuming $\|\Phi(0)\| = 1$, one sees that the coefficients $c_k = d_k(0) \leq 1$. Additionally the state $\Phi(t)$ decays monotonically.

So far, nothing surprising happened. However, things change for systems whose linear operator is not normal, i.e. $M^\dagger M \neq M M^\dagger$. As we mentioned in Section 3.1, several physically important systems fall into this category, most notably fluid systems with mean flow and systems under localized control, the latter being the subject of our study. In fact in both instances the nonnormality can be rather pronounced. We will describe later how to quantify nonnormality. For now it is important to note that every nonnormal (but diagonalizable) operator has a complete set of eigenfunctions $\{e_k\}$ which are *not orthogonal*. The fact that we have non-orthogonal eigenfunctions allows for the possibility that an initial condition $\Phi(0)$ with unit norm has large coefficients $|c_k| \gg 1$. Due to cancellations between the non-orthogonal eigenfunctions in (18), this can nevertheless result in $\|\Phi(0)\| = 1$. Fig. 5 shows this schematically for a two-dimensional system. The coefficients $c_k = d_k(0)$ are

larger than $\|\Phi(0)\|$, cancellations between the eigenvectors lead to a state with smaller magnitude. As time progresses, the amplitudes of all the e_k are exponentially decaying with rates $\lambda_k < 0$. However, since the decay rate of each eigenfunction is in general different from those of the other eigenfunctions, it is possible that an initial cancellation of large coefficients c_k is partially removed, which leads to growth in the state $\Phi(t)$. This can also be seen by again considering (21). We now have $(e_k^\dagger, e_n) \neq \delta_{kn}$ and therefore it is possible that even if all $\lambda_k < 0$, an initial state with certain coefficients c_k will have a positive value for the change in energy, indicating growth. Fig. 5 shows this for a two-dimensional system. Of course for $t \rightarrow \infty$, $\Phi(t)$ exponentially decays to zero. Nevertheless, short-term transient growth is possible.

We mentioned earlier the argument that the transient growth could be ignored if one is interested in the long-term dynamics of the system rather than its short-term behavior. When using linear stability theory, this is the viewpoint taken, either knowingly or sometimes unknowingly. For a purely linear systems, this point of view is justified, since any stable state is globally stable, no matter how large a transient growth one might encounter. Indeed, often the transient growth exists for only a very short time before exponential decay dominates. However, for nonlinear systems, the situation can be dramatically different. In those systems, transient growth of a small initial disturbance, or transient amplification of small background noise, can be large enough to produce a state $\Phi(t)$ of $O(1)$. This can trigger a nonlinear instability, potentially resulting in a permanent change of the system dynamics. If the system is strongly nonnormal, this mechanism can lead to instability even for minute disturbances, despite linear stability. In the context of the already mentioned fluid flows, this triggers transition to turbulence. In our context, it will lead to failure of linear control.

Before we discuss some more details of nonnormality and the associated transient growth in the next section, we want to mention a point that is sometimes brought up when people first learn about nonnormality. The comment is that, as long as the eigenfunctions of M span the full space, one can always transfer to a set of equivalent functions that span the same space and that are orthogonal. Therefore one should be able to circumvent this

somewhat unpleasant phenomenon of nonnormality by simply working in the appropriate space. Unfortunately, this idea is of limited usefulness. The reason being that for a given physical system, the observables such as $\Phi(t)$, which for instance represent the velocity in fluid flows, are independent of the choice of basis. To analyze the given system and the behavior of $\Phi(t)$, one can certainly express it in a more suitable basis, such as a basis with orthogonal eigenvectors. However, while a certain representation might be computationally advantageous, one still wants to know the behavior of $\Phi(t)$ in the physical space, which is independent of the basis one works in. In this situation, the transformation matrix which moves from the orthogonal to the original basis will re-introduce the nonnormality. One in effect shifts the nonnormality from one quantity to another [44]. Therefore nothing is gained in terms of preventing nonnormality. A system that is nonnormal in its physical description will exhibit real physical transient growth, no matter how the calculations are done. We therefore need to be able to quantify nonnormality and transient growth, which we set out to do in the following section.

3.3 Characterization of nonnormality and transient growth

After having introduced nonnormality and transient growth in a qualitative manner, we now want to introduce several concepts that allow a more quantitative description. Several conditions must be satisfied for strong nonnormality and transient growth to occur. First, since we can assume the e_k to be normalized, substantial growth in (17) can only occur for $c_k \gg 1$. The c_k are given by

$$c_k = (e'_k, \Phi(0)). \quad (24)$$

where $\{e'_k\}$ are the adjoint eigenfunctions, normalized according to $(e'_k, e_n) = \delta_{kn}$. Since we can require any initial condition to be normalized to $\|\Phi(0)\| = 1$, $c_k \gg 1$ is only possible for $\|e'_k\| \gg 1$. For a normal operator, the adjoint eigenfunctions $\{e'_k\}$ coincide with the eigenfunctions $\{e_k\}$, and therefore $\|e'_k\| = 1$. For $\|e'_k\|$ to become large, it is necessary that the operator is strongly nonnormal. The more the eigenfunctions e_k become aligned, the larger the norms of the e'_k become [44]. This shows, that one needs closely aligned eigenfunctions to allow for possible strong transient growth to occur. It also shows that the

magnitude of the coefficients c_k and of the adjoint eigenfunctions e'_k – which are determined by the eigenfunctions e_k – can give a quantitative measure for nonnormality. Note the connection to a useful quantity in numerical analysis, the so called condition number. The condition number $\kappa = \|E^{-1}\| \|E\|$ is used to measure how close to singular a matrix E is [74, 56]. A small κ means E is numerically invertible with great accuracy, while a large κ means that the inversion of E becomes less reliable, indicating that E approaches a singular matrix. For the case that E is non-invertible, $\kappa = \infty$. Since the e'_k can be written as the rows of the matrix E^{-1} where E is the matrix containing the e_k as columns, one sees that as the eigenfunctions become closely aligned, E becomes closer and closer to being singular, and $\|E^{-1}\|$ and κ become large. Nonnormality has been well known in the numerical analysis community [94], however its identification as being an important property in dynamical systems has only been made through the studies mentioned in Section 3.1.

An important fact to note is that the c_k not only depend on the e'_k but also on the initial disturbance $\Phi(0)$. This means that even if the system is strongly nonnormal with closely aligned eigenfunctions and large κ , not all initial conditions experience transient growth. Rather, only those $\Phi(0)$ whose inner product with the largest adjoint eigenvector e'_k is large, produce large c_k and have the potential for transient growth. As is shown in Fig. 6, random initial conditions lead to values of c_k that are comparable to those from initial conditions that are known to produce large c_k . However certain initial conditions do not experience growth. For instance choosing a unit magnitude initial state $\Phi(0)$ to be an eigenfunction e_m leads to only one nonzero coefficient $c_m = 1$ which decays without any transient growth. In general, significant transient growth is possible only for initial conditions that do not have significant projection onto the nonnormal eigenfunctions. For the two-dimensional case, this can again easily be seen from Fig. 5. In this figure, consider a $\Phi(0)$ pointing roughly in the direction of the two nonnormal eigenvectors, and it is immediately clear that it cannot experience any significant transient growth. The initial condition experiencing the most transient growth is roughly orthogonal to the non-normal subspace and sometimes referred to as the bi-orthogonal vector [42]. The fact that only certain initial conditions are transiently amplified is an important feature of nonnormality. It plays a crucial role in the

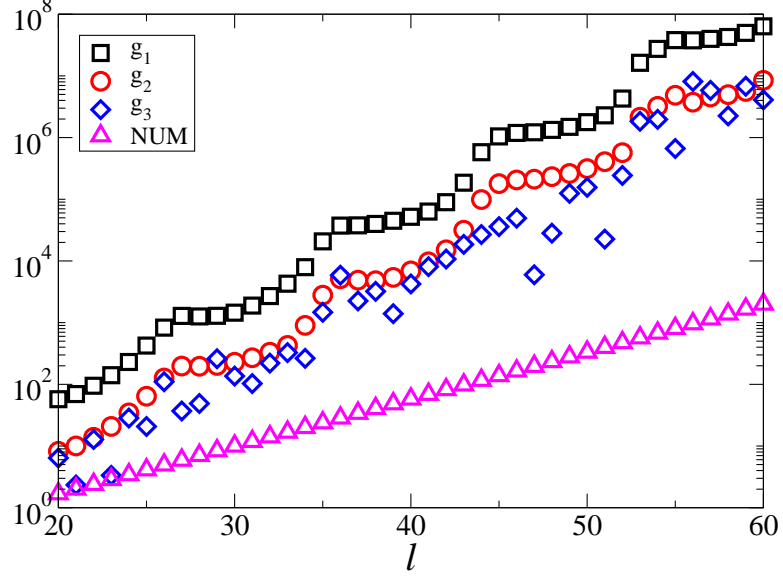


Figure 6: Largest expansion coefficient $g = \max_k |c_k|$ as a function of system size l for the controlled GL equation. The different g are computed through (24) with a $\Phi(0)$ normalized to unit magnitude. We choose $\Phi(0)$ to be the largest adjoint eigenfunction (g_1), the disturbance that leads to maximum transient growth (g_2) and a random state (g_3). For comparison, we also plot the maximal transient growth in the system as given by $\max_{t, \Phi(0)} [\Phi(t)/\Phi(0)]$, determined from numerical simulation (NUM).

explanation of control limits and we will therefore discuss it in more detail in Chapter 6 where we analyze control breakdown.

While the requirement $c_k \gg 1$ is a necessary one in order to achieve a large $\|\Phi(t)\|$ at some intermediate time, it is not sufficient. As mentioned earlier, for transient growth to occur, it is also necessary that the evolution of the e_k in the sum (17) is such that initial cancellations of different eigenvectors are at least partially removed. When considering dynamical systems, the maximum $\|\Phi(t)\|$ the state can reach is an important quantity one would like to know. Sometimes, the amount of nonnormality for a given M , as described for instance through the largest c_k or the condition number κ , can provide a good measure for the transient growth of $\Phi(t)$. However, since these quantities only consider the nonnormal eigenvectors e_k , and not how the eigenvalues λ_k influence the removal of initial cancellations, they sometimes overestimate the dynamically realizable growth in $\Phi(t)$. This can be seen for the coefficients c_k in Fig. 6.

We therefore require another quantity that can capture the maximum magnitude of

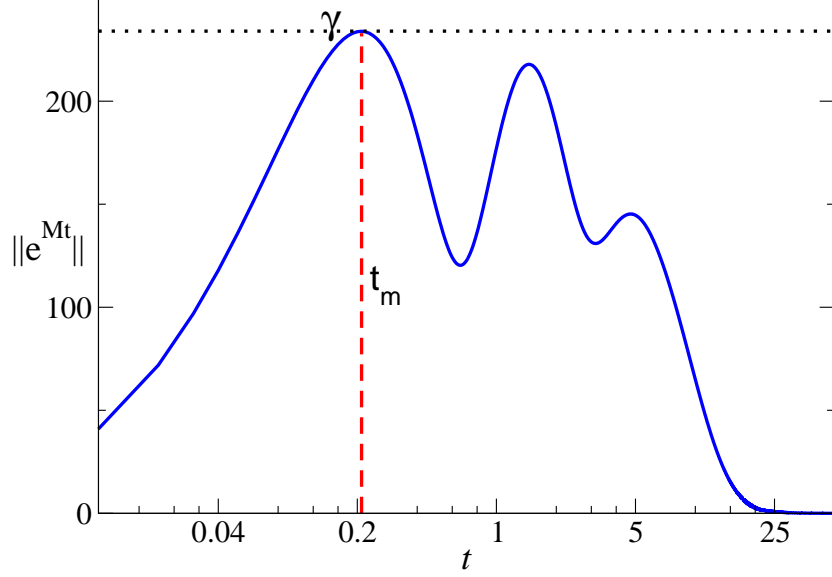


Figure 7: $\|e^{Mt}\|_2$ for the controlled GL equation. Also shown is the maximum transient amplification γ and the corresponding time t_m at which the maximum is reached. Note the logarithmic scale in the time direction to better resolve the fast transient growth.

$\|\Phi(t)\|$. To that end, we can define a transient amplification factor according to

$$\gamma \equiv \max_{t, \Phi(0)} \frac{\|\Phi(t)\|_2}{\|\Phi(0)\|_2} = \max_t \|e^{Mt}\|_2 = \|e^{Mt_m}\|_2 = \sqrt{\lambda_{max}(e^{M^\dagger t_m} e^{Mt_m})} \quad (25)$$

which measures the maximum amplitude of an evolved disturbance $\Phi(t)$ for all possible initial conditions $\Phi(0)$ and all times t . The initial condition that leads to maximum growth at time t_m is sometimes called the optimal disturbance Φ_{opt} [42]. The symbol λ_{max} denotes the largest eigenvalue. For normal operators one finds $\gamma = 1$, but for non-normal ones, it can be significantly larger. Several authors have introduced quantities similar to (25) in their studies of non-normality and transient growth, see for instance [42, 107, 111, 110]. Further, (25) is similar to the so called transfer norms and input-output description commonly used in control theory. As mentioned earlier, some authors recently started to use such control theoretical ideas in their analysis of nonnormality and transient growth [10, 80, 85].

To get some intuition to what (25) describes, we show in Fig. 7 the time evolution of $\|e^{Mt}\|_2$ as well as t_m and γ for one of the systems under study. Additionally, in Fig. 8 we plot γ computed via the matrix norm in (25) and compare it with direct numerical simulations (SIM). The values are shown as a function of the system size l , a dependence

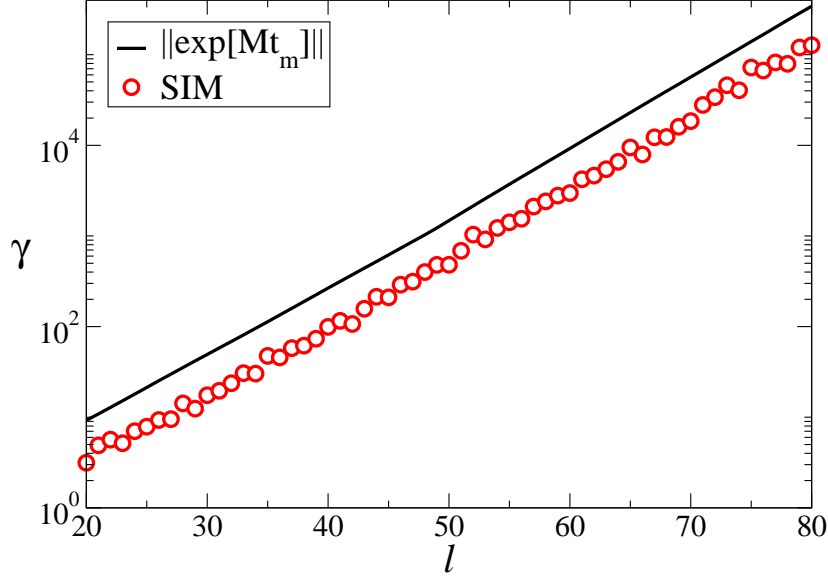


Figure 8: Amplification factor γ given by (25) and direct numerical simulation (SIM) with random initial disturbances as described in the text for the case of the controlled GL equation.

that we will strongly focus on later. For the direct numerical simulation, we start with 100 random initial conditions $\Phi(0)$ and determine $\max_{t, \Phi(0)} \frac{\|\Phi(t)\|_2}{\|\Phi(0)\|_2}$. This is expected to give a somewhat lower value than γ since it is unlikely that any of the 100 random initial conditions corresponds to the one resulting in maximum growth. Still one sees that the agreement is good and (25) can therefore be considered a good quantitative measure for the possible transient amplification of a generic disturbance in a nonnormal system.

So far, we considered nonnormality and transient growth from the perspective of an initial value problem. That is, we investigated how an initial disturbance $\Phi(0)$ evolves with time. A different scenario, which better represents many physical systems, is that of a system with stochastic background noise instead of a single initial disturbance. Several authors have studied nonnormal systems with stochastic noise [10, 41, 46]. The ideas we present in the following are very similar to material found in [41]. It is easy to introduce a quantity in analogy to (25) for the case of stochastic noise. In the presence of such noise, the linearized system is described by

$$\dot{\Phi}(t) = M\Phi(t) + \eta(t) \quad (26)$$

where the vector η describes the stochastic noise. In the following we assume that η is δ -correlated Gaussian white noise:

$$\langle \eta_i \rangle = 0, \quad \langle \eta_i^\dagger(t), \eta_j(t') \rangle = \sigma \delta_{ij} \delta(t - t'). \quad (27)$$

The square brackets denote ensemble averaging. We refer to σ as the magnitude or strength of the noise. This choice for the noise often provides a reasonably good approximation to the type of noise found in real physical systems.

The solution of (26) is given by

$$\Phi(t) = e^{Mt} \Phi(0) + \int_0^t e^{M(t-\tau)} \eta(\tau) d\tau. \quad (28)$$

Since we want to focus on the background noise, we set $\Phi(0) = 0$. In analogy to (25) we can define a growth factor γ_c representing the ratio of the statistical average of the state to the statistical average of the noise. We define

$$\gamma_c \equiv \frac{\langle \|\Phi(t)\|_2 \rangle}{\langle \|\eta(t)\|_2 \rangle} \quad (29)$$

$$\begin{aligned} &= \frac{1}{\langle \|\eta(t)\|_2 \rangle} \langle \left(\int_0^t \eta^\dagger(\tau) e^{M^\dagger(t-\tau)} d\tau, \int_0^t e^{M(t-\tau')} \eta(\tau') d\tau' \right)^{1/2} \rangle \\ &= \left\| \int_0^t e^{M^\dagger(t-\tau)} e^{M(t-\tau)} d\tau \right\|_2^{1/2} \equiv \sqrt{\|B(t)\|_2} \end{aligned} \quad (30)$$

where we used the properties (27) of η . Since the evolution matrix M is stable, there exists a statistically steady limit for $(t \rightarrow \infty)$ and in that limit

$$\gamma_c = \left\| \int_0^\infty e^{M^\dagger t} e^{Mt} dt \right\|_2^{1/2} \equiv \sqrt{\|B\|_2}. \quad (31)$$

which also implies

$$\lim_{t \rightarrow \infty} \frac{d}{dt} B(t) = 0. \quad (32)$$

Using the Leibniz integral rule one obtains from (30) the expression

$$\frac{d}{dt} B(t) = M^\dagger B(t) + B(t) M + I \quad (33)$$

which leads in the steady state asymptotic limit $t \rightarrow \infty$ to

$$M^\dagger B + B M = -I. \quad (34)$$

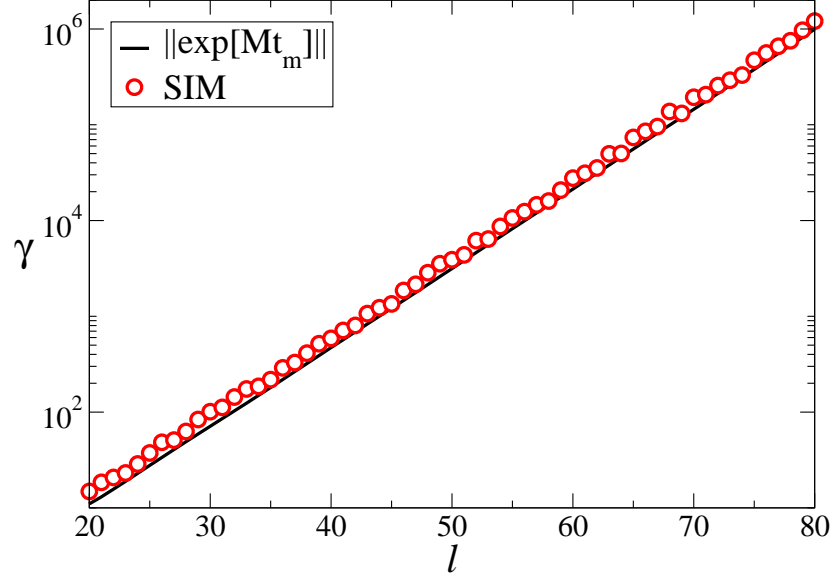


Figure 9: Amplification factor γ_c given by (30) and direct numerical simulation (SIM) with continuous noise as described in the text for the case of the controlled GL equation.

This last equation is a so-called Lyapunov equation, commonly found in control and linear system theory [30]. For a discrete, finite-dimensional system, B is simply a matrix and can be easily solved for using standard numerical algorithms. In Fig. 9 we show γ_c computed from (31) and compare it with direct simulation of the system. We apply noise of the form (27) to the controlled GL equation and determine the time average of $\|\Phi(t)\|_2$ for a sufficiently long interval. This allows computation of γ_c according to (29). One again finds good agreement between the theoretical value (30) and the numerically obtained results. Therefore γ_c is found to be a good measure for the possible growth given a certain amount of noise.

Note that in performing a time average for the simulations above, rather than an average over different realizations, we assume ergodicity. While this is not truly the case since the noise is cumulative, we can nevertheless assume that it is at least approximately true, due to the fact that the exponential decay results in some kind of ‘short term memory’ of the noise, which for long time intervals should lead to results that do not show a significant difference between the time and ensemble averages. Numerical checks confirm that this assumption is valid. We further want to remark that when numerically implementing the

noise, one ends up with band-limited Gaussian white noise. For a discussion of these issues and an introduction to the numerical implementation of stochastic differential equations, we refer to [23] and [71].

While one can extend the ideas we presented here by including structured noise or other generalizations, for our purpose, the Gaussian white noise suffices. Some additional details and generalizations can be found in [41, 10].

3.4 *Two toy models*

We end this chapter on nonnormality and transient growth by considering two simple toy models. Since these are low dimensional models, they have no direct application to the extended systems that we study later. However, they are simple enough to allow calculation of some of the quantities introduced. This allows us to illustrate the somewhat abstract concepts from the previous sections. We hope it adds further insight and understanding to the ideas outlined so far.

For our first model, which is similar to a model discussed in [42], we choose a two-dimensional system with eigenvalues $\lambda_2 < \lambda_1 < 0$ and eigenvectors

$$e_1 = \begin{pmatrix} 1 \\ 0 \end{pmatrix}, \quad e_2 = \begin{pmatrix} \cos(\theta) \\ \sin(\theta) \end{pmatrix}. \quad (35)$$

The angle θ is chosen to be in $[0, \pi/2]$. For $\theta = \pi/2$, the second eigenvector is $e_2 = (0 \ 1)$ and the system is normal with two orthogonal eigenvectors, corresponding to the scenario shown in Fig. 4. As θ decreases, the second eigenvector approaches the first one and the system becomes nonnormal. The Jacobian M for this system is given by

$$M = \begin{pmatrix} \lambda_1 & (\lambda_2 - \lambda_1) \cot(\theta) \\ 0 & \lambda_2 \end{pmatrix}. \quad (36)$$

While the eigenvectors are not orthogonal for $0 < \theta < \pi/2$, they form a basis, and we can express any state of the system through the linear combination

$$\Phi(t) = c_1 e^{\lambda_1 t} \begin{pmatrix} 1 \\ 0 \end{pmatrix} + c_2 e^{\lambda_2 t} \begin{pmatrix} \cos(\theta) \\ \sin(\theta) \end{pmatrix}. \quad (37)$$

Since both eigenvalues are negative, the state $\Phi(t)$ is asymptotically decaying with time. Nevertheless, as illustrated in Fig. 5, it is possible to have transient growth before asymptotic decay dominates. We noted earlier that a necessary condition for transient growth is to have large expansion coefficients c_k . And we also noted that for these coefficients to be large, the norm of the adjoint eigenfunctions needs to be large. Here we can easily calculate the adjoint eigenfunctions and find

$$e'_1 = \begin{pmatrix} 1 \\ -\cot(\theta) \end{pmatrix}, \quad e'_2 = \begin{pmatrix} 0 \\ \csc(\theta) \end{pmatrix}. \quad (38)$$

Their norm is found to be

$$\|e'_1\| = \|e'_2\| = |\csc(\theta)|. \quad (39)$$

As expected, this norm becomes large for small θ , that is for a strongly nonnormal system with closely aligned eigenvectors.

Another sign that indicates nonnormality is a non-vanishing commutator $[M, M^\dagger]$. We can compute the commutator and find

$$[M, M^\dagger] = (\lambda_2 - \lambda_1)^2 \cot(\theta) \begin{pmatrix} \cot(\theta) & 1 \\ 1 & -\cot(\theta) \end{pmatrix}. \quad (40)$$

The norm of the commutator is found to be

$$\|[M, M^\dagger]\|_2 = (\lambda_2 - \lambda_1)^2 \frac{\cos(\theta)}{\sin^2(\theta)}, \quad (41)$$

which is nonzero for $0 < \theta < \pi/2$, and strongly increasing with a decrease in θ , again showing that M becomes strongly nonnormal for small angles.

Next we compute γ using (25). One finds

$$\gamma^2 = \max_t \left| \frac{1}{2 \sin^2(\theta)} \left[(l_1 - l_2)^2 + \sqrt{(l_1 - l_2)^2 (l_1^2 + l_2^2 - 2l_1 l_2 \cos(2\theta))} \right] + l_1 l_2 \right| \quad (42)$$

with $l_1 = e^{\lambda_1 t}$, $l_2 = e^{\lambda_2 t}$. For a strongly nonnormal system with closely aligned eigenvectors, $\theta \ll 1$. In this limit, γ can be approximated by

$$\gamma \sim \frac{1}{\theta} \max_t |e^{\lambda_1 t} - e^{\lambda_2 t}|. \quad (43)$$

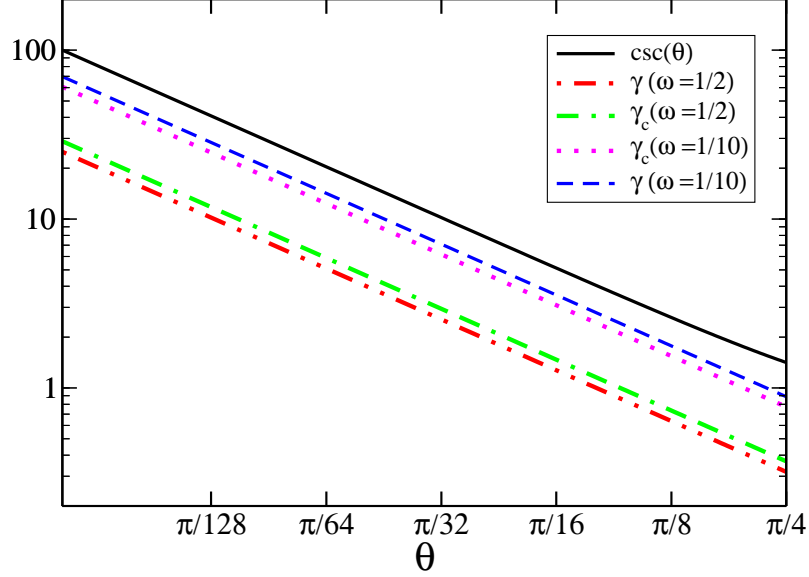


Figure 10: Norm of adjoint eigenfunctions $\|e'_i\|$, given by (39) and amplification factor γ and γ_c given by (45) and (46) for several choices of the eigenvalue ration ω .

Calculating the time t_m at which (43) reaches its maximum, one obtains

$$t_m = \frac{1}{\lambda_2 - \lambda_1} \ln\left(\frac{\lambda_1}{\lambda_2}\right). \quad (44)$$

Substituting (44) into (43) then leads to

$$\gamma \sim \frac{1}{\theta} \left| \omega^{\frac{\omega}{1-\omega}} - \omega^{\frac{1}{1-\omega}} \right| \quad (45)$$

with $\omega = \lambda_1/\lambda_2$. For both large and small ω , (45) approaches $1/\theta$, which for small θ agrees with the limit given by (39). For intermediate values of ω , corresponding to eigenvalues with similar magnitude, (45) has values lower than (39) with a minimum for $\omega = 1$.

As the last quantity of interest, we compute γ_c by first computing B according to (34) and then finding γ_c through (31). In the limit of small θ , this is found to be

$$\gamma_c \sim \frac{1}{\theta} \left| \frac{(\lambda_1 - \lambda_2)}{\sqrt{2\lambda_1\lambda_2(\lambda_1 + \lambda_2)}} \right|. \quad (46)$$

Now that we computed all the quantities of interest, let us briefly discuss the results. In Fig. 10, we show the norm of the adjoints as a function of θ , together with $\gamma(\theta)$ and $\gamma_c(\theta)$ for different λ_1, λ_2 . First we note that as expected, all three quantities strongly increase as θ decreases, diverging as $1/\theta$ for small θ . Comparing γ and γ_c with $\|e'_k\|$ one also sees that

the adjoints – and therefore through (24) the coefficients c_k – represent an upper limit for the transient amplification. This confirms our earlier explanation that the largest growth possible is given by the largest c_k . This growth could be realized if all eigenvectors e_n , $n \neq k$ were to decay very fast ($\lambda_n \ll 0$) while the eigenvector e_k experienced almost no decay ($\lambda_k \gtrsim 0$). It would lead to removal of almost all initial cancellations between the eigenvectors, leaving a state whose magnitude would be of order c_k .

For more realistic values of the λ_k , the transient growth is lower. The exact values of the λ_k determine how much growth will be realized. The more the eigenvalues differ, the more transient growth can be expected. For the simple system studied here, this is shown by the fact that γ only depends on the ratio of the two eigenvalues. This can easily be understood, again with the help of Fig. 5. If the nonnormal eigenfunctions decrease at different rates, initial cancellation of large coefficients c_k is strongly reduced. If, on the other hand, the eigenfunctions decrease at similar rates, the cancellation effects persist and no, or only very small, transient growth occurs. This consideration also explains the fact that γ has a minimum for $\omega = 1$ and that it increases, approaching $|e_k|$, as ω becomes large or small. We therefore find that all the analytic expressions computed for this simple example agree well with our general explanations presented in earlier sections. The simplicity of the example helps to get a better understanding of the general idea of nonnormality and the various quantities describing it.

An additional point merits mentioning. For the system presented here, the nonnormality as measured by the alignment of the eigenvectors is solely determined by θ – it is a purely geometric quantity. On the other hand, the transient growth γ and γ_c (and the commutator) also depend on the dynamics of the system as described by the eigenvalues. The separation between nonnormality due to the geometric alignment of the eigenvectors only, and transient amplification due to the eigenvector alignment as well as dynamical properties of the evolution operator is a nice property. Unfortunately it is rather exceptional and arises only because of the very specific way we set up the system. With the next example, we want to illustrate that in the general case, and specifically in the systems we will study later, the alignment of the eigenvectors and the dynamics of the system are interdependent.

To illustrate this point, we choose a second two-dimensional model, which is a low dimensional version of the systems we will study in more detail in Section 4.1. This model can be understood as the unstable subspace of a PDE having two positive eigenvalues, presented in its appropriate eigenspace. In the eigenspace, the evolution matrix is diagonal and the evolution equation is given by

$$\dot{\Phi} = \begin{pmatrix} 1 & 0 \\ 0 & 2 \end{pmatrix} \Phi = A\Phi, \quad (47)$$

where we arbitrarily choose the eigenvalues to be 1 and 2. To this equation we add the control term as given by (6) and (7), using one controller. As we show later, for a system with control at the right boundary, the 2×1 matrix B representing the control location and the 1×2 matrix K representing the feedback gain are given in the eigenspace representation by

$$B = \begin{pmatrix} -1 \\ 1 \end{pmatrix}, \quad K = \begin{pmatrix} K_1 & K_2 \end{pmatrix}. \quad (48)$$

With this choice, the evolution matrix of the controlled system is

$$M = A - BK = \begin{pmatrix} 1 + K_1 & K_2 \\ -K_1 & 2 - K_2 \end{pmatrix}. \quad (49)$$

As we will show in Section 4.1, we can use the PP method mentioned earlier to change the positive eigenvalues to negative eigenvalues $\lambda'_1, \lambda'_2 < 0$ if we choose the gain coefficients K_1, K_2 to be

$$K_1 = (1 - \lambda'_1)(1 - \lambda'_2), \quad K_2 = (2 - \lambda'_1)(2 - \lambda'_2). \quad (50)$$

Substituting (50) in (49) then leads to the evolution matrix

$$M = \begin{pmatrix} 1 + (1 - \lambda'_1)(1 - \lambda'_2) & (2 - \lambda'_1)(2 - \lambda'_2) \\ -(1 - \lambda'_1)(1 - \lambda'_2) & 2 - (2 - \lambda'_1)(2 - \lambda'_2) \end{pmatrix}. \quad (51)$$

The normalized eigenvectors of M are found to be

$$e_1 = \frac{1}{\sqrt{5 - 6\lambda'_1 + 2\lambda'^2_1}} \begin{pmatrix} 2 - \lambda'_1 \\ \lambda'_1 - 1 \end{pmatrix}, \quad e_2 = \frac{1}{\sqrt{5 - 6\lambda'_2 + 2\lambda'^2_2}} \begin{pmatrix} 2 - \lambda'_2 \\ \lambda'_2 - 1 \end{pmatrix}, \quad (52)$$

the adjoints are given by

$$e'_1 = \frac{\sqrt{5 - 6\lambda'_1 + 2\lambda'^2_1}}{\lambda'_1 - \lambda'_2} \begin{pmatrix} \lambda'_2 - 1 \\ \lambda'_2 - 2 \end{pmatrix}, \quad e'_2 = \frac{\sqrt{5 - 6\lambda'_2 + 2\lambda'^2_2}}{\lambda'_1 - \lambda'_2} \begin{pmatrix} \lambda'_1 - 1 \\ \lambda'_1 - 2 \end{pmatrix} \quad (53)$$

and their norms are found to be

$$\|e'_1\| = \|e'_2\| = \frac{1}{\lambda'_1 - \lambda'_2} \sqrt{(5 - 6\lambda_1 + 2\lambda'^2_1)(5 - 6\lambda_2 + 2\lambda'^2_2)}. \quad (54)$$

One sees that if $\lambda'_2 \rightarrow \lambda'_1$, the eigenvectors become aligned and the norms grow strongly, reflecting strong nonnormality.

While it is possible for this system to compute the commutator, γ and γ_c as we did in the first example, one obtains complicated expressions that do not provide additional insight beyond what we explained in the first example. To illustrate the point we set out to make, we do not need these quantities. We can use the results obtained so far. As mentioned, the eigenvectors in the first example did not depend on the dynamics of the system, i.e., on the eigenvalues. We claimed this to be an exception. Indeed, in this example, the eigenvectors, and therefore the adjoints and expansion coefficients c_k , depend on the eigenvalues of M . So do γ and γ_c . In fact, one can see from (51) that the old and new eigenvalues are the only quantities determining the amount of nonnormality of M and simultaneously the amount of transient growth a state that is being evolved by M can experience.

It is easy to make the point that this second example is the more generic one. In a generic extended system, the eigenfunctions are extended modes, usually characterized by a wavenumber q . This wavenumber determines at the same time the eigenfunctions e_q and their potential non-orthogonality $(e_q, e_{q'}) \neq 0$ as well as the eigenvalues λ_q , responsible for the amount of realizable transient growth. In a generic system, one therefore can not split the geometry of the underlying eigenspace from the dynamics described by the eigenvalues, instead, these are related to each other and have to be treated together.

This concludes the discussion of the examples. We hope to have illustrated and given further insight to some of the concepts introduced in prior sections. We will now use the tools and ideas outlined so far to compute nonnormality and transient growth in locally controlled systems.

CHAPTER IV

LOCALIZED CONTROL OF EXTENDED SYSTEMS

4.1 *Control at one boundary*

In this chapter, we will compute the feedback gains for several control scenarios. We will further derive expressions that show how the feedback gain scales with the size of the system. We begin by discussing the simplest case possible, the control problem with feedback applied at one of the boundaries.

To that end, consider any of the equations (2)-(4), on a finite domain $0 < x < l$. Linear feedback control will be implemented by modulating the flux of the quantity characterizing the state of the system, e.g., mass, temperature or concentration, at the right boundary, $x = l$. The feedback is given by

$$\phi'(l, t) = \int_0^l k(x)\phi(x, t)dx \quad (55)$$

where the prime denotes a spatial derivative. For instance, in the case of Rayleigh-Bénard convection, one could control the dynamics of the fluid by changing the heat flux through the bottom boundary of the convection cell [75]. The feedback gain $k(x)$ describes how different regions inside the domain affect the flux. There is a lot of flexibility in choosing the remaining boundary conditions. We pick $\phi(0, t) = 0$ as one of the boundary conditions at the other end of the domain. To provide a sufficient number of boundary conditions for the fourth order equations (3) and (4) we also choose $\phi''(0, t) = 0$ and $\phi'''(L, t) = 0$ for those equations.

Without control, that is for $k(x) \equiv 0$, there exists a uniform steady state $\phi(x, t) = 0$. While this state is stable in small systems due to strong confinement effects, it usually becomes unstable for large l . Our objective is to design a control that renders $\phi(x, t) = 0$ stable for any l .

As first step in the computation of $k(x)$, we want to convert any of the PDEs into a

system of ODEs. To find a suitable set of eigenfunctions that we can use as basis for our expansion, let us consider the eigenvalue problem

$$L\phi = \lambda\phi, \quad (56)$$

where L is the linear part of the evolution operator of the equation under study. Using the ansatz $\phi = e^{qx}$, we obtain for the three equations (2)-(4) the relations

$$q_{GL} = \pm i\sqrt{1-\lambda}, \quad \lambda < 1, \quad (57)$$

$$q_{KS} = \pm i\sqrt{1/2 \pm \sqrt{1/4 - \lambda}}, \quad \lambda < 1/4, \quad (58)$$

$$q_{SH} = \pm i\sqrt{1 \pm \sqrt{\epsilon - \lambda}}, \quad \lambda < \epsilon. \quad (59)$$

For the GL equation, one always obtains two imaginary solutions. For the KS and SH equations, one obtains either four imaginary or two real and two imaginary solutions, depending on the value of λ . For the KS equation, we have four imaginary solutions for $\lambda \in [0, 1/4]$ and two real and two imaginary ones for $\lambda < 0$, while for the SH equation we have four imaginary solutions for $\lambda \in [\epsilon - 1, \epsilon]$ and two real and two imaginary ones for $\lambda < \epsilon - 1$.

From (57-59) one finds the general solution of (56) in the case of the GL equation to be

$$\phi = c_0 \sin(qx) + c_1 \cos(qx) \quad (60)$$

while the KS and SH equations have as solutions either

$$\phi = c_2 \sin(q_1x) + c_3 \sin(q_2x) + c_4 \cos(q_1x) + c_5 \cos(q_2x) \quad (61)$$

or

$$\phi = c_6 e^{q_1x} + c_7 e^{-q_1x} + c_8 \sin(q_2x) + c_9 \cos(q_2x) \quad (62)$$

depending on λ as explained above.

Next, we need to incorporate the boundary conditions. For the GL equation, we have on the left boundary $\phi(0) = 0$. This leads to $c_1 = 0$. Without control, the right boundary condition is $\phi'(L) = 0$, which leads to $q_n = (n - 1/2)(\pi/l)$, $n = 1, 2, \dots$. Note that once control is implemented, the right boundary condition changes, therefore changing the wavenumber q . We will come back to this later in Section 4.4. Finally choosing the coefficient $c_0 = 1$,

which amounts to some arbitrary (but for our purpose convenient) normalization, we find as solution of (56) for the GL equation

$$\phi = \sin(q_n x). \quad (63)$$

For the KS and SH equations, the left BCs are $\phi(0) = \phi''(0) = 0$, leading to

$$\phi = c_2 \sin(q_1 x) + c_3 \sin(q_2 x) \quad (64)$$

or

$$\phi = c_7 \sinh(q_1 x) + c_8 \sin(q_2 x), \quad (65)$$

again depending on the value of λ . Without control, the right BCs are $\phi'(L) = \phi'''(L) = 0$, leading to the conditions $c_3 = 0$ and $c_7 = 0$. We further find the same conditions for q as in the case of the GL equation. Using again the same normalization for the remaining coefficients as above, we obtain for the KS and SH equations the same result (63) found for the GL equation.

Therefore, for the uncontrolled, linearized system the set of eigenfunctions is given by $f_n(x) = \sin(q_n x)$. The eigenvalues are $\lambda_n^{GL} = 1 - q_n^2$ for the GL equation, $\lambda_n^{KS} = q_n^2 - q_n^4$ for the KS equation and $\lambda_n^{SH} = (\epsilon - 1) + 2q_n^2 - q_n^4$ for the SH equation. One sees that for the uncontrolled system, the eigenfunctions are orthogonal, $(f_n^\dagger, f_m) = \delta_{nm}$, which means the linearized evolution operator L is normal. We use the eigenfunctions f_n as basis for the modal expansion of any of the PDEs and computation of the feedback. Projecting the linearized evolution equation onto this basis, we obtain

$$\dot{\Phi}_n = \lambda_n \Phi_n - (-1)^n \sum_{m=1}^{\infty} K_m \Phi_m \equiv (M\Phi)_n, \quad (66)$$

where $\Phi_n(t)$ and K_n are the expansion coefficients of $\phi(x, t)$ and $k(x)$, respectively:

$$\begin{aligned} \phi(x, t) &= \sum_{n=1}^{\infty} \Phi_n(t) f_n(x), & \Phi_n(t) &= \frac{2}{l} \int_0^l \phi(x, t) f_n(x) dx, \\ k(x) &= \sum_{n=1}^{\infty} K_n f_n(x), & K_n &= \frac{2}{l} \int_0^l k(x) f_n(x) dx. \end{aligned} \quad (67)$$

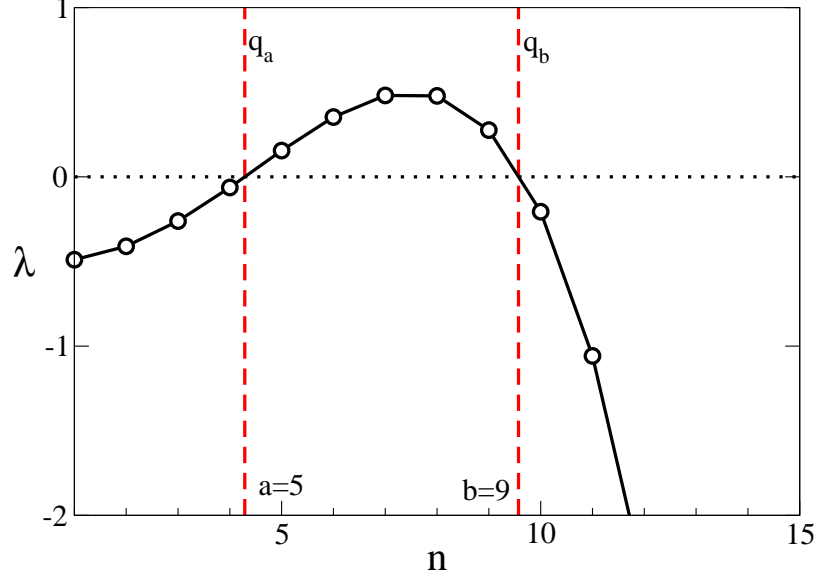


Figure 11: Eigenvalues λ_n versus wavenumber n for the SH equation ($\epsilon = 0.5$). For this system size ($l = 22$), $a = 5$ and $b = 9$. The lines marked by q_a and q_b are the limits of the continuous wavenumber band for which $\lambda(q) > 0$.

The matrix $M = A + Q$ is composed of the diagonal matrix of eigenvalues $A = \text{diag}(\lambda_1, \lambda_2, \lambda_3, \dots)$ and the matrix containing the feedback coefficients

$$Q = \begin{pmatrix} K_1 & K_2 & K_3 & \cdots \\ -K_1 & -K_2 & -K_3 & \cdots \\ K_1 & K_2 & K_3 & \cdots \\ \vdots & \vdots & \vdots & \ddots \end{pmatrix}. \quad (68)$$

Note that Q is a combination of the matrices B and K shown earlier, $Q = -BK$. The signs in (68) represent the $N \times 1$ matrix B , while the K_m constitute the $1 \times N$ matrix K . In the following we will work with the matrix Q since it allows a more concise treatment. Also note that without control, $M = A$ and $[A^\dagger, A] = 0$, therefore the uncontrolled system is normal. From the form of (68), it can also be seen that the controlled M , for which $K_m \neq 0$, will have $[M^\dagger, M] \neq 0$, which shows that the control renders M nonnormal, a point we will discuss in detail in Section 4.4.

In order to stabilize the state $\phi(x, t) = 0$, we need to find a set of coefficients K_m which will render the matrix M stable. It turns out that the special structure of Q simplifies the

problem remarkably. First we note that for an uncontrolled system of given length l , we only have a finite number of positive eigenvalues corresponding to unstable modes. We will assume that $\lambda_n \geq 0$ for $n = a, \dots, b$ and $\lambda_n < 0$ otherwise (see Fig. 11). The eigenvalues λ_n can always be re-indexed to achieve such an ordering. To render the matrix M stable, we only need to change these $s = b - a + 1$ non-negative eigenvalues. As we did earlier, we again assume the eigenvalues to be real valued. The results can easily be generalized to the case of complex eigenvalues. In that instance, the real part of the new eigenvalues needs to be negative. This can be achieved by setting all $K_m = 0$ with the exception of K_a, K_{a+1}, \dots, K_b . To see this, let us write the matrix M in block form as

$$M = \begin{pmatrix} A_1 & Q_1 & 0 \\ 0 & A_s + Q_s & 0 \\ 0 & Q_2 & A_2 \end{pmatrix}. \quad (69)$$

A_1 and A_2 denote the diagonal matrices containing the negative eigenvalues of A , A_s is the part of A containing the s positive eigenvalues. Q_1 , Q_2 and Q_s are the respective nonzero blocks of (68). The block structure of (69) shows that the change in the eigenvalues of A_s through an appropriate choice of Q_s does not affect the rest of the eigenvalues of M . We therefore need to focus on the s -dimensional block matrix $M_s = A_s + Q_s$ and choose the coefficients K_a, \dots, K_b such that M_s becomes stable. This automatically renders the infinite matrix M stable.

The coefficients K_m can be computed analytically. Consider choosing the s new negative eigenvalues of M_s as a sequence $\lambda'_a, \dots, \lambda'_b$. We then need to find K_m that satisfy the set of equations

$$\det(M_s - \lambda'_m I) = 0, \quad m = a, \dots, b. \quad (70)$$

Due to the special structure of (68), one can solve (70) for K_m and finds

$$K_m = \frac{(-1)^m \prod_{p=a}^b (\lambda_m - \lambda'_p)}{\prod_{p=a}^{m-1} (\lambda_m - \lambda_p) \prod_{p=m+1}^b (\lambda_m - \lambda_p)}, \quad m = a, \dots, b. \quad (71)$$

Using (67) then allows us to determine the feedback gain $k(x)$ in real space that achieves control via the boundary condition (55) and renders the system linearly stable with new

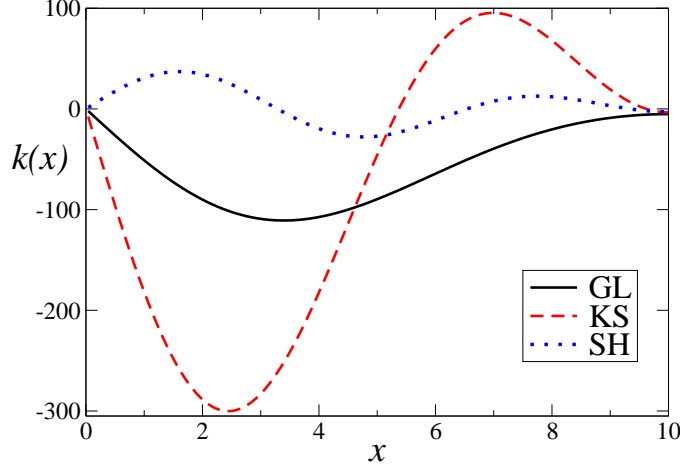


Figure 12: Gain function $k(x)$ for the three equations under study. The system size is $l = 10$, the new eigenvalues are $\lambda'_a = \dots = \lambda'_b = -1$, the parameter in the SH equation is chosen as $\epsilon = 0.5$.

eigenvalues $\lambda'_k < 0$ that we are free to choose. In Fig. 12 we show the feedback gain $k(x)$ for the three equations under study.

Since in most cases, the feedback gain can only be obtained numerically, the analytic expression (71) is an important result, it allows for further analysis of various aspects of the control problem. We can now compute a controller that stabilizes $\phi(x, t) = 0$ for *any* l . However, as we explained in Section 1.1, control fails for sufficiently large systems. To understand the origin of control failure, we need to determine the behavior of the coefficients K_m for large l . We first rewrite (71) as an exponential

$$|K_m| = \exp \left\{ \sum_{p=a}^b \ln |\lambda_m - \lambda'_p| - \sum_{p=a}^{m-1} \ln |\lambda_m - \lambda_p| - \sum_{p=m+1}^b \ln |\lambda_m - \lambda_p| \right\}. \quad (72)$$

In the large l limit, the eigenvalues are dense enough to allow approximation of the sums with integrals. It is natural to choose the wavenumber $q = q_a + (p-a)(\pi/l)$ as the integration variable, with integrals going over the unstable band $q_a < q < q_b$ of the uncontrolled system (see Fig. 11). To leading order in l we obtain

$$|K_m| \sim \exp \left\{ \frac{l}{\pi} \left(\int_{q_a}^{q_b} \ln |\lambda_m - \lambda'(q)| dq - \int_{q_a}^{q_b} \ln |\lambda_m - \lambda(q)| dq \right) \right\}. \quad (73)$$

Note that the second term includes a finite number of integrable singularities at $\lambda(q) = \lambda_m$, which are excluded in (72). Since the singularities contribute $O(\ln l)$ terms in the argument

of the exponential, which are small compared with the $O(l)$ dominant contribution, they do not alter the scaling relation.

The general result (73) applies to all systems in the class considered here and allows us to draw several important conclusions. First of all, since the terms inside the parentheses are independent of l , one immediately concludes that the Fourier coefficients K_m , and hence the gain function $k(x)$, blow up exponentially with the size l of the system. Second, since all the λ' are negative, the first term in (73), and therefore the strength of feedback, is minimized by choosing all new eigenvalues very close to zero, $\lambda'_p \lesssim 0$, $p = a, \dots, b$. Larger absolute values of the λ' requires stronger feedback, which is an intuitively sensible conclusion.

We can obtain the scaling relations in a more explicit form if we use our freedom to choose the new eigenvalues and set

$$\lambda'_a = \dots = \lambda'_b = \Lambda < 0. \quad (74)$$

For the GL equation, substituting (74) together with the dispersion relation $\lambda(q) = 1 - q^2$ into (73) yields

$$|K_m^{GL}| \sim \exp \left\{ \frac{l}{\pi} \left(2 + \ln \frac{|\lambda_m - \Lambda|}{|\lambda_m|} - 2\sqrt{\lambda_m - 1} \cot^{-1} \sqrt{\lambda_m - 1} \right) \right\}. \quad (75)$$

The scaling of $k(x)$ is determined by the largest coefficient K_m^{GL} . Since

$$\frac{dK_m}{dm} = \frac{\partial K_m}{\partial \lambda} \frac{\partial \lambda}{\partial q} \frac{dq}{dm}, \quad (76)$$

the maximum of K_m with respect to m corresponds to the maximum of λ with respect to q . For the GL equation the maximum of $\lambda(q)$ is achieved at $q = 0$, for which $\lambda_m = 1$, so for the largest K_m and therefore $k(x)$ we obtain the scaling

$$|K^{GL}| \sim \exp \left\{ \frac{l}{l_{GL}} \right\}, \quad (77)$$

with

$$l_{GL} = \pi (2 + \ln(1 + |\Lambda|))^{-1} \quad (78)$$

being a characteristic system size that can be controlled by applying feedback of moderate strength. An alternative derivation of this result can be found in Appendix A. Similar

expressions can be derived for the other model equations. For the KS equation the substitution $\lambda(q) = q^2 - q^4$ yields the exponential scaling (77) with the characteristic length l_{GL} replaced by

$$l_{KS} = \pi \left(4 - \sqrt{8} \ln(\sqrt{2} + 1) + \ln(1 + 4|\Lambda|) \right)^{-1}. \quad (79)$$

Equivalently, for the SH equation with $\lambda(q) = \epsilon - (1 - q^2)^2$, the respective characteristic length is

$$l_{SH} = \pi \left((q_b - q_a)(4 + \ln(\epsilon + |\Lambda|)) + 2 \ln \left[\frac{(1 + q_a)(1 - q_b)(q_a^2 - 1)^{q_a}}{(1 - q_a)(1 + q_b)(q_b^2 - 1)^{q_b}} \right] \right)^{-1}, \quad (80)$$

where $q_a = \sqrt{1 - \sqrt{\epsilon}}$, $q_b = \sqrt{1 + \sqrt{\epsilon}}$.

To check these analytical results, we compare them with the maximum of the feedback gain $\max_x k(x)$, numerically computed using two different control schemes. In the first method, the feedback is computed directly from (71), where all positive eigenvalues are set to $\Lambda < 0$ and the negatives ones are left unchanged. Though we have not yet specifically mentioned it, the approach presented here is of course the one introduced as “pole placement” (PP) method in Section 2.2, where one chooses the eigenvalues of the controlled system and computes K accordingly. The second method we use in our numerical schemes is the linear quadratic regulator (LQR) control that we also explained in Section 2.2. Since we did not make it explicit earlier, we want to point out that in LQR, the new eigenvalues λ'_k are not chosen a priori. Instead, K is computed according to the functional minimization explained earlier, resulting in a matrix M whose eigenvalues are negative but otherwise not specified. However, we can easily check numerically what those eigenvalues are, and we mention it where appropriate.

The results for the numerical control computations together with the analytic scaling relation are shown in Fig. 13 for the KS and SH equations. The agreement between analytical and numerical scaling is quite impressive despite the fact that the asymptotic results ($l \rightarrow \infty$) are used for a relatively small system size. One sees that the numerically calculated values in this figure (as well as several of the figures we show later) display some fluctuations around the theoretical value. This can be attributed to mostly finite size effects, that is the unstable dimension s changes at certain values of l , leading to jumps in

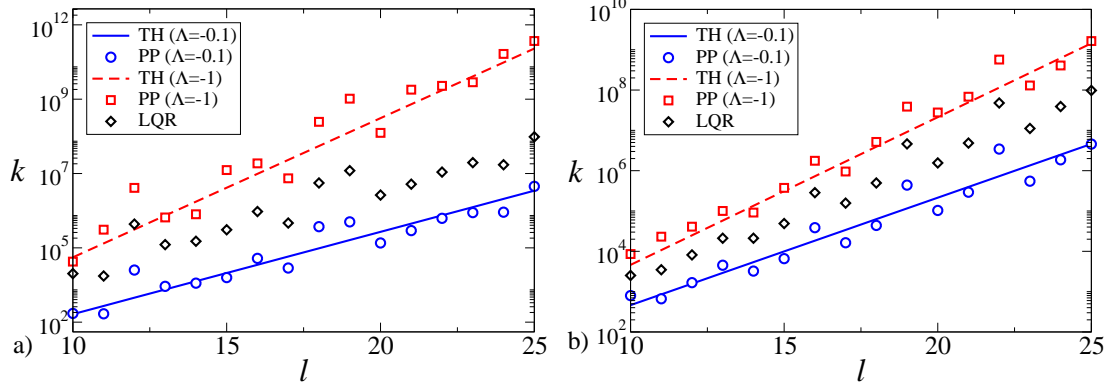


Figure 13: Maximal feedback gain $\max_x k(x)$ and analytical result (TH) as given by (77) as a function of the system size l for (a) the KS equation, (b) the SH equation ($\epsilon = 0.75$). The control schemes are PP control with $\Lambda = -0.1$ and $\Lambda = -1$ and LQR control, where the λ'_k are found to lie between -1 and -0.1 .

the feedback strength. The agreement would improve further for larger l . Unfortunately, the numerical solutions become unreliable for large l , reflecting the fact that the matrix M_s becomes increasingly nonnormal. Nevertheless, it is clear that the slope is correctly predicted by our analysis, even for system sizes that are not yet very large. These figures also show (and eqs. (78), (79) and (80) confirm) that the slope increases with $|\Lambda|$, as predicted by the general scaling expression (73).

We therefore find that the feedback gain $k(x)$ diverges exponentially with the system size, with exponents that depend on the particular equation and choice of the new eigenvalues λ'_k .

While we performed a quantitative analysis in this section, one can also make a simple physical argument that suggests that exponential scaling is expected. Since the system is locally unstable, even after control is applied, a disturbance away from a controller will grow exponentially with maximum growth rate λ_1 . It will grow for a time τ as long as it takes for the control signal to travel from the position of the controller to the location of the perturbation, where it then suppresses further growth of the perturbation. The travel time τ is roughly proportional to the size l of the system. The exponential growth of the disturbance will result in its amplification by a factor $\exp(\lambda_1 \tau) \sim \exp(\alpha l)$. To suppress the amplified disturbance, we need to apply a control perturbation at least as large as

the disturbance itself, which requires exponential growth with l in the feedback gain, in agreement with our quantitative result.

In addition, this argument also sheds light on the possibility for transient growth. The locally unstable system can have a disturbance which grows transiently until the control signal reaches it. Since the control signal (55) consists of the system state, integrated with the feedback gain, an increase in both the feedback gain and the size of the disturbance results in an increased control signal, inducing increased transient growth before the disturbance is eventually suppressed. The exponential scaling in $k(x)$ means that, for l large, the magnitude of the control signal $\phi'(l, t)$ can via (55) become many orders of magnitude larger than the magnitude of the disturbance $\phi(x, t)$, leading to transient growth.

Depending on the magnitude of the initial disturbance and the strength of the feedback gain, this transient growth might eventually die out without destabilizing the system, as Fig. 2 illustrates. Or it might be large enough to lead to breakdown of linear approximation at the location of the controller and consequent destabilization as seen in Fig. 3. We will establish a quantitative connection between the magnitude of the feedback gain and the strength of transient growth in Chapter 5.

4.2 *Control at both boundaries*

In this section, we take the next logical step and apply feedback control at both the left and the right boundary. With two controllers available, we expect the control to function more efficiently. Specifically, the control authority can be split in such a way that the left controller is primarily responsible for suppressing the disturbances in the left half of the system, while the right controller is responsible for the right half. Naively this would lead one to believe that this arrangement would be able to stabilize a system of about twice the size, all else being equal. To test this idea, let us replace the left boundary condition $\phi(0, t) = 0$ with another feedback controller of the form

$$\phi'(0, t) = \int_0^l p(x)\phi(x, t)dx. \quad (81)$$

The control at the right boundary is still chosen according to (55). For the fourth order equations we additionally require the third derivatives on the boundaries to be zero.

The eigenfunctions of the uncontrolled system can be determined as described in Section 4.1 and are found to be $f_n(x) = \cos(q_n x)$ with $q_n = (n-1)(\pi/l)$, $n = 1, 2, \dots$, while the eigenvalues are given by the same equations as before. Projecting the linear part of the evolution equation (1) onto the basis $\{f_n\}$ we obtain

$$\dot{\Phi}_n = \lambda_n \Phi_n + \sum_{m=1}^{\infty} P_m \Phi_m - (-1)^n \sum_{m=1}^{\infty} K_m \Phi_m \equiv (M\Phi)_n, \quad (82)$$

where $\Phi_n(t)$, K_n and P_n are the Fourier coefficients of $\phi(x, t)$, $k(x)$ and $p(x)$, respectively.

The matrix $M = A + Q$ is composed of $A = \text{diag}(\lambda_1, \lambda_2, \lambda_3, \dots)$ and

$$Q = \begin{pmatrix} K_1 + P_1 & K_2 + P_2 & K_3 + P_3 & \cdots \\ -K_1 + P_1 & -K_2 + P_2 & -K_3 + P_3 & \cdots \\ K_1 + P_1 & K_2 + P_2 & K_3 + P_3 & \cdots \\ \vdots & \vdots & \vdots & \ddots \end{pmatrix}. \quad (83)$$

We again need to find the coefficients K_m and P_m which will render the matrix M stable. As discussed earlier, we only need to focus on the block matrix M_s that contains the unstable eigenvalues. The s non-negative eigenvalues $\lambda_a, \dots, \lambda_b$ can be made negative by an appropriate choice of K_a, \dots, K_b and P_a, \dots, P_b . However, the procedure described in the previous section only yields s equations for the $2s$ unknowns. Therefore we have the freedom to impose another s equations on the unknown coefficients. We choose

$$P_m = (-1)^{m-1} K_m, \quad (84)$$

which corresponds to taking the feedback gains $p(x) = -k(l-x)$, preserving the reflection symmetry of the uncontrolled system. One could, of course, choose the gains differently by ignoring the symmetry. This would however lead to sub-optimal control [11]. The choice (84) leads to

$$Q = \begin{pmatrix} 2K_1 & 0 & 2K_3 & \cdots \\ 0 & -2K_2 & 0 & \cdots \\ 2K_1 & 0 & 2K_3 & \cdots \\ \vdots & \vdots & \vdots & \ddots \end{pmatrix}. \quad (85)$$

To find the remaining coefficients K_m , we again set the new eigenvalues to $\lambda'_a, \dots, \lambda'_b$, to obtain the set of s equations $\det(M_s - \lambda'_m I) = 0$. We can again solve these equations and

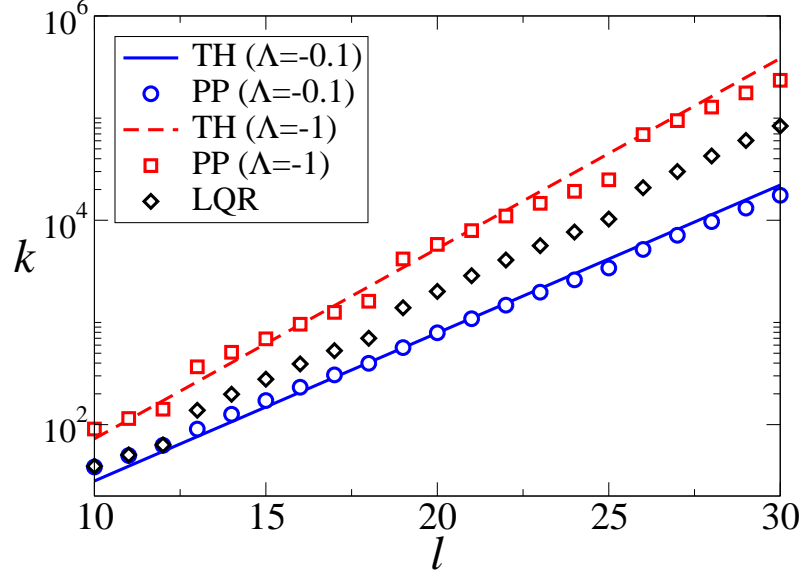


Figure 14: Maximal feedback gain $\max_x k(x)$ and analytical result (TH) as given by (89) as a function of the system size l for the GL equation with control at both boundaries. The control schemes are PP control with $\Lambda = -0.1$ and $\Lambda = -1$ and LQR control, where the λ'_k are found to lie between -1 and -0.1 .

find the coefficients K_m to be

$$K_m = \frac{(-1)^m (\lambda_m - \lambda'_m) \prod'_p (\lambda_m - \lambda'_p)}{2 \prod'_p (\lambda_m - \lambda_p)}, \quad m = a, \dots, b. \quad (86)$$

The prime on the products denotes that the index goes over integers $p = \dots, (m-4), (m-2), (m+2), (m+4), \dots$ in steps of two, with an additional restriction $a \leq p \leq b$. To obtain the scaling with l , we again rewrite (86) in exponential form

$$|K_m| = \exp \left\{ \ln |\lambda_m - \lambda'_m| - \ln(2) + \sum'_p \ln \frac{|\lambda_m - \lambda'_p|}{|\lambda_m - \lambda_p|} \right\} \quad (87)$$

and approximate the sums with integrals in the large l limit. Changing as before the integration variable to q , we obtain to leading order in l

$$|K_m| \sim \exp \left\{ \frac{l}{2\pi} \left(\int_{q_a}^{q_b} \ln |\lambda_m - \lambda'(q)| dq - \int_{q_a}^{q_b} \ln |\lambda_m - \lambda(q)| dq \right) \right\}. \quad (88)$$

This is the same equation as (73) apart from an additional prefactor of $1/2$. This prefactor arises due to the fact that the sum over p in (87) goes in steps of two. Therefore, all conclusions obtained for the case of control on one boundary naturally carry over to the

case of control on both boundaries. In particular, the large l scaling of the feedback gain is again exponential and given by

$$|K^{EQ}| \sim \exp \left\{ \frac{l}{2l_{EQ}} \right\}. \quad (89)$$

EQ is a placeholder for a specific evolution equation and l_{EQ} is determined by (78)-(80) for the three examples considered here, provided we choose the new eigenvalues according to (74). Since there is an additional factor of $1/2$ in the exponent, we conclude that doubling the number of controllers doubles the characteristic system size, as the naive argument made earlier suggested. Fig. 14 shows for the GL equation that (89) again agrees well with the numerics. One sees that the scaling exponent is indeed reduced by a half, in agreement with (77) and (89). The data for the KS and SH equations are similar and therefore not shown.

4.3 *Control at multiple locations*

Finally, we consider the general case of a system with r localized controllers. This is a natural generalization of the two cases considered previously. As the system size grows, first the one-controller and then the two-controller arrangement will fail. In order to control a system of arbitrary size l , we expect to need a number of controllers on the order of l/l_{EQ} since the maximum distance between controllers is restricted by the characteristic length l_{EQ} (provided we want to use a feedback gain $k(x)$ of reasonable magnitude). In other words, control authority is now split in such a way that each controller is responsible for a segment of the system of size roughly equal to l_{EQ} . With this more general arrangement the system is described by

$$\partial_t \phi(x, t) = N [\phi(x, t)] + \sum_{p=1}^r d_p(x) u_p(t) \quad (90)$$

where the $d_p(x)$ are functions describing the location and extent of the controllers. In the limit of spatially localized control, the $d_p(x)$ are δ -functions. Again, to preserve the symmetry of the system, we will assume periodic boundary conditions and place the controllers in a regular array. However, we cannot arrange them periodically, as that would make the

system uncontrollable [59]. We can achieve controllability (or more precisely, stabilizability) using a periodic array of *pairs* of controllers, which corresponds to

$$d_p(x) = \begin{cases} \delta(x - \frac{l}{r}(p - \Delta)), & p \text{ odd} \\ \delta(x - \frac{l}{r}((p - 1) + \Delta)), & p \text{ even} \end{cases} \quad (91)$$

For instance, four controllers would be placed as two pairs, one pair at $x = (1 \pm \Delta)l/4$ and the other at $x = (3 \pm \Delta)l/4$. The spacing $2l\Delta/r$ between the two controllers in each pair has to be chosen to satisfy the controllability constraints [59], but is otherwise arbitrary. As a rule of thumb, in order to achieve stabilizability the spacing should be smaller than the wavelength of the shortest unstable mode of the uncontrolled system. The functions $u_p(t)$ describe the strength of feedback and are chosen as

$$u_p(t) = \int_0^l k_p(x) \phi(x, t) dx. \quad (92)$$

With the periodic boundary conditions, the eigenfunctions of the system without control are Fourier modes $f_n(x) = \exp(iq_n x)$ with wavenumbers $q_n = 2\pi n/l$ and $n = -\infty, \dots, \infty$. Projecting the linearized version of (90) onto the set of Fourier modes $\{f_n\}$, we obtain

$$\dot{\Phi}_n = \lambda_n \Phi_n + \sum_{p=1}^r D_n^p \sum_{m=-\infty}^{\infty} K_{-m}^p \Phi_m, \quad (93)$$

with the definitions

$$\begin{aligned} \phi(x, t) &= \sum_{n=-\infty}^{\infty} \Phi_n(t) f_n(x), & \Phi_n(t) &= \frac{1}{l} \int_0^l \phi(x, t) f_n^*(x) dx, \\ k_p(x) &= \sum_{n=-\infty}^{\infty} K_n^p f_n(x), & K_n^p &= \frac{1}{l} \int_0^l k_p(x) f_n^*(x) dx, \\ d_p(x) &= \frac{1}{l} \sum_n B_n^p f_n(x), & B_n^p &= \int_0^l d_p(x) f_n^*(x) dx. \end{aligned} \quad (94)$$

We can simplify (93) by exploiting the remaining symmetry. The system with the chosen arrangement of controllers remains invariant under translations $x \rightarrow x + nl/r$, $n = 2, 4, \dots$ by a multiple of the distance between pairs of controllers. The feedback control preserving this symmetry requires gain functions $k_{p+2}(x)$ to have the same shape as $k_p(x)$, only shifted by $2l/r$. Further, the reflection symmetry implies that for each controller pair the gain function for $k_{p+1}(x)$ should have the same shape as $k_p(x)$, reflected at the midpoint between

the controllers. Combining these two results, every gain function $k_p(x)$ can be expressed via $k_1(x)$:

$$k_p(x) = k_1 \left((-1)^p \left\{ \frac{pl}{r} - \frac{l}{2r} - x \right\} + \frac{l}{2r} \right), \quad p = 2, \dots, r. \quad (95)$$

This also means that the respective Fourier coefficients K_m^p can be expressed in terms of the Fourier coefficients K_m^1

$$K_m^p = K_{-(-1)^p m}^1 \exp \left\{ -i \frac{\pi m}{r} (2p - 1 + (-1)^p) \right\}. \quad (96)$$

The resulting control has translational and reflectional symmetry. As shown in [11], such control is optimal with respect to general measures that respect the symmetry of the system.

With the result (96) and the Fourier coefficients B_n^p of (91), which are given by

$$B_n^p = \exp \left\{ -i \frac{\pi n}{r} (2p - 1 + (-1)^p (2\Delta - 1)) \right\}, \quad (97)$$

the evolution equation (93) can be written in the form

$$\dot{\Phi}_n = \lambda_n \Phi_n + \sum_{p=1}^r \sum_{m=-\infty}^{\infty} F_{nm}^p K_{(-1)^p m} \Phi_m, \quad (98)$$

where we defined

$$F_{nm}^p = \exp \left\{ i \frac{\pi}{r} [(2p - 1)(m - n) + (-1)^p (m - 2n\Delta + n)] \right\} \quad (99)$$

and dropped the superscript on K_m^1 for notational convenience. We can again write (98) in matrix notation

$$\dot{\Phi} = M\Phi = (A + Q)\Phi, \quad (100)$$

where $A = \text{diag}(\dots, \lambda_2, \lambda_1, \lambda_0, \lambda_1, \lambda_2, \dots)$ and Q is a matrix with elements

$$Q_{nm} = \sum_{p=1}^r F_{nm}^p K_{(-1)^p m}. \quad (101)$$

Note that the matrix B from standard control theoretical notation as introduced in Section 2.2 is represented by D_n^p , the feedback gain matrix K by K_m^p . Expression (101), is $Q = -BK$, though written in a nonstandard form. We can further manipulate (101) and obtain

$$\begin{aligned} Q_{nm} &= e^{\frac{2\pi i}{r}(n-n\Delta)} K_m \sum_p^{\text{even}} e^{\frac{2\pi i}{r}p(m-n)} + e^{\frac{2\pi i}{r}(-m+n\Delta)} K_{-m} \sum_p^{\text{odd}} e^{\frac{2\pi i}{r}p(m-n)} \\ &= \left[e^{\frac{2\pi i n}{r}(1-\Delta)} K_m + e^{-\frac{2\pi i n}{r}(1-\Delta)} K_{-m} \right] \sum_p^{\text{even}} e^{\frac{2\pi i}{r}p(m-n)} \\ &= \left[e^{\frac{2\pi i n}{r}(1-\Delta)} K_m + e^{-\frac{2\pi i n}{r}(1-\Delta)} K_{-m} \right] R(m, n, r) \end{aligned} \quad (102)$$

where

$$R(m, n, r) = \begin{cases} r, & 2(m - n)/r \in \mathbb{N} \\ 0, & \text{otherwise} \end{cases} \quad (103)$$

From (102) and (103), one can see that for a given number $r/2$ of controller pairs, Q consists of $\frac{r}{2} \times \frac{r}{2}$ blocks of diagonal matrices. This is a generalization of the case with two controllers where we had 2×2 blocks of diagonal matrices, as (85) shows.

To find the gain coefficients K_m , we can again split the matrix M into blocks containing positive and negative eigenvalues of the diagonal matrix A . Note that for the SH equation, A has positive eigenvalues in the columns $[-b, -a] \cup [a, b]$ and negative eigenvalues in columns $(-\infty, -b) \cup (-a, a) \cup (b, \infty)$. We could reorder the Fourier coefficients Φ_n in (98) to obtain a matrix with the same structure as (69). A more convenient way is to define the matrix M_s such that it not only contains the positive eigenvalues but also the negative eigenvalues in the columns $(-a, a)$. We then have $2b + 1$ eigenvalues λ_m in $[-b, b]$ which can be modified with an appropriate choice of K_{-b}, \dots, K_b . Replacing the eigenvalues λ_m with new eigenvalues λ'_m for $m = -b, \dots, b$ we obtain a set of $2b + 1$ equations $\det(M_s - \lambda'_m I) = 0$. All systems used as examples are real and therefore $\lambda_m = \lambda_{-m}$. To ensure that the state of the system remains real in the presence of feedback, we choose $\lambda'_m = \lambda'_{-m}$. Solving for K_m one finds that, if we do not change the stable eigenvalues in $(-a, a)$ and choose $\lambda'_m = \lambda_m$ for $|m| < a$, the only nonzero coefficients are given by

$$K_m = K_{-m}^* = C_m \frac{2(\lambda_m - \lambda'_m) \prod_p' (\lambda_m - \lambda'_p)}{r \prod_p' (\lambda_m - \lambda_p)}, \quad m = a, \dots, b, \quad (104)$$

which corresponds to a set of real gain functions $k_p(x)$, $p = 1, \dots, r$. The primes on the products indicate that the index $p = \dots, (m - r), (m - r/2), (m + r/2), (m + r), \dots$ goes in steps of $r/2$ subject to an additional restriction $a \leq p \leq b$. The prefactor is given by

$$C_m = \frac{\exp \left[\frac{2\pi i m (\Delta - 1)}{r} \right]}{\exp [2\pi i g_m \Delta] - 1}, \quad (105)$$

where g_m is a positive integer, which depends on both m and r . In the scaling analysis this prefactor is of no importance, since it is independent of both the system size l and the

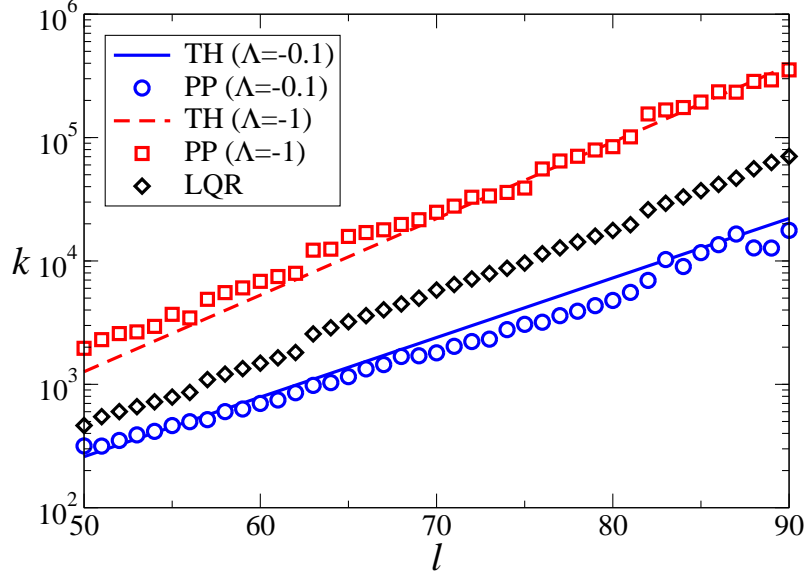


Figure 15: Maximal feedback gain $\max_x k_1(x)$ and analytical result (TH) as given by (108) as a function of the system size l for the GL equation with six controllers placed according to (91). The control schemes are PP control with $\Lambda = -0.1$ and $\Lambda = -1$ and LQR control, where the λ'_k are found to lie between -1 and -0.1 .

choice of new eigenvalues. We again rewrite (104) as an exponential and obtain

$$|K_m| = \exp \left\{ \ln \left| \frac{2C_m}{r} (\lambda_m - \lambda'_m) \right| + \sum_p' \ln \frac{|\lambda_m - \lambda'_p|}{|\lambda_m - \lambda_p|} \right\}. \quad (106)$$

As previously we approximate the sums by integrals and change the integration variable to q . Ignoring the sub-leading $O(\ln l)$ terms we obtain

$$|K_m| \sim \exp \left\{ \frac{l}{\pi r} \left(\int_{q_a}^{q_b} \ln |\lambda_m - \lambda'(q)| dq - \int_{q_a}^{q_b} \ln |\lambda_m - \lambda(q)| dq \right) \right\}. \quad (107)$$

Equation (107) is identical to (73), apart from the prefactor $1/r$. We therefore find the scaling in the general case to be

$$|K^{EQ}| \sim \exp \left\{ \frac{l}{r l_{EQ}} \right\}, \quad (108)$$

with the characteristic lengths l_{EQ} found in Section 4.1 (for new eigenvalues chosen according to (74)) increasing by a factor of r . This result again supports our naive expectations: by employing r controllers, the system size can be increased by a factor of r without either losing control or increasing the magnitude of feedback applied by each controller. The scaling determined by (108) together with the numerical results for $\max_x k_1(x)$ are illustrated

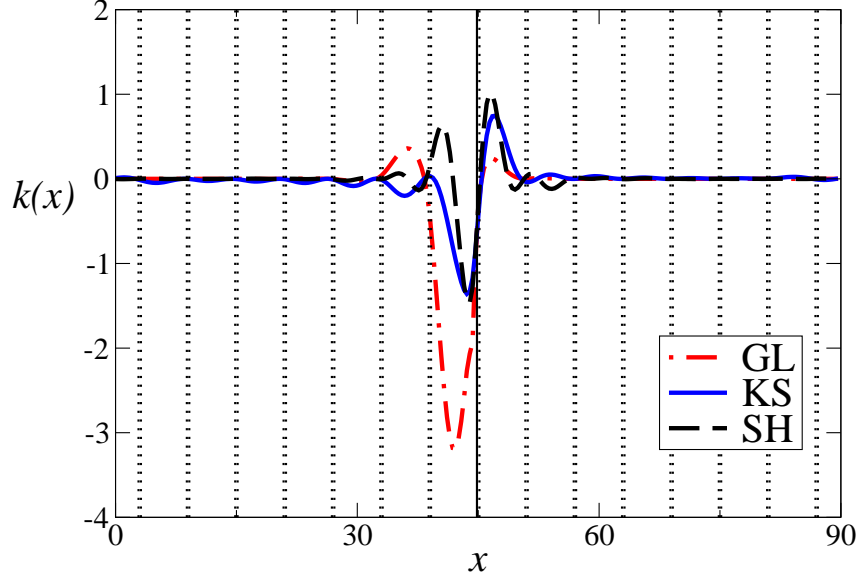


Figure 16: Gain function $k_{15}(x)$ for the three equations under study with LQR control and 30 controllers, $l = 90$. The dotted straight lines indicate positions of the controllers, the solid straight line the location of controller 15.

in Fig. 15 for the case of the GL equation with six controllers. Similarly good agreement is found for different numbers of controllers and different choices of the evolution equation.

It is interesting to note that a particular arrangement of controllers in the array (i.e., the distance between controllers in each pair) has a very small effect on the magnitude of the feedback signal. This result follows directly from (104) and (105). Indeed, the magnitude of feedback depends on Δ only through C_m , which diverges for $\Delta = n/g_m$ with any integer n , which correspond to the loss of stabilizability. For instance, when $4m$ is a multiple of r , $g_m = 4m/r$ and C_m diverges when the location of all controllers coincides with the nodes of a Fourier mode with wave number $q = \pm 2\pi m/l$. Choosing Δ outside of small neighborhoods of such values yields $C_m = O(1)$, making the coefficients K_m very weakly dependent on the spacing between controllers in each pair.

It is also worthwhile to point out that localized feedback control is spatially localized in another sense as well: not only is the action of feedback local, but the information about the state of the system that is needed to compute the control signal applied by a particular controller is also local – the feedback gain function decays with the distance from

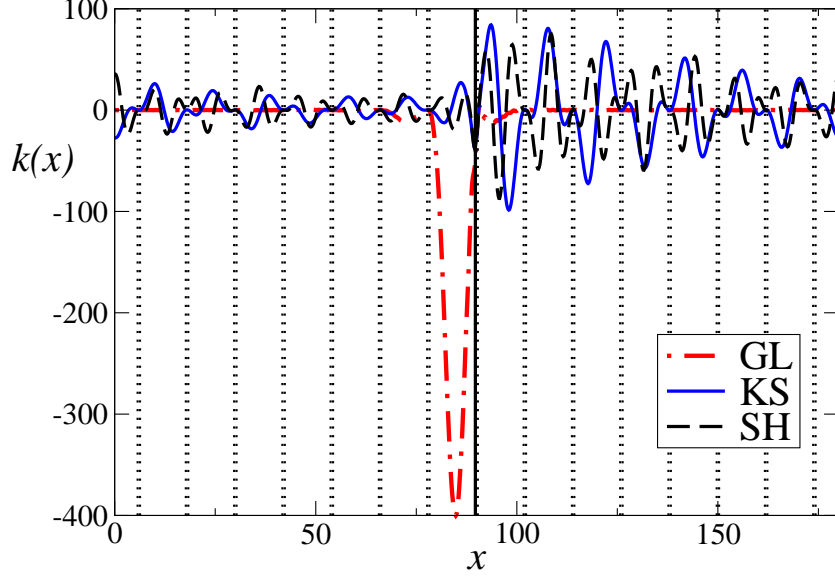


Figure 17: Gain function $k_{15}(x)$ for the three equations under study with LQR control and 30 controllers, $l = 180$. The dotted straight lines indicate positions of the controllers, the solid straight line the location of controller 15.

the controller. As Fig. 16 illustrates, for systems with the separation between controllers small compared with l_{EQ} , the decay is very fast (exponential, to be exact). Such a result was proved in [11] for control in the limit $r \rightarrow \infty$ where feedback is applied at every point $x \in (0, l)$. This result provides additional support for the idea that control authority is effectively split between regions immediately adjacent to the controllers.

On the other hand, when the separation between controllers is large compared with l_{EQ} , the decay is much slower (perhaps algebraic) for the fourth order evolution equations, as Fig. 17 shows. Although conventionally the notions of cheap and expensive control are associated with the magnitude of the feedback gain, for spatially localized feedback it is more natural to identify cheap control with a dense array of controllers and expensive control with a sparse array. Then our results are also consistent with the result obtained in [60] for a specific extended system in the limit of expensive control, where the feedback gain was also found to decay algebraically with the distance.

Summarizing the main results obtained so far, we found that the strength of the feedback gain scales exponentially with the size of the system. This exponential scaling holds for

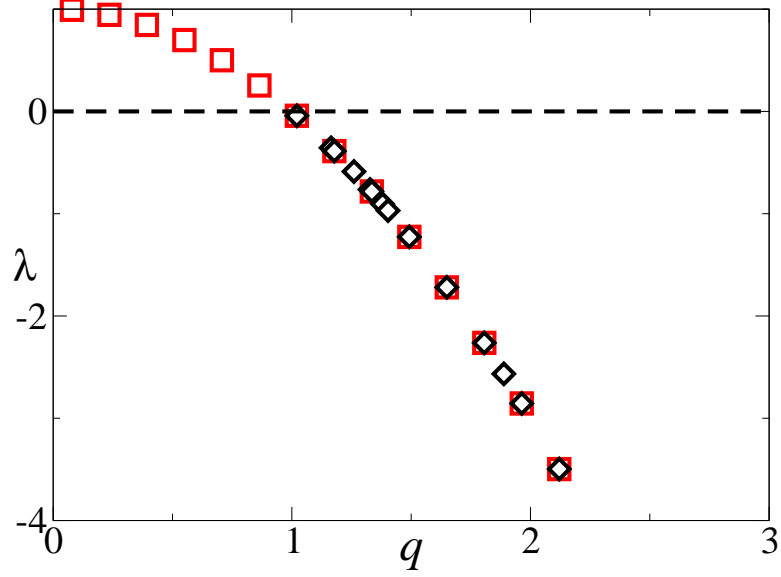


Figure 18: The wave number and corresponding eigenvalues for the linearized GL equation with one controller located at the right boundary and LQR control, $l = 20$. Shown are the eigenvalues for the uncontrolled (square) and controlled (diamond) system.

any choice of the evolution equation and for any number of controllers. The choice of the evolution equation mainly affects the characteristic length l_{EQ} , which determines the distance between controllers placed in a regular array. Furthermore, we expect our main results to hold also for irregular arrays, with l_{EQ} determining the maximal distance between controllers.

4.4 Control and nonnormality

After establishing the exponential scaling of the feedback gain, we end this chapter with a detailed explanation on how the strong growth in feedback gain with system size leads to strong nonnormality.

For all our equations under study, the evolution matrix A for the uncontrolled system is diagonal and therefore normal. To this matrix we add the matrix Q describing position of the controllers and choice of feedback gains. This matrix is not normal. In fact one can see from (68), (83) and (102) that Q is highly nonnormal. We just showed that some of the entries K_m in Q scale exponentially with increasing system size. Therefore, for large l , the matrix Q dominates M and that leads to $\|[M, M^\dagger]\| \sim \|QQ^\dagger - Q^\dagger Q\|$ which is expected to

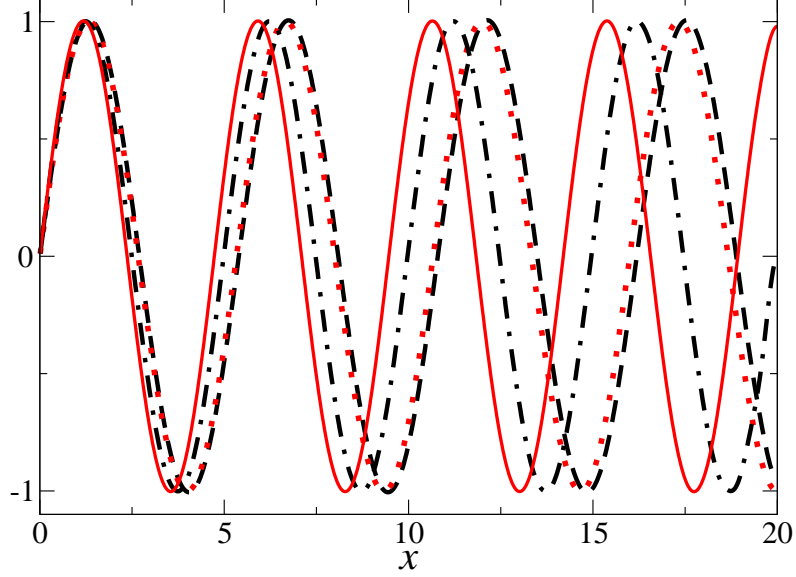


Figure 19: First four eigenfunctions of the GL equation with one controller at the right boundary for $l = 20$. Further closely aligned eigenfunctions exist for this value of l but are not shown. The control is computed using LQR.

grow with increasing l , providing a first indication of an increase in nonnormality.

Physically, this corresponds to an increasing alignment of the eigenfunctions of M . As explained in the previous sections, all the uncontrolled systems have eigenfunctions $f_k(x)$ that are given by orthogonal Fourier modes, $(f_k^\dagger, f_n) = \delta_{kn}$, with eigenvalues λ_k and wavenumbers q_k . The effect of the control is to change the unstable eigenvalues $\lambda_k > 0$ to stable eigenvalues $\lambda'_k < 0$. In the simplest case – the GL equation with control at one boundary – the feedback acts such that the eigenfunctions $f'_k(x)$ of the controlled system are still given by sine modes with new wavenumbers q'_k . We briefly mentioned this in Section 4.1. Fig. 18 shows the spectrum of the uncontrolled and controlled GL equation, Fig. 19 shows a few of the corresponding eigenfunctions. One sees from the figures that for this type of control choice, the LQR control, the new wavenumbers q'_k are tightly clustered just below the threshold wavenumber q^* for which $\lambda = 0$, and the corresponding eigenfunctions $f_{q'_k}(x) = \sin(q'_k x)$ become closely aligned. In this scenario, nonnormality arises due to the fact that the space of formerly orthogonal eigenfunctions is in effect divided into two subspaces. One subspace, with dimension approximately equal to the number of

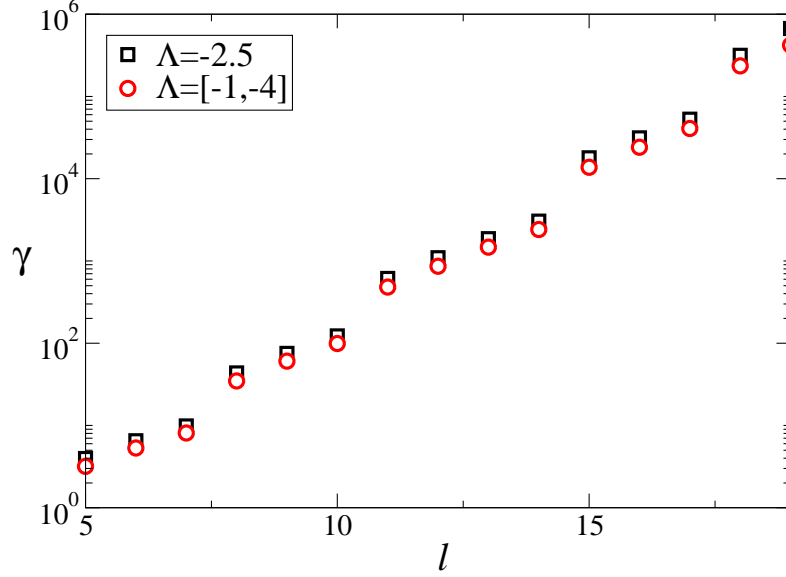


Figure 20: Nonnormality as defined by γ for PP control at the right boundary of the GL equation with all eigenvalues equal to -2.5 and with eigenvalues linearly spaced in the interval $[-1, -4]$.

previously unstable modes, consists of strongly aligned eigenfunctions. The second subspace consists of the eigenfunctions corresponding to the formerly stable eigenvalues. The latter eigenfunctions are not changed by the control, they remain orthogonal among each other and are mostly orthogonal to the nonnormal subspace. As the system size l and with it the dimension of the unstable subspace increases, control will produce more aligned eigenfunctions, increasing the nonnormality.

If instead of choosing LQR control, we use the PP method, we have the freedom to specify the λ'_k and therefore the wavenumbers q'_k . This allows us to remove the tight clustering of the q'_k and the resulting close alignment of the corresponding eigenfunctions. One might hope that this can reduce the nonnormality. However this is not the case. While one can indeed design control such that the new eigenvalues and wavenumbers are not as clustered as the ones shown in Fig. 18, it does not lead to reduced nonnormality. LQR control created two subspaces that are almost orthogonal to each other, one strongly nonnormal and one orthogonal subspace. The PP feedback, with a choice of λ'_k that avoids clustering, produces eigenfunctions with wavenumbers q'_k located between the original q_k .

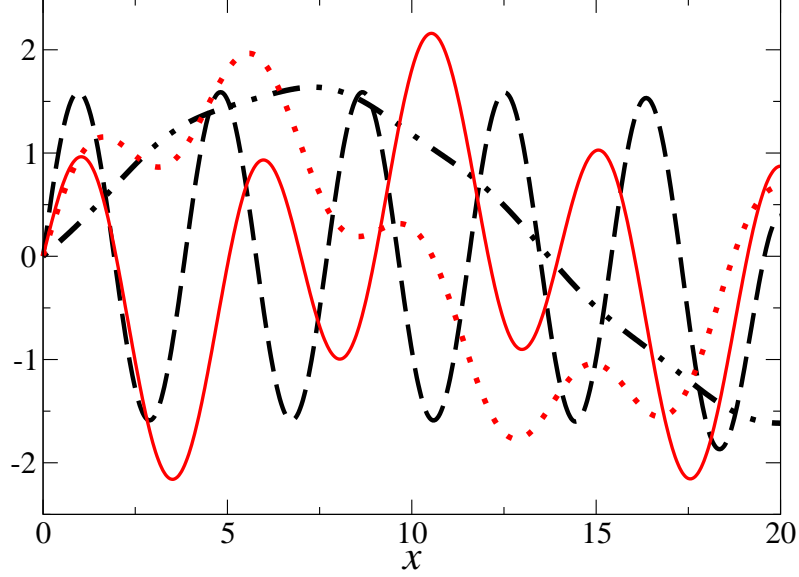


Figure 21: First four eigenfunctions of the SH equation with one controller at the right boundary for $l = 20$. The control is computed using LQR.

The result is that instead of having the two distinct subspaces as described above, we now have a set of eigenfunctions f'_k with less alignment between any two eigenfunctions but a significant overlap $(f'_k, f_n) \neq \delta_{kn}$ between more individual eigenfunctions. The overall effect on nonnormality does not change significantly, one still finds the same increase as the system size increases. Comparing the two different setups in Fig. 20 shows that indeed the nonnormality does not change.

For the case of the KS and SH equation, the control affects more than just the wavenumber. Consider the case with one controller on the right boundary. We found in Section 4.1 that the boundary conditions $\phi'(L) = \phi'''(L) = 0$ lead to eigenfunctions given by sine modes. With control implemented, we have $\phi(L)' \neq 0$, therefore the coefficients c_3 and c_7 can be nonzero, allowing for eigenfunctions that are given by the more general expressions (61) and (62).

Since for the controlled case, we have $\lambda < 0$, one obtains from the relation (58) for the KS equation two real and two imaginary solutions for q , which means the solution for the KS equation can only be given by

$$\phi = c_7 \sinh(q_1 x) + c_8 \sin(q_2 x). \quad (109)$$

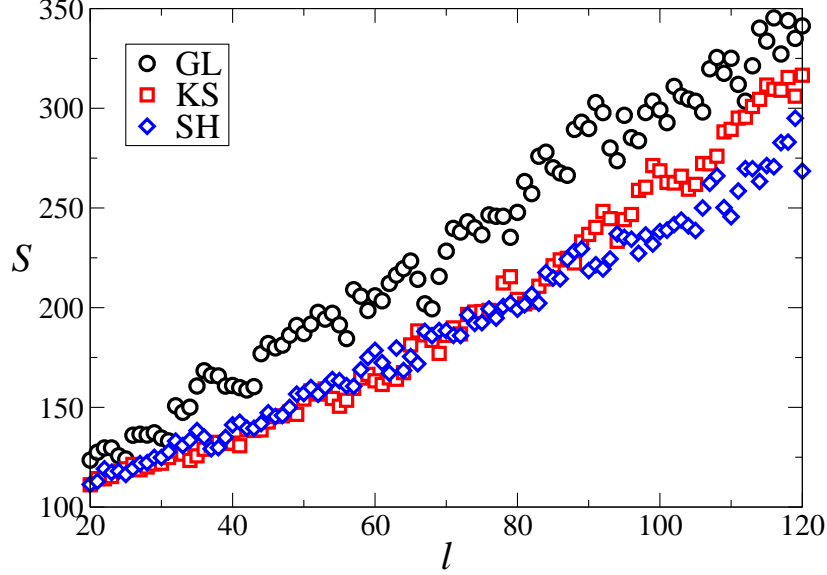


Figure 22: The sums of the inner products as defined by (110) as a function of l for the three different equations and eight controllers. The feedback gain is computed using LQR.

And indeed, one finds that for the controlled system, the eigenfunctions of the KS equation are of this form. For the SH equation the eigenfunctions of the controlled system can be either (61) or (62), again depending on λ .¹

We show in Fig. 21 as example the eigenfunctions of the SH equation with control located at the right boundary. The control happens to result in $\lambda'_k \in [\epsilon - 1, \epsilon]$ in a way that only leads to solutions of the form (61). Different choices of control can lead to both (61) or (62). One sees that for eigenfunctions of that form, the alignment is not as readily visible as before. Nevertheless, we can check that the nonnormality increases. We show in Fig. 22 the sum of all the inner products of the eigenfunctions

$$S = \sum_{k,n} |(f_k^\dagger, f_n)|. \quad (110)$$

The figure should only be understood in a qualitative fashion. Since S depends for instance on the number of modes kept in the numerical approximation of the matrix M ,

¹For control at both boundaries, one finds that for the GL equation, the feedback produces a change in wavenumber and a phase shift, but the eigenfunctions are still given by pure sine or cosine modes. For the KS and the SH one again finds eigenfunctions given by combinations of different cosine and sine terms. For control inside the domain, one encounters discontinuities at the location of the controllers and therefore above considerations are not readily applicable.

one should not attribute any importance to the numerical value of S . Still, on a qualitative level, the figure demonstrates that the overlap of the eigenfunctions does indeed increase with increasing system size. Similar figures can be found for all the equations and different control setups considered here. We therefore expect that for any of the systems studied, with any arrangement of the controllers, an increase in system size l and feedback gain K_m will lead to an increase in nonnormality. Further, from what we explained in Chapter 3, we know that increased nonnormality leads to increased transient growth. What is not clear so far is how exactly transient growth depends on l or K_m . In the next chapter, we will make this relation more quantitative, deriving an explicit expression for the transient growth (25) for the controlled systems.

CHAPTER V

TRANSIENT GROWTH IN THE CONTROLLED SYSTEM

5.1 *Scaling of the transient growth - method I*

We discussed qualitatively in the last section how increasing system size and therefore increasing feedback gain leads to strong nonnormality. Figs. 2 and 3 illustrate, and we also explained in Section 3.3, how this nonnormality can lead to strong transient growth in the magnitude of initial disturbances or continuous noise. In this section we describe more explicitly the connection between the magnitude of feedback gain and the strength of transient growth, the latter being described quantitatively via the transient amplification factor (25) and (29).

Since both matrix exponentials and matrix norms are difficult to compute analytically, γ or γ_c are usually computed numerically. Nevertheless, sometimes one can construct reasonably tight bounds without resorting to numerics, as has for instance been done in the analysis of continuous noise [10] for certain fluid systems. In the following we try to obtain an analytical expression for the transient amplification for the case of the controlled systems discussed in the last chapter. We will restrict ourselves to the analysis of γ , and mention what one should expect for γ_c .

We begin by noting that the instantaneous growth of the matrix exponential for $t \rightarrow 0$ is given by

$$\frac{d}{dt} \|e^{Mt}\|_{t=0} = \Gamma(M) \quad (111)$$

where

$$\Gamma(M) = \sup_{\|u\|=1} \Re(u^\dagger, Mu) \quad (112)$$

is the numerical abscissa [116]. In the large l limit, the elements of M vary by many orders of magnitude, so a tight lower bound is obtained by choosing a unit vector u which picks out the largest element of M . This largest element is $M_{nn} = \lambda_n + Q_{nn}$, where Q_{nn} is defined

by (102) with $K_n = K^{EQ}$. Choosing $u_k = \delta_{kn}$ we obtain $\Gamma(M) \gtrsim r|K^{EQ}|$. Therefore, for $t \ll 1$, we can approximate the norm of the matrix exponential by

$$\|e^{Mt}\|_2 = 1 + \Gamma(M)t + O(t^2) \approx 1 + r|K^{EQ}|t. \quad (113)$$

Taking $t = t_m$ we obtain the following estimate for the maximal transient amplification:

$$\gamma \sim |K^{EQ}|t_m. \quad (114)$$

Since (113) is only accurate for small times, (114) should provide an accurate estimate for γ as long as t_m is reasonably small, i.e., when transient amplification is a fast process.

In order to make further analytical progress let us again assume that the controlled system (100) has s identical eigenvalues $\lambda'_k = \Lambda$, $k = a, \dots, b$. The corresponding eigenvectors are identical and therefore do not form a complete basis. Hence the Jacobian matrix M is non-diagonalizable. In this case, M can be converted into the Jordan normal form

$$J = S^{-1}MS = \begin{pmatrix} J_1 & 0 & 0 \\ 0 & J_s & 0 \\ 0 & 0 & J_2 \end{pmatrix}, \quad (115)$$

where $J_1 = \text{diag}(\dots, \lambda_{a-2}, \lambda_{a-1})$, J_s is an $s \times s$ Jordan block with eigenvalues $\lambda_k = \Lambda$, $J_2 = \text{diag}(\lambda_{b+1}, \lambda_{b+2}, \dots)$, and S is the respective transformation matrix. The solution for the state $\Phi(t)$ is found to be

$$\Phi(t) = \sum_{p < a} c_p e^{\lambda_p t} e_p + \sum_{p=a}^b \left[\sum_{m=0}^{b-p} c_{p+m} \frac{t^m}{m!} \right] e^{\Lambda t} \hat{e}_p + \sum_{p > b} c_p e^{\lambda_p t} e_p, \quad (116)$$

where e_p are eigenvectors corresponding to blocks J_1 and J_2 and \hat{e}_p are the generalized eigenvectors such that $M\hat{e}_p = \Lambda\hat{e}_p + \hat{e}_{p-1}$ for $p = a+1, \dots, b$ and $\hat{e}_a = e_a$. The c_p are integration constants that depend on the choice of the initial condition. The first and the last sum in (116) monotonically decay to zero, since the corresponding eigenvectors are normal, and we can therefore neglect them. The second sum exhibits both algebraic growth and exponential decay, allowing for transient growth of $\Phi(t)$. Each term in the second sum describes a mode of the controlled system with amplitude

$$\hat{\Phi}_m(t) \sim \frac{t^m}{m!} e^{\Lambda t}, \quad m = 1, \dots, s-1. \quad (117)$$

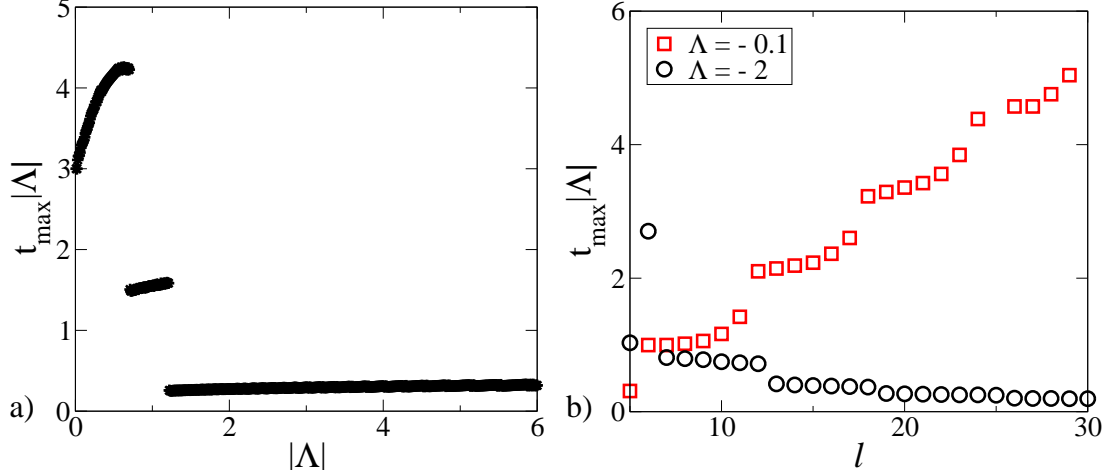


Figure 23: The time at which the maximum in transient amplification is achieved (a) as a function of $|\Lambda|$ for $l = 20$ ($s = 7$) and (b) as a function of the system size l . The numerical results shown are for the GL equation with control applied at the two boundaries.

The maximum of $\hat{\Phi}_m$ is achieved at

$$\hat{t} = \frac{m}{|\Lambda|}. \quad (118)$$

Substituting (118) back into (117) we obtain

$$\hat{\Phi}_m(\hat{t}) \sim \frac{m^m e^{-m}}{m! |\Lambda|^m}. \quad (119)$$

This expression as a function of m has a single extremum inside the domain, which is a minimum. The maximum occurs either on the left or on the right boundary, that is for $m = 1$ or $m = s - 1$, depending on the value of $|\Lambda|$. Using the Stirling formula

$$m! \approx m^m e^{-m} \sqrt{2\pi m} \quad (120)$$

we can write (119) as

$$\hat{\Phi}_m(\hat{t}) \sim \frac{1}{\sqrt{2\pi m} |\Lambda|^m}. \quad (121)$$

From this expression one sees that for $|\Lambda| > 1$, the maximum is achieved for $m = 1$, while for $|\Lambda| < 1$, and sufficiently large l , the maximum occurs for $m = s - 1$. For values $|\Lambda| \approx 1$, neither maximum is very dominant. These conclusions are supported by numerical computations of the time t_m at which the maximal transient amplification (25) occurs. Figs. 23a and 23b show the value of the product $t_m |\Lambda|$ as a function of $|\Lambda|$ and l , respectively. If

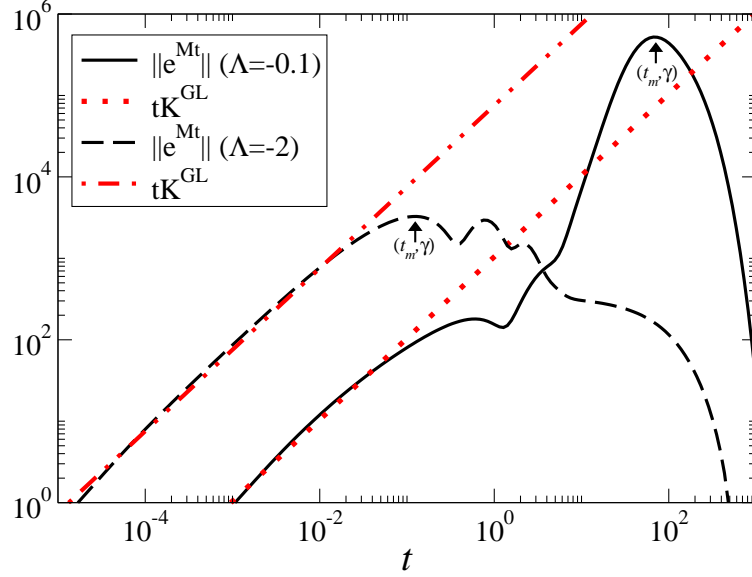


Figure 24: Matrix exponential $\|e^{Mt}\|$ and $K^{GL}t$ for the GL equation with control at the two boundaries, $l = 25$ ($s = 8$). Shown are plots for eigenvalues $\Lambda = -0.1$ and $\Lambda = -2$.

our ideas are correct, we expect \hat{t} to be a good approximation of t_m . This should result in $t_m|\Lambda| = s - 1 \sim l$ for small $|\Lambda|$ and $t_m|\Lambda| = 1$ for large $|\Lambda|$ and some undetermined value for $|\Lambda| \approx 1$. While no complete quantitative agreement is found – which is to be expected since the estimate (117) is rather crude – one finds good qualitative agreement with our expectations. We can therefore conclude that in the limiting cases when $|\Lambda|$ is either small or large, one of the two maxima is dominant.

Since for small $|\Lambda|$ the term with $m = s - 1$ dominates, the magnitude of transiently amplified disturbances close to t_m should be described by

$$\hat{\Phi}_{s-1}(t) = \frac{t^{s-1}}{(s-1)!} e^{\Lambda t}. \quad (122)$$

In this regime, t_m is large and therefore (114) is expected to produce a poor estimate of the maximum transient amplification. Fig. 24 shows that this is indeed the case. The growth in $\|e^{Mt}\|_2$ is linear only for small times and high order polynomial terms dominate near $t = t_m$. Therefore $K^{EQ}t$ at $t = t_m$ does not provide a good estimate of γ .

On the other hand, since for large $|\Lambda|$ the linear term with $m = 1$ dominates, the

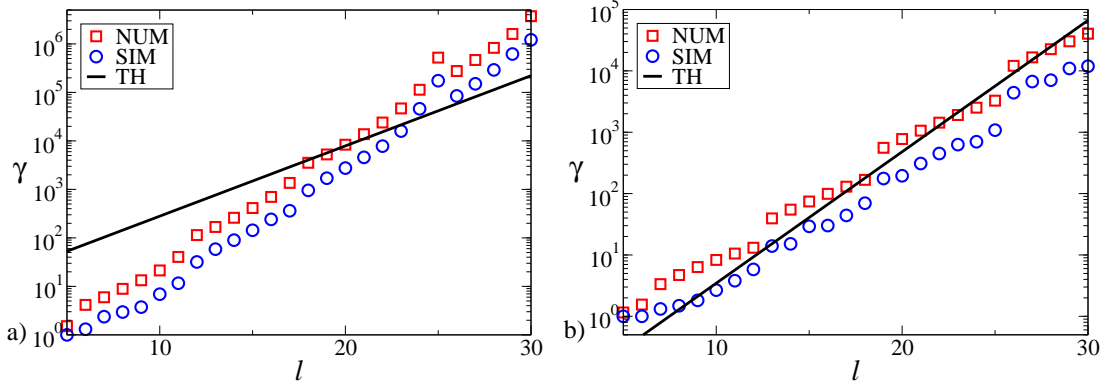


Figure 25: Transient amplification γ as a function of system size l for the GL equation with control at the two boundaries with (a) $\Lambda = -0.1$ and (b) $\Lambda = -2$. Squares show the numerical results (NUM) obtained using (25), circles are the numerical results obtained through simulation (SIM) of 100 initial conditions as explained in the text, the line is the theoretical estimate (TH) as given by (124).

magnitude of transiently amplified disturbances is well approximated by

$$\hat{\Phi}_1(t) = te^{\Lambda t}. \quad (123)$$

In this regime, t_m approximated by $\hat{t} = 1/|\Lambda|$ is small and we expect (114) to produce an accurate estimate for γ . As Fig. 24 shows, one does indeed find good agreement. The time t_m is small and $K^{EQ}t$ at t_m can well approximate γ . Further, since the transient growth in this case is a fast process, we expect only a small difference between γ and the time-integrated version γ_c , which means the obtained approximation should be valid for both initial disturbances and continuous noise.

In this regime for large $|\Lambda|$, we can therefore combine (114) with (118) to obtain to leading order in l

$$\gamma \sim K^{EQ}t_m \sim \frac{1}{|\Lambda|}K^{EQ} \sim \frac{1}{|\Lambda|} \exp\left\{\frac{l}{rl_{EQ}}\right\}, \quad (124)$$

where K_{EQ} and l_{EQ} depend on Λ . Just like the feedback gain, the transient amplification increases exponentially fast with the length of the system and decreases with the number of controllers.

The result (124) can also be understood through a simple qualitative argument we mentioned earlier: An initial disturbance of magnitude σ will get integrated with the gain

function $k(x)$ to generate a new ‘disturbance’ of $O(K^{EQ}\sigma)$, the control signal injected into the system. The ratio of the two norms is therefore K^{EQ} , in agreement with (124).

The scaling of (124) with l is compared with numerical results in Fig. 25. As expected, the agreement is quite good for $\Lambda = -2$ and relatively poor for $\Lambda = -0.1$. However, even though our estimate produces an incorrect exponent for small $|\Lambda|$, we see that γ still increases exponentially fast with l .

Since the optimal disturbances, which produce the largest transient amplification, might not be representative of typical random noise in the system, we additionally compute the amount of transient amplification $\max_t \|\Phi(t)\|_2 / \|\Phi(0)\|_2$ achieved for random initial conditions as done earlier. Fig. 25 shows the maximum over hundred initial conditions. Not surprisingly, since none of the random initial conditions are optimal, they are amplified less than the optimal ones. Nevertheless, the random initial conditions produce transient amplification which is rather close to γ and the scaling agrees with that of both (25) and (124). This shows that (124) provides a good estimate for the transient growth of both optimal and generic random initial conditions. The results for the KS and SH equations are similar to those for the GL equation and therefore not shown.

The estimate (124) also contains the dependence of transient amplification on the choice of the new eigenvalues (that is on Λ). Since l_{EQ} approaches a constant for $|\Lambda| \rightarrow 0$ and scales as $1/\ln|\Lambda|$ for $|\Lambda| \rightarrow \infty$ (at least for the examples we consider here), we should expect γ to diverge as a power law for both small and large values of $|\Lambda|$. For instance in the case of the GL equation, we have

$$\gamma \sim \frac{1}{|\Lambda|} \exp \left\{ \frac{l}{\pi} (2 + \ln(1 + |\Lambda|)) \right\}, \quad (125)$$

so that $\gamma \sim |\Lambda|^{-1}$ for $|\Lambda| \rightarrow 0$ and $\gamma \sim |\Lambda|^{l/\pi}$ for $|\Lambda| \rightarrow \infty$. Fig. 26 compares this estimate with γ computed numerically from (25).

The estimate (124) and hence (125) breaks down for small $|\Lambda|$, as expected. Yet the numerical results show that the transient amplification still diverges for small $|\Lambda|$ as a power law, $\gamma \sim |\Lambda|^{-2}$, albeit with a different exponent. From (114) we see that transient amplification can be reduced by minimizing either the feedback gain or the time it takes

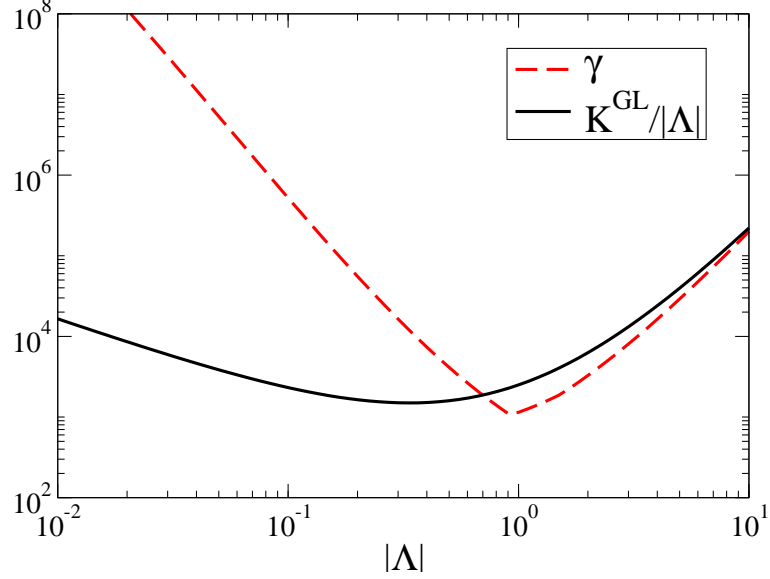


Figure 26: Transient amplification γ and estimate $K^{EQ}/|\Lambda|$ as a function of $|\Lambda|$, shown for the GL equation, $l = 25$, with control located at the boundaries. (The somewhat sharp kink in the γ -curve is due to switching between two different numerical routines at that point and of no significance.)

for control to suppress transient growth. The former is minimized by decreasing $|\Lambda|$, while the latter is minimized by increasing $|\Lambda|$. The minimum in $\gamma(\Lambda)$ is thus achieved for an intermediate value $|\Lambda| = O(1)$. This value is optimal with respect to the robustness toward “worst-case” disturbances. While we do not try to make a formal connection, this result might merit closer comparison with modern robust control methods, such as the H_∞ control mentioned in Sec. 2.2, which aim for a similar minimization toward worst-case disturbances.

The results obtained in this section still apply if we relax some of the assumptions. In the analysis presented above, we assumed that all new eigenvalues of the controlled system are identical. This allowed us to isolate the terms in the formal solution (116) responsible for transient amplification. For the case when the new eigenvalues are different, the matrix M is diagonalizable and all eigenvectors of M are distinct. Therefore the solution (116) is not valid anymore. If however M is strongly nonnormal with closely aligned eigenvectors, the evolution will still be characterized by strong transient amplification of disturbances. In this case (113) will still hold, provided the transient growth happens on a fast enough time scale. Since t_m is primarily determined by the spectrum of the eigenvalues $\{\lambda_k\}$, but is

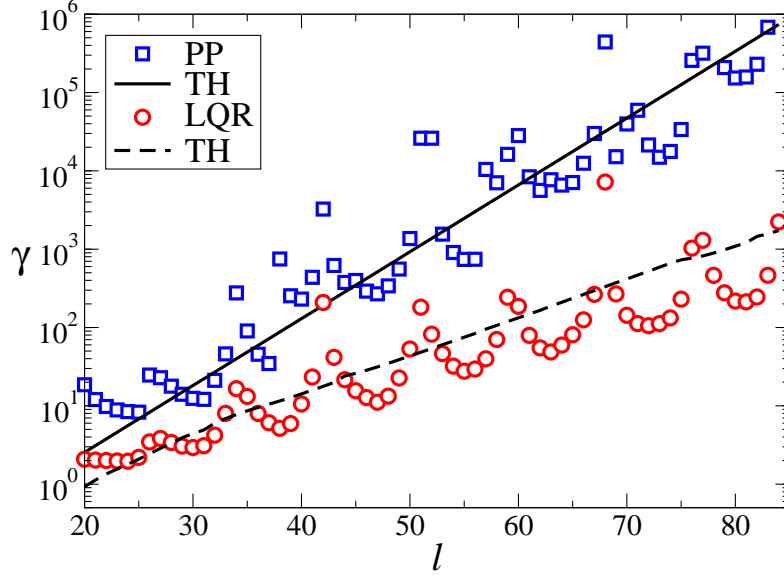


Figure 27: Transient amplification γ as a function of l for the case of the KS equation with 6 controllers located inside the domain. For PP control, the eigenvalues λ'_k are distributed evenly between $[-1, -3]$, the LQR control produces eigenvalues λ'_k mostly clustered around one. For the estimate (TH) as given by (124), we choose Λ as the median of the λ'_k .

weakly dependent on the system size l , we can expect (124) to hold as well. The numerical and analytical results presented in Fig. 27 support this conclusion. We find similarly good agreement for other choices of the equations, number of controllers r and new eigenvalues λ'_k .

5.2 Scaling of the transient growth - method II

In this section, we present an alternative way to derive the scaling of γ under certain circumstances. To that end, we again start with the matrix exponential e^{Mt} . We have obtained a convenient representation of the evolution operator $M = A + Q$ for our system (1) in the Fourier space. However, the full matrix M is infinite-dimensional and thus rather inconvenient for computational purposes. A good estimate of transient amplification can be obtained by considering only the matrix M_s instead of the full matrix M . To see this, consider the partition of the full state into the ‘normal’ and ‘nonnormal’ subspaces, $\Phi = (\Phi_1, \Phi_s, \Phi_2)$, according to the block structure (69) of M . The maximum transient amplification in the ‘nonnormal’ subspace, which corresponds to the component Φ_s , clearly

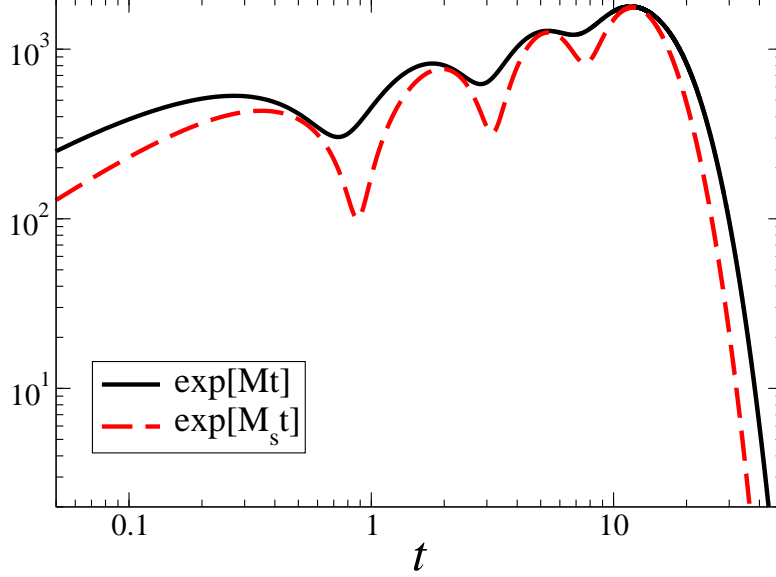


Figure 28: Transient amplification of $\|e^{Mt}\|_2$ and $\|e^{M_s t}\|_2$ as a function of time for the GL equation with control at the right boundary, $l = 15$ and $\Lambda = -0.5$. The double logarithmic scale is used to resolve the quick transient amplification and the slow exponential decay.

gives a lower bound for the maximum transient amplification in the full space. Furthermore, the equation for Φ_s decouples and one finds $\Phi_s(t) = \exp(M_s t)\Phi_s(0)$. Substituting this into the equation for Φ_1 yields

$$\Phi_1(t) = e^{A_1 t}\Phi_1(0) + \int_0^t e^{A_1(t-\tau)}Q_1\Phi_s(\tau)d\tau. \quad (126)$$

Since A_1 is stable and normal, any initial perturbation $\Phi_1(0)$ decays monotonically. On the other hand, the integral term in (126) scales with $\Phi_s(t)$. Similar arguments show that $\|\Phi(t)\|_2$ scales with $\|\Phi_s(t)\|_2$ and hence the lower bound produced by considering the ‘nonnormal’ space produces the correct scaling for the full space. The example presented in Fig. 28 shows that the typical difference between the norm of M and that of M_s is indeed very small. We will therefore restrict ourselves to the ‘nonnormal’ subspace for the analytical calculation of γ .

We further note that the only nonzero elements of the diagonal matrix A_s are the positive eigenvalues of the uncontrolled system which are $O(1)$. On the contrary, the entries in Q_s are exponentially large (in terms of the system size l). One can therefore consider A_s as an exponentially small perturbation of Q_s . It is well known that the eigenvalues of strongly

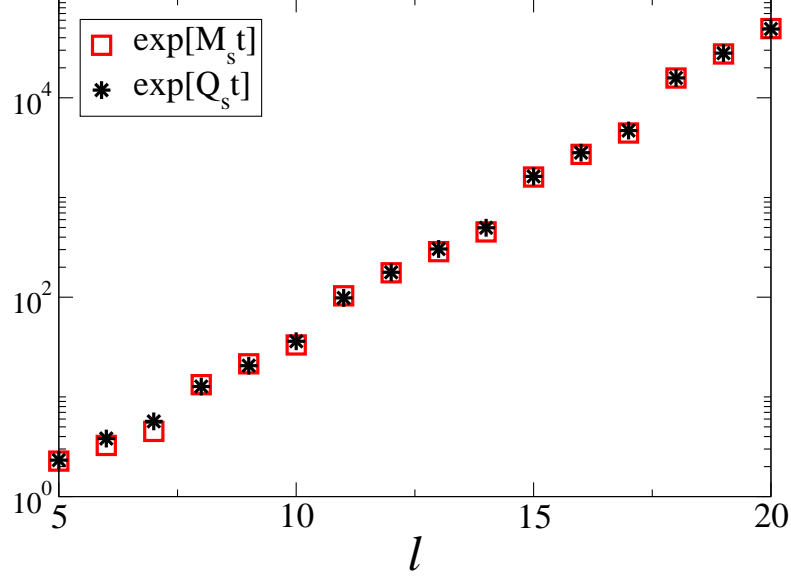


Figure 29: Maximum transient amplification γ for $\|e^{M_s t}\|_2$ and $\|e^{Q_s t}\|_2$ as a function of l for the GL equation with control at the right boundary, $\Lambda = -1$.

non-normal matrices such as Q_s are generally very sensitive to small perturbations. In fact, this is the case here. However, the norm is less sensitive toward small perturbations [108] and therefore one can approximate M_s by Q_s when computing the norm of the matrix exponential in (25). Fig. 29 indicates that this is indeed a valid approximation. We can therefore obtain as approximation for the transient amplification

$$\gamma = \|e^{M t_m}\|_2 \sim \|e^{M_s t_m}\|_2 \sim \|e^{Q_s t_m}\|_2 = \left\| \sum_{n=0}^{\infty} \frac{t_m^n}{n!} Q_s^n \right\|_2. \quad (127)$$

Next, let us write $Q_s^n = D^{n-1} Q_s$, $n > 0$, which leads to

$$\gamma \sim \|e^{Q_s t_m}\|_2 = \left\| I + \sum_{n=1}^{\infty} \frac{t_m^n D^{n-1}}{n!} Q_s \right\|_2 = \|I + (e^{t_m D} - I) D^{-1} Q_s\|_2. \quad (128)$$

We introduced the matrix D without further specification. Of course $D = Q_s$ is always possible, though of no further use. However if there exists a matrix D which is *normal* and furthermore has negative eigenvalues whose magnitudes grow with l , the matrix exponential in (128) is a monotonously decaying function of l and for large l becomes negligible. Note that for this to be a valid approximation, it is additionally necessary that t_m does not decay with l faster than D grows. We showed in Section 5.1 that t_m is indeed either growing with l or approaches a constant value, therefore neglecting the matrix exponential is possible. In

this case, the expression for γ can be further simplified to

$$\gamma \sim \|I - D^{-1}Q_s\|_2 \sim \|D^{-1}Q_s\|_2. \quad (129)$$

For the one-controller case, where Q_s is defined by (68), D is found to exist and given by $D = \text{tr}(Q_s)I$. This matrix is clearly normal. Substituting (71) and $\lambda'_m = \Lambda$ into (68), one finds

$$\text{tr} Q_s = s\Lambda - \sum_{m=a}^b \lambda_m = -s(|\Lambda| + \tilde{\lambda}), \quad (130)$$

where $\tilde{\lambda} > 0$ is the mean of the positive eigenvalues λ_m , $m = a, \dots, b$. Equation (130) shows that $\text{tr} Q_s < 0$ and that it scales linearly with l (recall that $s \sim l(q_b - q_a)/\pi$). Therefore D satisfies the requirements that allow us to use (129). Furthermore, noting that in the large l limit, $D^{-1} \sim \frac{1}{s(|\Lambda| + \tilde{\lambda})}I$, we arrive at

$$\gamma \sim \frac{1}{s(|\Lambda| + \tilde{\lambda})} \|Q_s\|_2. \quad (131)$$

Using the definition of the 2-norm and the scaling of K_m we obtain

$$\|Q_s\|_2 = \sqrt{\lambda_{\max}(Q_s^\dagger Q_s)} = \sqrt{s \sum_{m=a}^b K_m^2} \sim s^{1/2} K^{EQ} \quad (132)$$

with K^{EQ} computed for a particular evolution equation as described in Section 4.1. Next we substitute (132) into (131) and also discard the remaining prefactor $s^{-1/2}$ which is of the same order as the sub-dominant terms we neglected in computing the scaling for K^{EQ} . This leads to the final result for the large l scaling of the amplification factor

$$\gamma \sim \frac{K^{EQ}}{(|\Lambda| + \tilde{\lambda})} \sim \frac{1}{(|\Lambda| + \tilde{\lambda})} \exp\left(\frac{l}{l_{EQ}}\right), \quad (133)$$

which to leading order in l agrees with (124) obtained earlier. It is interesting to note that in the derivation above, we did not make any assumptions regarding the magnitude of Λ . Indeed, Fig. 30 shows a scenario for which we obtain good agreement between numerics and the estimate (133) for small $|\Lambda|$. However, as shown earlier in Fig. 25, there are other situations when the agreement for small $|\Lambda|$ is not good. One can attribute it to the fact that the magnitude of Λ does not completely determine the timescale of transient growth, instead, it also depends on the equation under study. If the timescale of transient growth

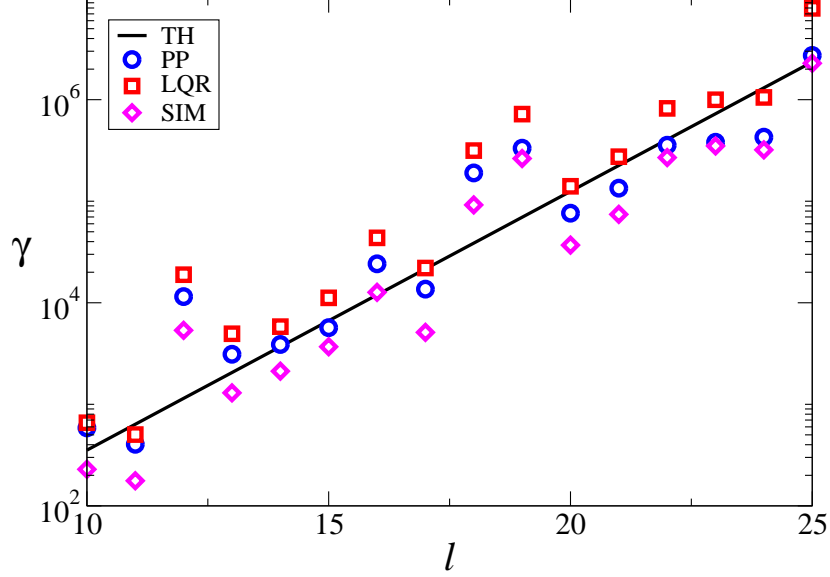


Figure 30: Transient amplification γ as a function of l for the case of the KS equation with control applied at the right boundary. For PP control, the eigenvalues are $\lambda'_k = \Lambda = -0.1$, the LQR control produces eigenvalues λ'_k mostly clustered around one. The symbols denoted (SIM) are obtained by numerical integration of 100 random initial conditions as explained earlier. The line denotes the estimate (TH) as given by (133).

is small enough, the estimates (124) and (133) give a reasonably good result even for small $|\Lambda|$.

Turning to the two-controller case, Q_s is now defined by (85). We can again obtain a normal matrix D , now given by $D = \text{diag}(d_1, d_2, d_1, d_2, \dots)$. The diagonal elements are

$$d_1 = -(\lceil s/2 \rceil |\Lambda| + \sum_{i=1}^{\lceil s/2 \rceil} \lambda_{a+2(i-1)}), \quad d_2 = -(\lfloor s/2 \rfloor |\Lambda| + \sum_{i=1}^{\lfloor s/2 \rfloor} \lambda_{a+2i-1}), \quad (134)$$

where $\lceil \cdot \rceil$ and $\lfloor \cdot \rfloor$ stand for the ceiling and floor functions respectively. One sees that again every diagonal element $d_i < 0$ scales linearly with l and can be approximated by $d_i \sim -s(|\Lambda| + \tilde{\lambda})/2$ in the large l limit. Thus D is again normal and has negative eigenvalues that grow with l , which allows us to again neglect the matrix exponential in (128) and use (129). Further noting that in the large l limit we can approximate $D^{-1} \sim -2/(s(|\Lambda| + \tilde{\lambda}))I$ leads to

$$\gamma \sim \frac{1}{s(|\Lambda| + \tilde{\lambda})} \|Q_s\|_2. \quad (135)$$

Finally, using (85) we find the 2-norm to be in the large l limit $\|Q_s\|_2 \sim (2s)^{1/2} K^{EQ}$, so

that to leading order in l

$$\gamma \sim \frac{1}{(|\Lambda| + \tilde{\lambda})} K^{EQ} \sim \frac{1}{(|\Lambda| + \tilde{\lambda})} \exp\left(\frac{l}{2l_{EQ}}\right), \quad (136)$$

again in agreement with the results obtained earlier.

For the general case of multiple controller pairs, where Q is given by (102), we were able to find normal matrices D with the required properties as described above for the case of $r = 2, 4$. Due to the complexity of the equations involved, we were not able to find a general expression for D , valid for arbitrary r .

Nevertheless, the results presented in this section confirm what we obtained in Section 5.1 using a different way of reasoning and approximation. This strengthens our earlier conclusion that the transient amplification factor γ scales linearly with the maximal feedback gain K^{EQ} and exponentially with the system length l . At some point the transient growth becomes so large that it leads to breakdown of linear control. Our analysis done so far provides part of the information necessary to determine under what circumstances control can be successful and when it will fail. In Chapter 6, we will complete the picture by looking at the relation between the transient amplification γ and the threshold amount of noise for a given system that still leads to control success. Before that, we want to briefly discuss in the next section the case of transient growth for a system with localized sensors in addition to localized controllers.

5.3 *Scaling of the transient growth - the sensing case*

So far, we assumed that the state of the system at every spatial location can be directly measured in order to compute the feedback. This is often not the case in practice. In this section we briefly discuss the extension of our approach to the more realistic situation in which the state of the system can only be measured at certain spatial locations x_i , $i = 1, \dots, w$. In this scenario, the full state of the system has to be reconstructed from these localized measurements, the well-known problem of state estimation in control theory. Since this is a standard problem, we only give a brief explanation. For additional details, we refer to any of the control theory textbooks mentioned in Section 2.2.

The sensor measurements $\xi_i(t)$ at locations x_i can be related to the Fourier space representation of the system state via

$$\xi_i(t) = \phi(x_i, t) = \sum_n f_n(x_i) \Phi_n(t) \equiv (C\Phi)_i, \quad (137)$$

where the matrix C is the Fourier space description of the the sensor locations. The estimate Ψ of the true state Φ can be constructed by taking an arbitrary initial condition, say, $\Psi(0) = 0$ and evolving it subject to the linear equation

$$\dot{\Psi} = A\Psi + Q\Psi + PC(\Phi - \Psi) \quad (138)$$

similar to (100), with matrix P chosen in such a way that the estimation error $\Xi = \Phi - \Psi$ converges to zero as time goes on. The evolution equation for Ξ is obtained by subtracting (138) from (100):

$$\dot{\Xi} = \dot{\Phi} - \dot{\Psi} = (A - PC)\Xi. \quad (139)$$

Therefore, in order to achieve a vanishing estimation error, P has to be chosen such that the matrix $A - PC$ is stable. One can notice that C^\dagger is the direct analog of the matrix B describing the location of controllers, while P^\dagger is analogous to the matrix K . As a result, if we assume for simplicity that the sensors are positioned at the same locations as the controllers, $C^\dagger = B$, the elements of P^\dagger can be chosen to be the same (up to the sign) as the controller gains, such that $-PC = Q^\dagger$. Finally, replacing the state $\phi(x, t)$ with its estimate

$$\psi(x, t) = \sum_n \Psi_n(t) f_n(x) \quad (140)$$

in (92) we obtain the following linear system describing the deviation Φ from the target state and the state estimation error Ξ :

$$\begin{pmatrix} \dot{\Phi} \\ \dot{\Xi} \end{pmatrix} = \begin{pmatrix} A + Q & -Q \\ 0 & A + Q^\dagger \end{pmatrix} \begin{pmatrix} \Phi \\ \Xi \end{pmatrix} \equiv S \begin{pmatrix} \Phi \\ \Xi \end{pmatrix}. \quad (141)$$

It is important to note that (138)-(141) can be truncated to the stable subspace, replacing $A \rightarrow A_s$, $Q \rightarrow Q_s$, etc., since the convergence of the estimate to the state in the stable subspace is assured. As a result, the controller will only need to compute the evolution of

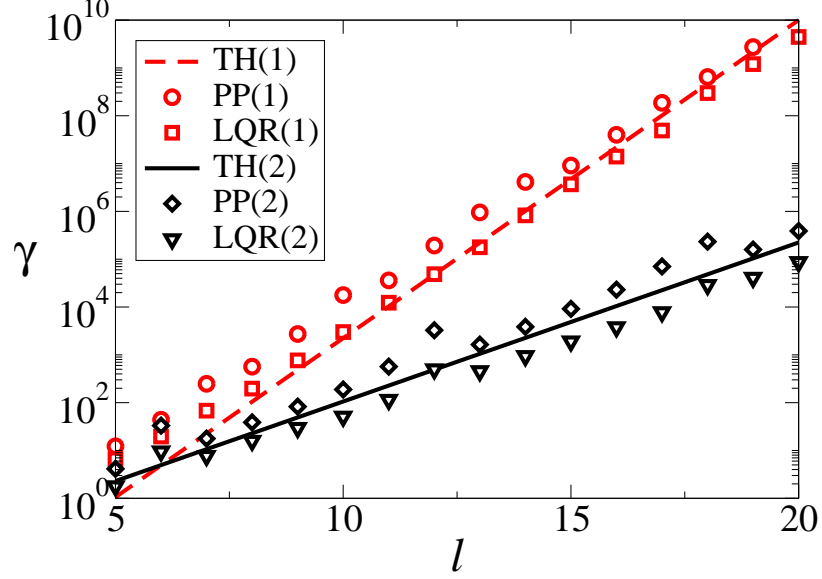


Figure 31: Transient amplification in the GL equation as a function of the system size l for the case of one and two controllers and sensors. For the one-controller case, both sensor and controller are located at the right boundary, for the two-controller case, the locations are both boundaries. The respective case is indicated by the numbers in parentheses. For the pole placement (PP) calculations we took $\Lambda = -0.5$, for LQR control, the λ'_k are in $[-1, -0.1]$. The theoretical value (TH) is given by (147).

the state estimate according to (138) in a $2(b-a+1)$ -dimensional space, which can be done very quickly and efficiently, as opposed to the numerical integration of the corresponding partial differential equation. In the following we will imply such truncation and drop the index s for brevity.

The transient amplification in the system with state estimation can be computed by replacing the norms of Φ in (25) with the norms of the extended state vector (Φ, Ξ) . We then obtain for the transient amplification factor $\gamma \approx \|e^{St_m}\|_2$. As before, we can neglect A compared with Q in the matrix exponential, which yields

$$\gamma \sim \left\| \exp \left[\begin{pmatrix} Q & -Q \\ 0 & Q^\dagger \end{pmatrix} t_m \right] \right\|_2 = \left\| \sum_{n=0}^{\infty} \frac{t_m^n}{n!} \begin{pmatrix} Q & -Q \\ 0 & Q^\dagger \end{pmatrix}^n \right\|_2. \quad (142)$$

Assuming a matrix D with the properties mentioned earlier exists, we can use the relation

$Q^n = D^{n-1}Q$ derived in the previous section and obtain

$$\gamma \sim \left\| I + \sum_{n=1}^{\infty} \frac{t_m^n}{n!} \begin{pmatrix} D^{n-1}Q & -D^{n-1}Q(I + (n-1)D^{-1}Q^\dagger) \\ 0 & D^{n-1}Q^\dagger \end{pmatrix} \right\|_2. \quad (143)$$

After some algebra (see Appendix B for the details) this can again be written via matrix exponentials

$$\gamma \sim \left\| I + (e^{\hat{D}t_m} - I)\hat{D}^{-1}\hat{A} + ([I - \hat{D}t_m]e^{\hat{D}t_m} - I)\hat{D}^{-1}\hat{B} \right\|_2, \quad (144)$$

where we have defined

$$\hat{D} = \begin{pmatrix} D & 0 \\ 0 & D \end{pmatrix}, \quad \hat{A} = \begin{pmatrix} Q & -Q \\ 0 & Q^\dagger \end{pmatrix}, \quad \hat{B} = \begin{pmatrix} 0 & D^{-1}QQ^\dagger \\ 0 & 0 \end{pmatrix}. \quad (145)$$

Since D satisfies the properties specified in Section 5.2, the matrix exponentials in (144) become negligible for large l and we can further simplify to obtain

$$\gamma \sim \frac{1}{s} \left\| \begin{pmatrix} Q & -Q + D^{-1}QQ^\dagger \\ 0 & Q^\dagger \end{pmatrix} \right\|_2. \quad (146)$$

Since the 2-norm in (146) is difficult to compute, we use a lower bound $\max_{i,j} |M_{i,j}| \leq \|M\|_2$, which to leading order in l gives

$$\gamma \gtrsim K_{EQ}^2 \sim e^{2l/r_{lEQ}}. \quad (147)$$

Therefore in the presence of localized sensors, collocated with the controllers, the transient amplification again scales exponentially with the system size, however, the characteristic length is now only half of that found for the case with complete state information. This result is intuitively clear, since now a perturbation inside the system first has to propagate to the sensor location, and then the feedback has to travel from the controller to the spatial location of the disturbance, doubling the total path and hence the effective time delay in the feedback loop. A similar result was found earlier for coupled map lattices [66, 58]. The analytical scaling (147) is only valid for the case where the matrix D with the properties specified earlier exists. As mentioned in Section 5.2, we can show existence of such a D for control at the boundaries, as well as for the system with two and four controllers located

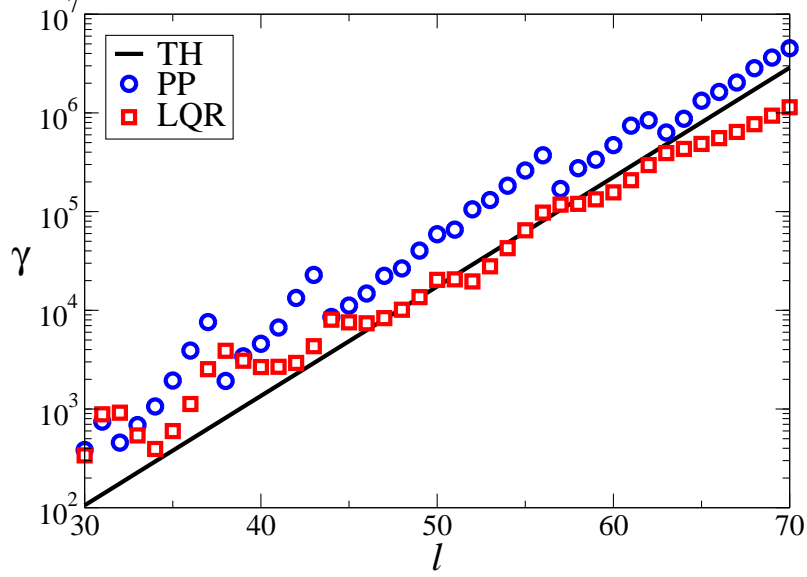


Figure 32: Transient amplification in the GL equation as a function of the system size l for the case of six collocated controllers and sensors located inside the domain. In the pole placement (PP) calculations we took $\Lambda = -0.5$, for LQR control, the λ'_k are in $[-1, -0.1]$. The theoretical value (TH) is given by (147).

inside the domain. For other scenarios, it is not clear if such a D exists. Additionally, as our analysis in Section 5.1 suggests, the scaling (147) will likely break down for small $|\Lambda|$. Nevertheless, as Fig. 31 and Fig. 32 show, (147) provides a good estimate, even for values of Λ whose magnitude is not too large and for control setups where we can not prove the existence of D . In all instances, we find exponential scaling with l that is reasonably well approximated by (147).

If the sensors are not collocated with the controllers the above analysis is not valid. Numerical simulations show that changing the location of the sensors can change the exponent. It is possible to reduce the exponent by placing the sensor pairs between the controller pairs. Nevertheless the exponential scaling of the transient amplification remains. Fig. 33 shows this scenario, using the GL equation as example. Further numerical simulations show that placing the localized sensors at various positions always leads to an exponential scaling with exponents that have as lower bound the exponent obtained from distributed sensing and as upper bound the exponent obtained from collocated sensors and controllers. Although it is likely that our analysis can be generalized for the case of sensors placed at arbitrary

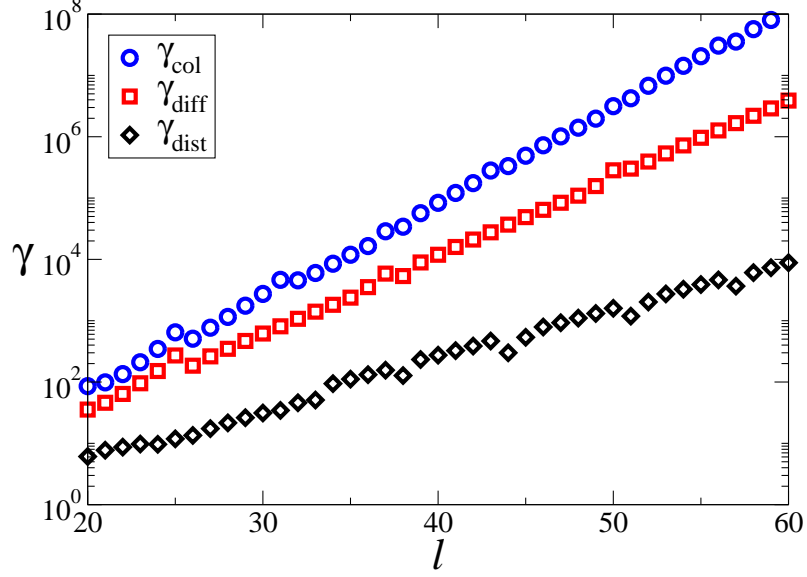


Figure 33: Transient amplification in the GL equation as a function of the system size l for the case of four controllers and sensors. Shown is the case of localized sensors and controllers collocated at the same points inside the domain (γ_{col}), the case of sensor pairs in the middle between controller pairs (γ_{diff}) and the case of distributed sensing everywhere in the domain, as discussed in Section 4.3 (γ_{dist}). The control is computed using the LQR scheme.

locations, our focus here is on the underlying mechanism of control failure and we therefore made no attempt to obtain an analytical solution for the general case of arbitrary sensor locations.

CHAPTER VI

BREAKDOWN OF CONTROL

6.1 Linear breakdown scenarios

We spent the previous two chapters obtaining explicit solutions for the feedback gain and then relating these results with the transient amplification. In this chapter we will complete the picture by connecting the transient amplification to disturbances or noise in the system and obtain results that explain under what circumstances control will break down, as it is shown in Fig. 3. In this section, we analyze how control can fail or become useless through purely linear, nonnormal effects. In the next section, we show how nonlinearity can further reduce the effectiveness of control.

For a purely linear system, an initial disturbance and its transient growth can not lead to control breakdown. No matter how large the transient amplification γ is, no transition to a different state can occur since the target state is the only global attractor. After the transient growth phase, asymptotic exponential decay sets in and the system approaches the target state. However, instead of a single initial disturbance, the more physically realistic scenario is that of continuous background noise. While for this case (continuous noise in a linear system) the control is theoretically working, it can become useless for all practical applications. Since the system is still linear, the target state is still the only attractor. If we had very rare occurrences of ‘dangerous’ disturbances, that is disturbances that can experience significant growth, control would be possible most of the time. One would find a system with occasional transient deviations from the target state whenever such a ‘dangerous’ disturbance occurs, followed by exponential decay toward the target state, induced by the control.¹ But generic continuous noise almost always has a nonzero projection onto

¹It is interesting to note that this is phenomenologically similar to intermittency phenomena in nonlinear systems. We do not know if some deeper connection between these phenomena can be established or if it is purely a phenomenological similarity. We tend to believe the latter, however, since we did not investigate any connections we cannot say for sure.

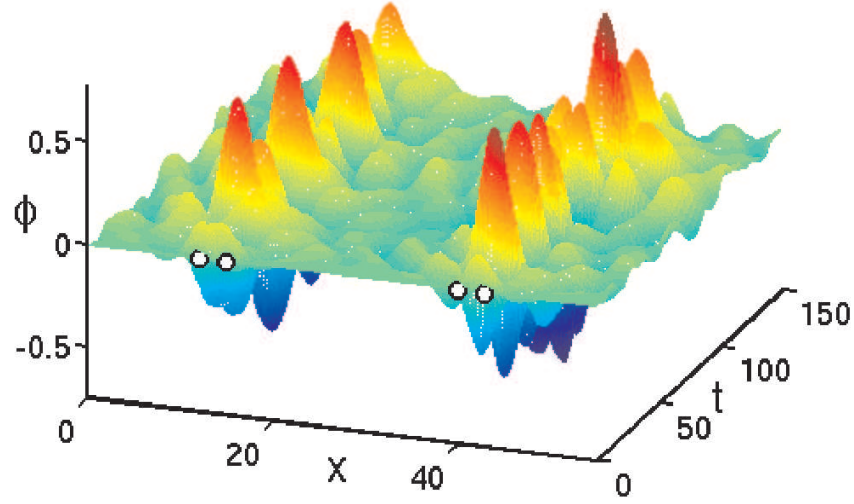


Figure 34: The evolution of the linearized Kuramoto-Sivashinsky equation with continuous random noise of magnitude $\sigma = 10^{-5}$ and system size $l = 55$. The nonnormal amplification is strong enough to produce continuous deviations from the target state of such magnitude that control fails to be effective for any practical application.

the nonnormal subspace. Therefore the noise drives a continuous nonnormal amplification, which results in continuous ‘transient departures’ away from the target state, overlaying the exponential decay induced by the controller. This continuous ‘transient departure’ can lead to a system that is practically non-stabilizable and most of the time far away from the target state. For noise of order σ , in a nonnormal system with amplification factor γ , noise will constantly be amplified to size $O(\gamma\sigma)$. If the latter value becomes large enough, the control becomes useless, even though it technically still works. One therefore finds that the maximum noise that still leads to adequate control scales like $\sigma \sim \gamma^{-1}$, as expected from a linear scenario. The phenomenon just described is shown in Fig. 34 for the linearized KS equation.

Another way control can fail, even if the system is noiseless, is through the inaccuracy in modeling the true physical system. Even in a truly linear and noiseless system, the operator M or even the original continuous, infinite-dimensional operator, always represent

an approximative model of the real physical system. The real system is never perfect in its geometries, boundary conditions, etc. For instance in a fluid system, the container walls can never be made perfectly smooth. Therefore, the real system is described by an operator $M + \sigma P$, where σP accounts for the discrepancies between model and real system. Since these discrepancies are unknown, σP is unknown. To model the unknown inaccuracies, one can instead use a random matrix P with $\|P\| = 1$, while σ represents the magnitude of those discrepancies. Note that adding the unknown error to M is only one way to describe the modeling error. One could also think of other ways, for instance through a multiplicative error or other forms of error modeling. However, it can be shown that these descriptions are equivalent [57].

Several recent studies [117],[107] pointed out that if the operator M is strongly nonnormal, its eigenvalues become very sensitive to small perturbations in M . Specifically, if we add σP to M , it can lead to changes in the eigenvalues of M that are of order $\sigma\gamma$. For strongly nonnormal M , a very small change σP can change the eigenvalues on a scale $O(1)$, potentially turning them positive and resulting in failure of control. We are therefore facing the problem that the design of a control which renders the evolution operator M stable, at the same time renders M so nonnormal that the ‘true’ unknown system $M + \sigma P$ is potentially unstable. This is independent of noise in the system. Rather, control fails due to the inability to accurately model the system and therefore potentially designing control that does not work for the real physical system. One could say that control fails due to ‘noise’ in the modeling process. From what we just explained, one expects the scaling relation between modeling uncertainty σ and transient amplification to again be given by $\sigma \sim \gamma^{-1}$. In Fig. 35 we show that this is indeed the case. For different system size l and associated transient amplification γ , we create 100 random matrices σP with $\|P\| = 1$ and check if any one of them results in at least one positive eigenvalue of $M + \sigma P$. We determine the threshold value of σ at which the eigenvalues do not change enough to result in at least one positive eigenvalue. While creating just 100 random matrices is clearly a crude estimate, Fig. 35 nevertheless shows very well that $\sigma \sim \gamma^{-1}$, as expected.

We can therefore conclude that for a purely linear system, the scaling of the tolerable

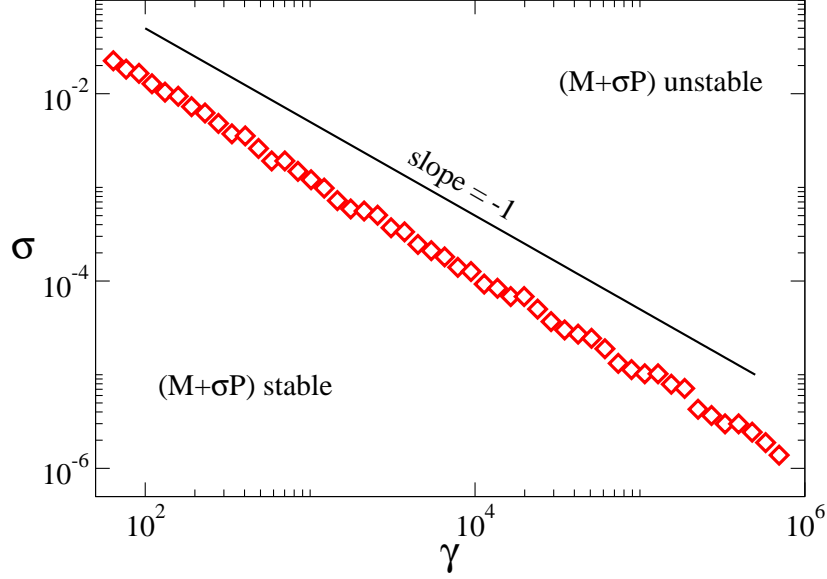


Figure 35: Limit of perturbation strength σ for a given γ such that the resulting perturbed matrix is still stable. The figure shows the scaling for the GL equation with four controllers.

noise or uncertainty goes with the transient amplification as

$$\sigma \sim \gamma^{-1}. \quad (148)$$

As we will show next, the amount of tolerable noise can be significantly reduced further if nonlinear effects are taken into account. In these instances, one can have a scaling coefficient that is smaller than -1 , leading to control breakdown for noise levels that are much smaller than the limits obtained by purely linear nonnormal effects.

6.2 *Nonlinear breakdown scenarios*

Up to this point, we solely focused on the linearized form of the systems under study. As we discussed in the Section 6.1, even in linear systems, control can fail to work if the non-normality becomes large. However, most physically important systems are nonlinear. It is therefore important to investigate what happens in a fully nonlinear system². If nonlinearities are present, the global system behavior can change significantly. First, the target state is not necessarily the only attractor. The controlled system might have other attractors,

²Additionally, since this work is performed in the Center for Nonlinear Sciences, I better include some nonlinearity.

including potentially strange attractors, corresponding to turbulent time evolution of the state. If in such a situation either an initial disturbance or background noise of magnitude σ gets amplified by γ , and the amplified state is of $O(1)$, the nonlinearities in the system become non-negligible. A nonlinear instability can occur, leading to control breakdown and transition into a different and potentially turbulent regime. Control in the nonlinear system can break down for even smaller amounts of noise than the ones given by (148). As we will explain below, for nonlinear systems, the scaling relation for the tolerable amount of noise σ as a function of the transient amplification γ is given by

$$\sigma \sim \gamma^\beta \tag{149}$$

with $\beta \leq -1$. In the following we study how the value of β depends on the specifics of a given controlled system.

A similar issue has recently received a lot of attention in the study of transition to turbulence. In [9], the authors asked the question: How does the minimum disturbance of magnitude σ that leads to transition to turbulence scale with the Reynolds number R , i.e., for $\sigma \sim R^\beta$, what is the value of β ? To find an answer to that question, several groups first proposed and studied low dimensional models. Most of them are reviewed in [9]. Recently, more accurate analysis for some of these fluid systems has been performed [37, 24, 29]. As these studies showed, for each system under consideration, the type of nonlinearity and its interaction with the nonnormality determine the value of β . Values that were found for different systems, by means of simple models, numerics or detailed analytical computations, range between -1 and -3 . The references just mentioned, as well as the references on turbulence transition mentioned in Section 3.1 and the recent overview article [67] provide additional information.

Since the Reynolds number scales with the size of the system, it is interesting to consider some parallels. One finds that in the fluid systems, γ or a similarly defined quantity scales like some small power of the Reynolds number, and since the Reynolds number depends linearly on l , one finds $\gamma \sim R^n \sim l^n$ for some small n . The nonnormality in these fluid systems stems from the fact that mean flow is present. In contrast, we have the much more

pronounced divergence $\gamma \sim e^{l/l_0}$, due to nonnormality induced by localized control.

Nevertheless, the question what the value of β is for a given nonnormal and nonlinear system is similar. While in the fluid systems just mentioned the nonnormality arises due to mean flow and in our systems it arises due to localized control, and further the scaling of γ is different, we nevertheless expect that most of the ideas presented in the following apply equally to other nonnormal, nonlinear systems, independent of the source of nonnormality.

To determine β , we first explain the most basic idea from which one can derive a value for β . This idea of interaction between nonnormality and nonlinearity was introduced in [117] and called the bootstrapping mechanism. Assume we have a nonnormal system with transient growth measured by a transient amplification constant $\gamma \gg 1$. Now consider the evolution of a small initial disturbance $u = \phi(0)$ with magnitude $\|u\| = \sigma \ll 1$ for which the nonlinear terms can be neglected. Generically, u will have a non-vanishing component along the maximal growing direction ϕ_{opt} . It will therefore be transiently amplified by the nonnormal M to a new state $v = \phi(t_1) \sim \gamma\sigma$ at time $t_1 \approx t_m$. Now let us consider what happens when nonlinearities come into play. At every instant, the nonlinearity takes the state $\phi(t)$ and transforms it. For instance a polynomial nonlinearity will create $P[\phi(t)] = \phi(t)^n$. For the state v , that leads to $P[v] = w$, $\|w\| \sim (\gamma\sigma)^n$, which leads to an integrated deviation of order $t_m(\gamma\sigma)^n$ in the same amount of time it takes the linear operator to amplify the initial disturbance by a factor $O(\gamma)$. In general, t_m might scale with γ . However, as we noted in Section 5.1, in our systems t_m scales at most linearly with l and we can therefore neglect it in the large l limit. Next, we assume that the state w will be further amplified by M . This leads to further nonnormal growth, establishing a positive feedback loop. The initial disturbance will therefore be ‘bootstrapped’ until it reaches $O(1)$ where a nonlinear instability can lead to control failure. Hence the name bootstrapping mechanism. The requirement for the positive feedback loop to exist is that the magnitude of the state w is larger than the magnitude of the initial disturbance u . Otherwise if $\|w\| < \|u\|$, no positive feedback loop exists and the system relaxes to the target state. The following diagram

shows what we just explained in words for a polynomial nonlinearity.

$$\|u\| \sim \sigma \xrightarrow[\text{nonnormal}]{e^{Mt_m} u=v} \|v\| \sim \gamma \sigma \xrightarrow[\text{nonlinear}]{P[v]=v^n=w} \|w\| \sim (\gamma \sigma)^n \xrightarrow[(\gamma \sigma)^n \lesssim \sigma]{(\gamma \sigma)^n \gtrsim \sigma} \begin{array}{l} \text{bootstrapping.} \\ \text{no bootstrapping.} \end{array}$$

Solving for the scaling of the threshold noise σ gives

$$\sigma \sim \gamma^{-n/(n-1)}. \quad (150)$$

Therefore the bootstrapping mechanism predicts an exponent $\beta = -n/(n-1)$. Clearly, this nonlinear mechanism would lead to breakdown before the linear breakdown mechanisms can set in.

Sometimes the bootstrapping idea gives accurate predictions for the maximum tolerable threshold noise σ . This type of scaling was indeed observed in the control problem for coupled rings [38]. However, sometimes the predictions of the bootstrapping mechanism do not lead to correct results. The reason for that is easily noted. In the above argument, we assume that the nonlinearities change the spatial structure of v into w in such a way that w again has nonzero projection onto the space of functions that can experience non-normal growth and therefore w experiences further amplification by M . This idea, that nonlinearities transfer energy back into the nonnormal part of the system, does not always hold true. While some authors early on suggested that the feedback loop should occur as a very generic mechanism for transition in fluid flows [9], more careful work that has been done recently shows that this is not so [29]. Instead, one needs to take into account the specific interaction between nonlinearity and nonnormality, especially with regards to their spatial structures. Several more recent studies paid attention to the possible nonlinear-nonnormal interactions for the case of transition in fluid flows [27, 29, 67]. We used a wavenumber analysis to investigate the spatial structures and the resulting scaling [65] in the case of the GL equation and localized control at one boundary. In the following we extend our earlier findings [65] and investigate the behavior of the scaling coefficient β for the different equations and control scenarios discussed earlier.

We start with the nonlinear GL equation and control at the right boundary. Instead of using the GL equation (2) in its standard form, we use different nonlinearities, namely

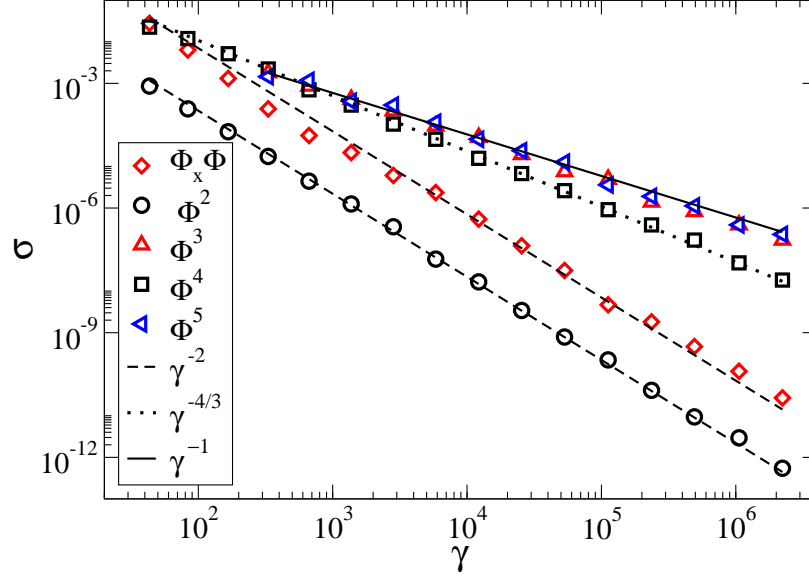


Figure 36: The noise level for which localized linear control fails as a function of the transient amplification factor. The system is the GL equation with control at the right boundary and different types of nonlinearities. The plot shows the range $l = [5, 20]$.

$\phi^2, \phi^3, \phi^4, \phi^5$ and $\phi_x \phi$. For each of these nonlinearities, we apply Gaussian white noise to the system and simulate it, thereby determining the maximum tolerable amount of noise σ that still allows successful control, as a function of the transient amplification γ_c obtained from (31). The nature of Gaussian noise is such that in theory there can always be a disturbance – or a series of disturbances, since the noise is short-term cumulative – that will lead to loss of control. However for all practical applications it is enough to investigate stability for a finite long time. If the system does not lose control for that time period, it can be considered stabilizable for all practical purposes. By varying the simulation time, we check for consistency and convergence.

As can be clearly seen from Fig. 36, the bootstrapping mechanism does not explain all the scaling relations found. Instead, one sees that the critical noise level resulting in control failure scales as given by (150) for ϕ^2, ϕ^4 and $\phi_x \phi$, while the scaling for ϕ^3 and ϕ^5 is given by the linear expression (148). This means the odd nonlinearities do not close the feedback loop and do not lead to bootstrapping.

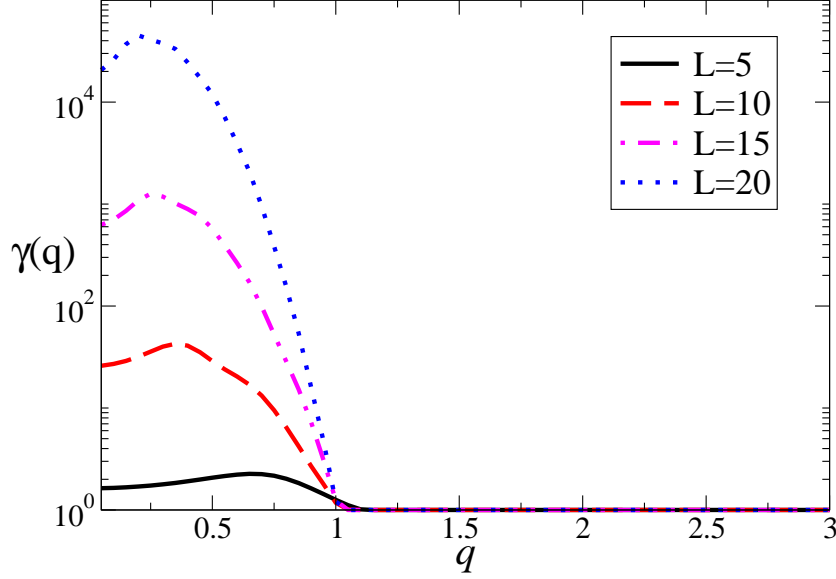


Figure 37: Amplification $\gamma(q)$ for an initial condition of the form $\sin(qx)$. Shown is the GL equation with LQR control applied at the right boundary.

To understand these results, we need to discuss the spatial features of nonnormal amplification. Without control, the equations under study can be expanded in Fourier modes with real wavenumbers. As noted in Section 4.4, for the GL equation and control at the right boundary, the feedback only changes the wavenumbers, the eigenfunctions are still given by sine modes. Therefore a good way to analyze the spatial selectiveness of the growth with regard to certain disturbances is by analyzing it in wavenumber space. We briefly mentioned in Section 3.3 the fact that nonnormality is rather ‘selective’, that is, only certain spatial structures in form of initial conditions or background noise are getting amplified. To investigate this selectiveness, we define the transient amplification as function of the wavenumber

$$\gamma(q) = \max_t \left\| \frac{\phi(x, t)}{\phi(x, 0)} \right\| \bigg|_{\phi(x, 0) = f_q(x)}, \quad (151)$$

where $f_q(x)$ represents a certain modal disturbance. Fig. 37 shows $\gamma(q)$ for the GL equation with control on one boundary. For this system, the initial disturbances are the eigenfunctions $f_q(x) = \sin(qx)$. We see from Fig. 37 that only disturbances with wavenumbers $0 \leq q \lesssim 1$ experience transient growth.

This suggests that we need to generalize the bootstrapping idea, including the spectral

(that is, spatial) dependence of γ . We can do this by writing

$$\|u\| \sim \sigma \xrightarrow[\text{nonnormal}]{e^{Mtm}u=v} \|v\| \sim \gamma(q)\sigma \xrightarrow[\text{nonlinear}]{P[v]=v^n=w} \|w\| \sim (\gamma(q)\sigma)^n \xrightarrow[(\gamma(q)\sigma)^n \lesssim \sigma]{(\gamma(q)\sigma)^n \gtrsim \sigma} \begin{array}{l} \text{bootstrapping.} \\ \text{no bootstrapping.} \end{array}$$

Formally, we simply replaced γ by $\gamma(q)$, explicitly indicating the wavenumber dependence.

However, this simple formal change allows us to explain the scaling shown in Fig. 36.

Before we can do that, we need to consider one more feature of nonnormality. In addition to the selectivity in transient growth, the nonnormality also transforms an initial state while it gets amplified. The change occurs in such a way that the completely amplified state has no component that can be further amplified. This behavior is of course intuitively clear, since otherwise the amplification would continue and it would not be transient. Still, while obvious, this phenomenon has important consequences, and therefore merits further analysis. For instance one can see in the Fig. 5 show earlier, that the amplified state $\Phi(t)$ is almost completely in the direction of e_1 , which means its further evolution will essentially follow that of e_1 , exponentially decaying with λ_1 , so no further growth is possible. This is generally the case. The amplified state will be in the direction of the strongly nonnormal eigenfunctions, such that no further growth can occur. We show in Fig. 38 the spectrum of the maximum amplified state for the controlled, linearized GL with random noise. Specifically, the state is expanded in the basis of the eigenfunctions $f'_k(x) = \sin(q'_k x)$ of the controlled system

$$\phi(x, t) = \sum_k c'_k(t) f'_k(x), \quad (152)$$

and the spectrum $F_k[\phi]$ is obtained by finding the maximal values $F_k[\phi] = \max_t |c'_k(t)|$ for each k . One sees that the amplified state has large coefficients c'_k that are strongly localized at a wavenumber q^* slightly larger than one. Here q^* denotes the wavenumber at which the spectrum $F_k[\phi]$ has its peak. This can be understood if one recalls the discussion in Section 4.4. There we explained how LQR control leads to a tight bunching of wavenumbers, with the wavenumbers corresponding to the new eigenvalues located approximately around the wavenumber that corresponds to the first negative eigenvalue. This is exactly what one sees in Fig. 38.

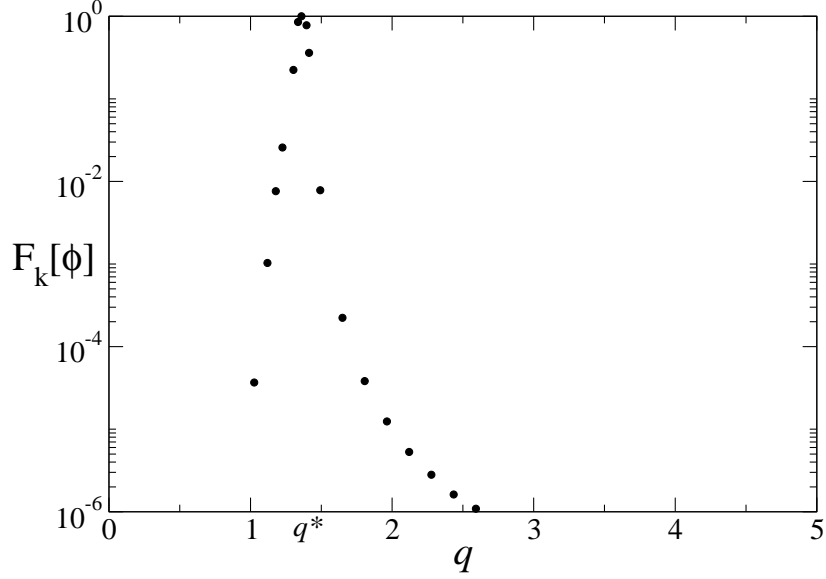


Figure 38: Normalized spectrum $F_k[\phi]$ for the linear GL equation driven by random noise. Control is applied at the right boundary, and computed according to the LQR scheme.

Thus Fig. 37 and 38 confirm the fact that the initial conditions that can experience large growth have to be largely orthogonal to the nonnormal eigenfunctions, which is the case for functions with strong components in $0 \lesssim q \lesssim 1$, and that the amplified function becomes aligned with the nonnormal eigenfunctions and orthogonal to the growing modes. We call this phenomenon focusing since a generic initial disturbance which has components everywhere in wavenumber space is focused into a few modes.

With these pieces of information, we can understand Fig. 36. Assume we start with a generic initial condition. It will get transiently amplified and focused into certain modes. As seen in Fig. 38, the spectral content is strongly focused to a small wavenumber band. Since the transiently amplified disturbances have a very narrow spectrum, the spectrum produced by the nonlinear terms will also consist of several narrow peaks, as long as we consider nonlinearities of the power law type $P[\phi] = \phi^n$ with moderate n . High powers are not interesting as the scaling exponents for the even and odd powers become indistinguishable. Besides, most physically interesting nonlinearities have low powers. For instance, the spectrum of a quadratic nonlinearity, be it ϕ^2 or $\phi_x \phi$, will only contain frequencies which are either sums or differences of frequencies q_k , i.e., 0 , $|q_m - q_n|$, $2q_m$, and $q_m + q_n$. This

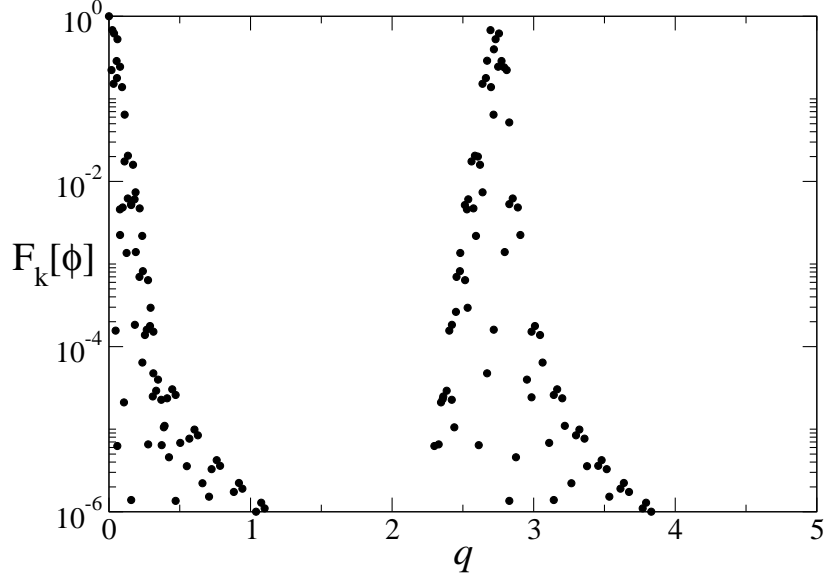


Figure 39: Normalized spectrum $F_k[\phi]$ for the quadratic term ϕ^2 of the GL equation driven by random noise. Control is applied at the right boundary, and computed according to the LQR scheme.

means that the spectrum of the quadratic term will be localized near $q = 0$ and $q = 2q^*$, as Fig. 39 shows. And as Fig. 37 shows, disturbances with $q \approx 0$ experience significant nonnormal amplification. Therefore the nonlinearity is able to transfer energy back into the nonnormally growing subspace where it will again be transiently amplified. This leads to a closed feedback loop and bootstrapping.

For odd powers of the nonlinearity, the spectrum will be focused around the maximum wavenumber q^* and $(2n+1)q^*$. For instance, the spectrum of a cubic nonlinearity, $f(\phi) = \phi^3$, will only contain wave numbers $|q_m \pm q_n \pm q_k|$. Therefore the spectrum will be strongly localized near $q = q^*$ and $q = 3q^*$, as can be seen in Fig. 40. The quintic nonlinearity, $f(\phi) = \phi^5$, is expected to produce similar results as its spectrum will be localized near q^* , $3q^*$, and $5q^*$, and so on. Therefore, odd nonlinearities will not transfer excitations into the subspace $0 \lesssim q \lesssim 1$ that can experience further amplification. The feedback loop is not closed and no bootstrapping will occur, leaving $\beta = -1$. This explains the scaling relations found in Fig. 36.

The same arguments above can be made for the GL equation with control applied at both

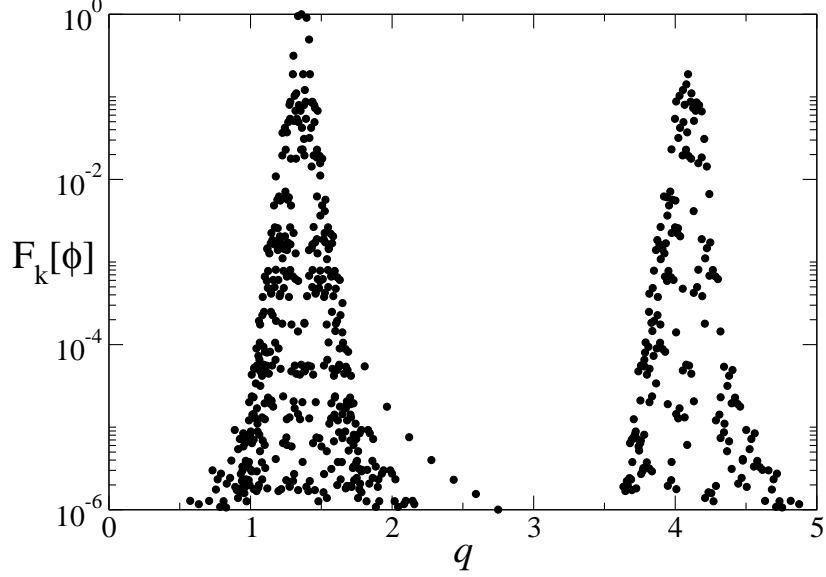


Figure 40: Normalized spectrum $F_k[\phi]$ for the cubic term ϕ^2 of the GL equation driven by random noise. Control is applied at the right boundary, and computed according to the LQR scheme.

boundaries, where again the eigenfunctions under feedback are given by pure sine or cosine modes and the same wavenumber analysis just outlined can be applied, leading to the same scaling results. For the case of localized control applied inside the domain, discontinuities can occur at the locations of the controllers. Therefore the eigenfunctions are not global sine or cosine modes. Nevertheless, between controllers the eigenfunctions are still described by these modes with changed wavenumbers. As Fig. 41 shows, this leads to the same scaling results as found for the boundary control. An additional point worth mentioning can be observed in Fig. 41. Namely for small l , the $\phi_x\phi$ nonlinearity as well as the ϕ^4 nonlinearity scale with $\beta = -1$, only for larger l does one find scaling according to the bootstrapping mechanism. We can understand this at least on a qualitative level. For small l , the partial re-population of the wavenumber space around $q \approx 0$ through the nonlinearities, and the subsequent nonnormal amplification of those structures, is not strong enough to compete with the linear amplification mechanism. Therefore linear scaling is found. Only for larger l does the partial re-population of $q \approx 0$ and subsequent amplification become strong enough to dominate, which leads to a switch in the scaling behavior.

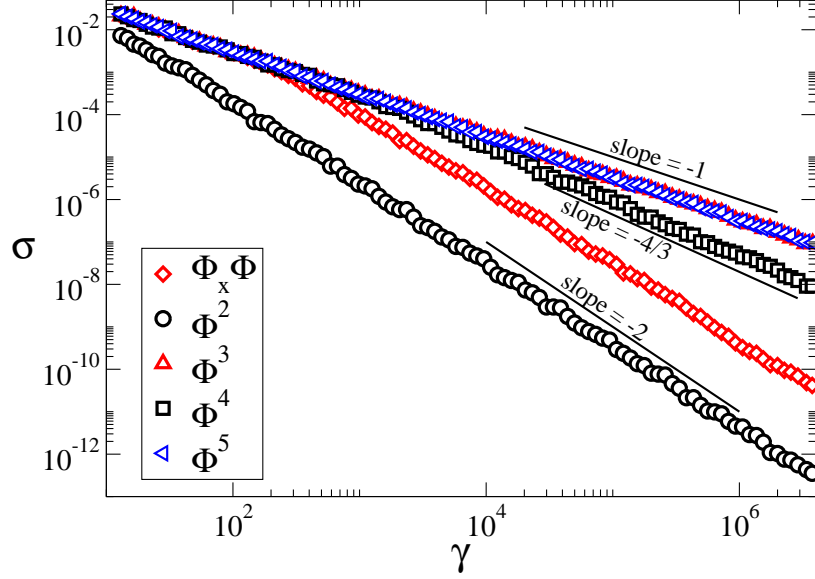


Figure 41: The noise level for which localized linear control fails for the GL equation with six controllers (LQR) as a function of the transient amplification factor for different types of nonlinearities. The plot shows the range $l = [30, 130]$

The situation changes for the KS and SH equations. One sees from Figs. 42 and 43 that for both equations, all nonlinearities are able to close the feedback loop and the scaling coefficient is given by $\beta = -n/(n - 1)$. The figure shows the scaling for the case of six controllers inside the domain, the same results are found for boundary control. We can understand these results as follows. In Section 4.4 we showed that the eigenfunctions of the controlled KS and SH equations are not given by pure Fourier modes. Therefore, figures such as Fig. 37 are of little value, and equivalent figures to Fig. 38 do not exist. Nevertheless, we can understand the scaling without such figures. For the KS equation, the eigenfunctions of the controlled system are a combination of sine and sinh modes. They are therefore not monochromatic and no sharp localization in wavenumber space occurs. Therefore the nonlinearity can always ‘rotate’ the amplified state such that some of the power gets redistributed into the wavenumber space corresponding to the formerly unstable eigenfunctions, which is the wavenumber space corresponding to structures that can experience transient growth. For the controlled SH equation, we can either have a combination of sine and sinh modes, resulting in exactly the same scenario as for the KS

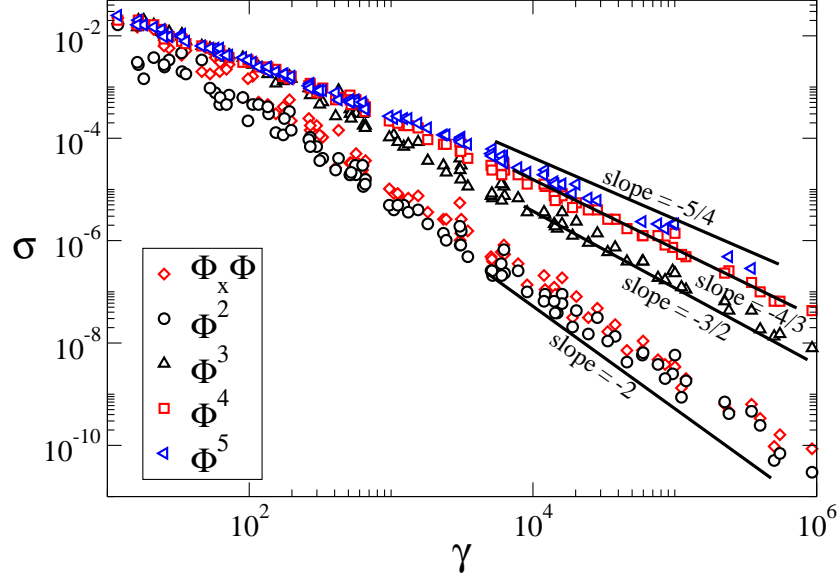


Figure 42: The noise level for which localized linear control fails for the KS equation with six controllers (LQR) as a function of the transient amplification factor for different types of nonlinearities. The plot shows the range $l = [30, 130]$

equation. Additionally, for certain λ , we can have a combination of two sine modes. While this does not lead to a broad spectrum, the new wavenumbers of the controlled system are found to be such that again the ‘rotation’ of the amplified state by the nonlinearities is such that some of the power gets redistributed into the wavenumber that can experience transient growth. This leads to scaling according to the bootstrapping mechanism in these equations for all nonlinearities.

We are therefore able – with the help of spectral considerations – to explain the scaling for all the equations and control setups considered here. Taking into account the spatial aspects of transient amplification helps to explain in which instances one finds a scaling coefficient β according to the idea of nonlinear bootstrapping mechanism and in which instances the scaling is given by the linear, nonnormal effects.

Finally, we want to point out that there are still some minor issues involving the value of β that are not yet completely clear to us and that are still under ongoing investigation. Most notably, it is found that switching between different control schemes (PP versus LQR) for a given equation with specified nonlinearity and specified number of controllers, one can

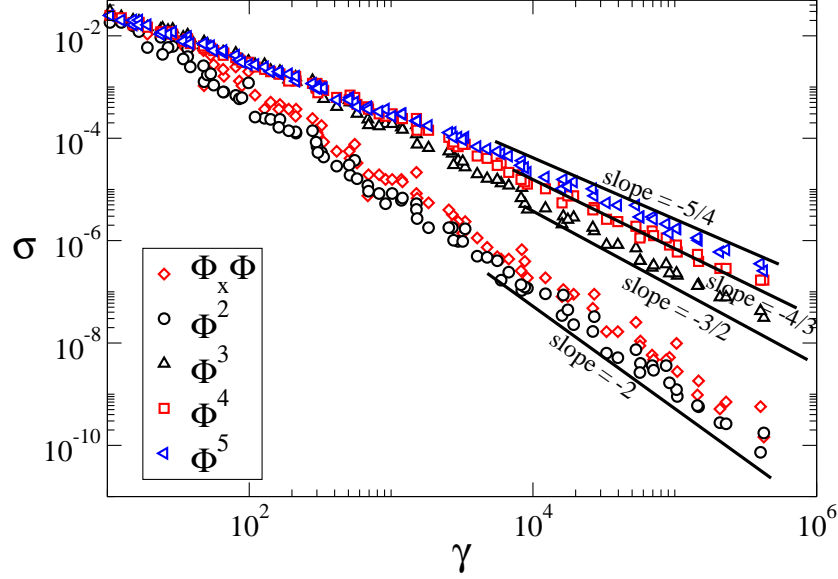


Figure 43: The noise level for which localized linear control fails for the SH equation with six controllers (LQR) as a function of the transient amplification factor for different types of nonlinearities. The plot shows the range $l = [30, 130]$

switch between the nonlinear and the linear scaling relation. Specifically, if one uses the PP scheme and chooses λ'_k that are strongly negative, one finds the linear scaling relation to be dominant. It seems that spectral considerations do not explain this switch in scaling. We suspect the reason to lie in the temporal behavior of the system. As we noted in Section 5.1, strongly negative λ'_k lead to a very fast transient amplification, which might result in transient growth and exponential decay that is so fast that there is not enough time for a potential feedback loop to close. However, this is so still a preliminary assumption and needs confirmation. We are confident to have a full description in the very near future.

Summarizing this chapter, we find that control always fails due to nonnormal, linear effects. Moreover, under certain circumstances, nonlinearities can accelerate control failure through a feedback loop between nonnormality and nonlinearity, reducing the amount of tolerable noise even further. To understand when the feedback loop is effective, one needs to carefully analyze the system with given control, taking into account spatial considerations. A possible way to perform this analysis is by studying a spectral representation of the system.

CHAPTER VII

CONCLUSIONS AND OUTLOOK

We set out to answer the question: “What are the limits of localized control?”, which we noted in Section 1.1 can be split into the two questions: “How does the transient growth and noise amplification arise in locally controlled systems?” and “How much noise can a given controlled system tolerate before control fails?” We now review the main answers we found and their implications, followed by a discussion of some of the questions that remain open and that allow for possible future work.

In Chapter 4, we derived explicit expressions for the feedback gain for a relatively broad class of systems and different control setups. We further found that the feedback diverges exponentially with the system size, with an exponent dependent on the specifics of the equation and the control. This result, together with the explanation how a large feedback gain leads to strong nonnormality provided the first indication how transient growth can come about. In Chapter 5, we were able to make this connection more quantitative, obtaining an analytical expression, showing that the exponential scaling with system size also applies to the transient growth. This answered the first question, explaining how localized control leads to transient growth and noise amplification.

The exponential scaling we obtained already indicated strong limitations on the maximum system size or level of noise. In Chapter 6 we were able to obtain more quantitative limits, showing how linear nonnormal effects and nonlinear-nonnormal interactions can lead to different scaling relations between the amount of tolerable noise and the transient growth, and therefore the system size. This answered the second question.

Combining all the results, we are able to explain the limits of localized control for the rather general class of PDEs and control setups studied here.

While we were able to answer the questions we set out to answer, there are of course extensions that might be worthwhile pursuing. One extension could be to study systems in

two or three spatial dimensions. We expect that while the specific analytic expressions will change, the main results will still hold true, since our reasoning does not explicitly depend on the fact that only one space dimension is present. This should also be the case for a generalization to complex or vector valued functions that could be studied.

Further work could be done in the direction of utilizing more advanced concepts from control theory like the H_∞ control or nonlinear control schemes and to study how these schemes affect the ability to locally control extended systems. We expect studies in that direction to be performed by the control theory community in the very near future. In fact, some very recent work in that direction has already been performed [85], albeit so far with a focus on controlling an unstable nonnormal system, rather than studying the limits of control itself. From the arguments we presented, one can expect that the exponential scaling for the feedback gain and the transient growth will persist and continue to pose strong limitations on the control. Still, schemes like H_∞ should allow one to minimize the exponents of the scaling relations. Some indications of this can be found for instance in [85] and another recent study [17]. We expect that significant progress can be made by merging state of the art approaches from control theory with the concept of nonnormality.

Another extension that might be of interest to control engineers concerns the case of localized sensing. Since in all real applications, localized sensors are as important as localized controllers, researchers in the control community might want to study the issue of localized sensors combined with localized control in more detail. We only gave a brief exposure to it in Section 5.3. More in depth study is certainly possible and potentially important from an applications point of view.

While we were able to obtain an analytical result for the feedback gain scaling – which is an important result by itself since it allows for further analysis – the analytic expression for the transient amplification is an approximation. Despite being a rather good approximation in most instances, it might be possible to manipulate the matrix exponential further to obtain a further improved result. The same can be said for the scaling analysis as it concerns control breakdown. While the analysis presented explains very well what happens in the system, there might be the possibility to introduce further qualitative or quantitative

analytical tools, for instance by making use of the singular value analysis [42].

Lastly, while it is not a direct extension to our work, we believe that the concept of nonnormality, which is so essential to our work, merits study in different contexts pertaining to dynamical systems – with or without control present. We believe that the nonnormality concept will spread into other areas of physics and engineering and potentially enable to solve longstanding problems similar to the flow transition problem we mentioned repeatedly or the control problem we discussed in this work. Following that route of investigation seems to us a rather promising approach. For instance we mentioned in Section 2.1 the strong interest in synchronization that has emerged recently. This is an area of study that can clearly profit from some of the nonnormality concepts.

In any case, we think we have done our part, and we leave these studies to others. At least for the time being, since we decided to do what seems to be the trendy thing to do for physicists these days, to try and mess with biology. But even there, we suspect, at some point nonnormal dynamical systems that require control might be awaiting us...

APPENDIX A

ALTERNATIVE COMPUTATION OF THE FEEDBACK GAIN SCALING

In the following, we present an alternative derivation of the scaling result for the feedback gain K_m . We show it for the case of the GL equation and the three different control scenarios.

A.0.1 Computation of feedback scaling for the one-controller case

For the case of control located at one boundary, we start with (71) given by

$$K_m = \frac{(-1)^m \prod_{p=a}^b (\lambda_m - \lambda'_p)}{\prod_{p=a}^{m-1} (\lambda_m - \lambda_p) \prod_{p=m+1}^b (\lambda_m - \lambda_p)}, \quad m = a, \dots, b. \quad (153)$$

Substituting $\lambda_m = 1 - q_m^2$, $\lambda'_p = \Lambda$ and $q_m = (m - \frac{1}{2}) \frac{\pi}{l}$ into (153) we obtain

$$\begin{aligned} |K_m| &= \frac{(1 - (m - \frac{1}{2})^2 (\frac{\pi}{l})^2 - \Lambda)^s}{\prod_{p=1}^{m-1} (\frac{\pi}{l})^2 ((m - \frac{1}{2})^2 - (p - \frac{1}{2})^2) \prod_{p=m+1}^s (\frac{\pi}{l})^2 ((p - \frac{1}{2})^2 - (m - \frac{1}{2})^2)} \\ &= \left(\frac{l^2}{\pi^2} \right)^{s-1} \frac{(1 - (m - \frac{1}{2})^2 (\frac{\pi}{l})^2 - \Lambda)^s}{\prod_{p=1}^{m-1} (m^2 - m - p^2 + p) \prod_{p=m+1}^s (p^2 - p - m^2 + m)} \\ &= \left(\frac{l}{\pi} \right)^{2(s-1)} \frac{(1 - (m - \frac{1}{2})^2 (\frac{\pi}{l})^2 - \Lambda)^s}{\prod_{p=1}^{m-1} (m - p)(m + p - 1) \prod_{p=m+1}^s (p - m)(p + m - 1)} \\ &= \left(\frac{l}{\pi} \right)^{2(s-1)} \frac{(m - 1)!(2m - 1)! \prod_{p=1}^s (1 - (m - \frac{1}{2})^2 (\frac{\pi}{l})^2 - \Lambda'_p)}{(m - 1)!(2m - 2)!(s - m)!(s + m - 1)!} \\ &= \left(\frac{l}{\pi} \right)^{2(s-1)} \frac{(1 - 2m)(1 - (m - \frac{1}{2})^2 (\frac{\pi}{l})^2 - \Lambda)^s}{(s - m)!(s + m - 1)!} \\ &= \exp \left[(2s - 2) \ln \left(\frac{l}{\pi} \right) + \ln(1 - 2m) + s \ln(1 - (m - \frac{1}{2})^2 (\frac{\pi}{l})^2 - \Lambda) \right. \\ &\quad \left. - \ln((s - m)!) - \ln((s + m - 1)!) \right]. \end{aligned}$$

Since we are interested in the large l scaling, we can use Stirling's formula $\ln(n!) \approx (n + \frac{1}{2}) \ln(n) - n$, which preserves the proper scaling. This leads to

$$\begin{aligned}
|K_m| &\approx \exp \left[(2s-2) \ln\left(\frac{l}{\pi}\right) + \ln(1-2m) + s \ln\left(1 - \left(m - \frac{1}{2}\right)^2 \left(\frac{\pi}{l}\right)^2 - \Lambda\right) \right. \\
&\quad \left. - \left(s - m + \frac{1}{2}\right) \ln(s-m) + 2s - 1 - \left(s + m - \frac{1}{2}\right) \ln(s+m-1) \right] \\
&= \exp \left[s \left(2 - \ln(s+m-1) - \ln(s-m) + 2 \ln\left(\frac{l}{\pi}\right) \right. \right. \\
&\quad \left. \left. + \ln\left(1 - \left(m - \frac{1}{2}\right)^2 \left(\frac{\pi}{l}\right)^2 - \Lambda\right) \right) \right. \\
&\quad \left. + \left(m - \frac{1}{2}\right) \ln\left(\frac{s-m}{s+m-1}\right) - 1 - 2 \ln\left(\frac{l}{\pi}\right) + \ln(1-2m) \right] \\
&= \exp \left[s \left(2 + 2 \ln\left(\frac{l}{\pi}\right) - 2 \ln(s) + \ln\left(1 - \left(m - \frac{1}{2}\right)^2 \left(\frac{\pi}{l}\right)^2 - \Lambda\right) \right. \right. \\
&\quad \left. \left. - \ln\left(1 - \frac{m^2}{s^2} - \frac{1}{s} + \frac{m}{s^2}\right) \right) \right. \\
&\quad \left. + \left(m - \frac{1}{2}\right) \ln\left(\frac{s-m}{s+m-1}\right) - 1 - 2 \ln\left(\frac{l}{\pi}\right) + \ln(1-2m) \right]. \tag{154}
\end{aligned}$$

Finally, for l large, $s \approx \frac{l}{\pi}$ and from (76) we know that the maximum of K_m is at $m = 1$. Using these facts and keeping only leading terms in l , we obtain

$$|K^{GL}| \sim \exp\left(\frac{l}{\pi} \{2 + \ln(1 + |\Lambda|)\}\right), \tag{155}$$

which is the same as (77) and (78). We expected the results to be the same since the Stirling approximation is nothing else but the integral approximation expressed in a different form. Still, it is a good check to confirm the earlier results.

To arrive at equation (155), we assumed $m = 1$. It is of interest to check that the scaling result for K obtained for that value is indeed the largest possible. Especially for m large, the scaling of (154) is not immediately obvious. For that case, let's write $m = s - p$ where p is now a small integer. Further using $s \approx l/\pi$ we can write

$$\begin{aligned}
|K_m| &\approx \exp \left[s \left(2 + \ln\left(1 - \left(s - p - \frac{1}{2}\right)^2 \left(\frac{1}{s}\right)^2 - \Lambda\right) - \ln\left(\frac{2ps - p^2 - p}{s^2}\right) \right) \right. \\
&\quad \left. + \left(s - p - \frac{1}{2}\right) \ln\left(\frac{p}{2s - p - 1}\right) - 1 - 2 \ln(s) + \ln(1 - 2s + 2p) \right] \\
&= \exp \left[s \left(2 + \ln\left(\frac{2ps + s - p - p^2 - \frac{1}{4}}{s^2} - \Lambda\right) + \ln\left(\frac{s^2}{2ps - p^2 - p}\right) + \ln\left(\frac{p}{2s - p - 1}\right) \right) \right. \\
&\quad \left. - \left(p + \frac{1}{2}\right) \ln\left(\frac{p}{2s - p - 1}\right) - 1 - 2 \ln(s) + \ln(1 - 2s + 2p) \right] \\
&= \exp \left[s \left(2 + \ln\left(\frac{2ps + s - p - p^2 - \frac{1}{4}}{s^2} - \Lambda\right) + \ln\left(\frac{s^2}{4s^2 - 4ps - 4s + 2p + p^2 + 1}\right) \right) \right. \\
&\quad \left. - \left(p + \frac{1}{2}\right) \ln\left(\frac{p}{2s - p - 1}\right) - 1 - 2 \ln(s) + \ln(1 - 2s + 2p) \right].
\end{aligned}$$

From this one finds to leading order in l

$$|K_m| \sim \exp \left[\frac{l}{\pi} \left(2 + \ln(|\Lambda|) - 2 \ln(2) \right) \right]. \quad (156)$$

The scaling coefficient in this case is clearly lower than for $m = 1$, consistent with our earlier result that K_m has its maximum for $m = 1$.

A.0.2 Computation of feedback scaling for the two-controller case

For the case of two controllers, we start with (86) given by

$$K_m = \frac{(-1)^m (\lambda_m - \lambda'_m) \prod'_p (\lambda_m - \lambda'_p)}{2 \prod'_p (\lambda_m - \lambda_p)}, \quad m = a, \dots, b. \quad (157)$$

We again choose $\lambda'_1 = \lambda'_2 = \dots = \lambda'_s = \Lambda$. To avoid considering different cases, we also choose m and s even. Further we use $\lambda_m = 1 - q_m^2$ and $q_m = (n-1)(\pi/l)$. This leads to

$$\begin{aligned} |K_m| &= \frac{(1 - (\frac{(m-1)\pi}{l})^2 - \Lambda)^{s/2}}{2 \prod_j (\frac{\pi}{l})^2 (j+m-2)(j-m)} \\ &= \left(\frac{l}{\pi} \right)^{(s-2)} \frac{(1 - (\frac{(m-1)\pi}{l})^2 - \Lambda)^{s/2}}{2 \prod_j (j+m-2)(j-m)} \\ &= \left(\frac{l}{\pi} \right)^{(s-2)} \frac{(m-2)!! (1 - (\frac{(m-1)\pi}{l})^2 - \Lambda)^{s/2}}{2(s+m-2)!! (s-m)!! (m-2)!! (-1)^{\frac{m}{2}-1}} \\ &= \left(\frac{l}{\pi} \right)^{(s-2)} \frac{(1 - (\frac{(m-1)\pi}{l})^2 - \Lambda)^{s/2}}{2(-1)^{(\frac{m}{2}-1)} (s+m-2)!! (s-m)!!} \\ &= \left(\frac{l}{\pi} \right)^{(s-2)} \frac{(1 - (\frac{(m-1)\pi}{l})^2 - \Lambda)^{s/2}}{2^s (-1)^{(\frac{m}{2}-1)} \frac{s+m-2}{2}! \frac{s-m}{2}!}. \end{aligned}$$

The ‘!!’ represents the double factorial function. For m and/or s odd one finds similar expressions. Next rewriting the equation in exponential form and using Stirling’s formula

leads to

$$\begin{aligned}
|K_m| &= \exp \left[(s-2) \ln\left(\frac{l}{\pi}\right) + \frac{s}{2} \ln\left(1 - \left(\frac{(m-1)\pi}{l}\right)^2 - \Lambda\right) - s \ln(2) \right. \\
&\quad \left. - \left(\frac{m}{2} - 1\right) \ln(-1) - \ln\left(\frac{s+m-2}{2}\right)! - \ln\left(\frac{s-m}{2}\right)! \right] \\
&\approx \exp \left[(s-2) \ln\left(\frac{l}{\pi}\right) + \frac{s}{2} \ln\left(1 - \left(\frac{(m-1)\pi}{l}\right)^2 - \Lambda\right) - s \ln(2) \right. \\
&\quad \left. - \left(\frac{m}{2} - 1\right) \ln(-1) - \frac{s+m-1}{2} \ln\left(\frac{s+m-2}{2}\right) + s-1 - \frac{s-m+1}{2} \ln\left(\frac{s-m}{2}\right) \right] \\
&= \exp \left[s \left(\ln\left(\frac{l}{\pi}\right) + \frac{1}{2} \ln\left(1 - \left(\frac{(m-1)\pi}{l}\right)^2 - \Lambda\right) - \ln(2) + 1 - \frac{1}{2} \ln\left(\frac{s^2 - m^2 - 2s + 2m}{4}\right) \right) \right. \\
&\quad \left. - 2 \ln\left(\frac{l}{\pi}\right) - \left(\frac{m}{2} - 1\right) \ln(-1) - \frac{m-1}{2} \ln\left(\frac{s+m-2}{2}\right) - 1 + \frac{m-1}{2} \ln\left(\frac{s-m}{2}\right) \right] \\
&= \exp \left[s \left(\ln\left(\frac{l}{\pi}\right) + \frac{1}{2} \ln\left(1 - \left(\frac{(m-1)\pi}{l}\right)^2 - \Lambda\right) + 1 - \ln(s) - \frac{1}{2} \ln\left(1 - \frac{m^2}{s^2} - \frac{2}{s} + \frac{2m}{s^2}\right) \right) \right. \\
&\quad \left. - 2 \ln\left(\frac{l}{\pi}\right) - \left(\frac{m}{2} - 1\right) \ln(-1) + \left(\frac{m}{2} - \frac{1}{2}\right) \ln\left(\frac{s-m}{s+m-2}\right) - 1 \right].
\end{aligned}$$

Finally using $s \approx l/\pi$ and one finds to leading order in l

$$|K_m| \sim \exp\left(\frac{l}{2\pi} \{2 + \ln(1 + |\Lambda|)\}\right), \quad (158)$$

in agreement with (89).

A.0.3 Computation of feedback scaling for the r -controller case

In the general case of r controllers, the feedback gain coefficients are given by (104), which is

$$K_m = C_m \frac{2(\lambda_m - \lambda'_m) \prod'_p (\lambda_m - \lambda'_p)}{r \prod'_p (\lambda_m - \lambda_p)}, \quad m = a, \dots, b. \quad (159)$$

We again choose all the new eigenvalues to be Λ . Also again to avoid considering different cases, we assume that s and m are divisible by r . Using $\lambda_m = 1 - q_m^2$ and $q_m = 2\pi m/l$, we

obtain

$$\begin{aligned}
|K_m| &= C_m \frac{(1 - (\frac{2\pi(m-1)}{l})^2 - \Lambda) \prod_j (1 - (\frac{2\pi(m-1)}{l})^2 - \Lambda)}{\prod_j (\frac{2\pi}{l})^2 (j+m-2)(j-m)} \\
&= C_m (\frac{l}{2\pi})^{(2s/r-2)} \frac{(1 - (\frac{2\pi(m-1)}{l})^2 - \Lambda)^{s/r}}{\prod_j (j+m-2)(j-m)} \\
&= C_m (\frac{l}{2\pi})^{(2s/r-2)} \frac{f_r(m-2)(1 - (\frac{2\pi(m-1)}{l})^2 - \Lambda)^{s/r}}{f_r(s+m-2)f_r(s-m)f_r(m-r)} \\
&= C_m (\frac{l}{2\pi})^{(2s/r-2)} \frac{r^{\frac{m-2}{r}} (\frac{m-2}{r})! (1 - (\frac{2\pi(m-1)}{l})^2 - \Lambda)^{s/r}}{r^{(s+m-2)/r} (\frac{s+m-2}{r})! r^{(s-m)/r} (\frac{s-m}{r})! r^{(m-r)/r} (\frac{m-r}{r})!} \\
&= C_m (\frac{l}{2\pi})^{(2s/r-2)} \frac{(\frac{m-2}{r})! (1 - (\frac{2\pi(m-1)}{l})^2 - \Lambda)^{s/r}}{r^{(2s/r-1)} (\frac{s+m-2}{r})! (\frac{s-m}{r})! (\frac{m-r}{r})!}.
\end{aligned}$$

Here $f_r(n)$ represents the r -multifactorial function of n . Rewriting as exponential and using Stirling's formula leads to

$$\begin{aligned}
|K_m| &= \exp \left[\ln(C_m) + \frac{s}{r} \ln(1 - (\frac{2\pi(m-1)}{l})^2 - \Lambda) + (2\frac{s}{r} - 2) \ln(\frac{l}{2\pi}) - (2\frac{s}{r} - 1) \ln(r) \right. \\
&\quad \left. + \ln(\frac{m-2}{r}!) - \ln(\frac{s+m-2}{r}!) - \ln(\frac{s-m}{r}!) - \ln(\frac{m-r}{r}!) \right] \\
&\approx \exp \left[\ln(C_m) + \frac{s}{r} \ln(1 - (\frac{2\pi(m-1)}{l})^2 - \Lambda) + (2\frac{s}{r} - 2) \ln(\frac{l}{2\pi}) - (2\frac{s}{r} - 1) \ln(r) \right. \\
&\quad \left. + (2\frac{s}{r} - 1) + 2\frac{s}{r} \ln(r) - \frac{s}{r} \ln(1 - \frac{m^2}{s^2} - \frac{2}{s} + \frac{2m}{s^2}) - \frac{2s}{r} \ln(s) \right. \\
&\quad \left. + \frac{m}{r} \ln(\frac{(m-2)(s-m)}{(s+m-2)(m-r)}) + \frac{2}{r} \ln(\frac{(s+m-2)}{(m-2)}) + \frac{1}{2} \ln(\frac{(m-2)(m-r)}{(s+m-2)(s-m)}) \right] \\
&= \exp \left[\frac{s}{r} \left(\ln(1 - (\frac{2\pi(m-1)}{l})^2 - \Lambda) + 2(\ln(\frac{l}{2\pi}) + 1 - \ln(s)) - \ln(1 - \frac{m^2}{s^2} - \frac{2}{s} + \frac{2m}{s^2}) \right) \right. \\
&\quad \left. + \frac{m}{r} \ln(\frac{(m-2)(s-m)}{(s+m-2)(m-r)}) + \ln(C_m) - 1 - 2\ln(\frac{l}{2\pi}) + \ln(r) + \frac{2}{r} \ln(\frac{(s+m-2)}{(m-2)}) \right. \\
&\quad \left. + \frac{1}{2} \ln(\frac{(m-2)(m-r)}{(s+m-2)(s-m)}) \right].
\end{aligned}$$

Finally using $s \approx \frac{l}{2\pi}$ one finds to leading order in l

$$|K_m| = \exp(\frac{l}{2\pi r} (2 + \ln(1 + |\Lambda|))), \quad (160)$$

in agreement with (108).

APPENDIX B

COMPUTATION OF TRANSIENT GROWTH IN THE CASE OF LOCALIZED SENSING

We start the derivation of γ for a system with localized control and sensing with equations (142) and (143).

$$\begin{aligned}\gamma &\sim \left\| \exp \left[\begin{pmatrix} Q & -Q \\ 0 & Q^\dagger \end{pmatrix} t_m \right] \right\|_2 = \left\| \sum_{n=0}^{\infty} \frac{t_m^n}{n!} \begin{pmatrix} Q & -Q \\ 0 & Q^\dagger \end{pmatrix}^n \right\|_2 \\ &= \left\| I + \sum_{n=1}^{\infty} \frac{t_m^n}{n!} \begin{pmatrix} D^{n-1}Q & -D^{n-1}Q(I + (n-1)D^{-1}Q^\dagger) \\ 0 & D^{n-1}Q^\dagger \end{pmatrix} \right\|_2. \quad (161)\end{aligned}$$

We assume that a D exists that satisfies the requirements described in Section 5.2. We can manipulate (161) by extracting all terms that depend on n and then rewriting as matrix exponentials. Making use of the definitions (145) given by

$$\hat{D} = \begin{pmatrix} D & 0 \\ 0 & D \end{pmatrix}, \quad \hat{A} = \begin{pmatrix} Q & -Q \\ 0 & Q^\dagger \end{pmatrix}, \quad \hat{B} = \begin{pmatrix} 0 & D^{-1}QQ^\dagger \\ 0 & 0 \end{pmatrix},$$

and also using the fact D and Q commute, we obtain

$$\begin{aligned}\gamma &\sim \left\| I + \sum_{n=1}^{\infty} \frac{t_m^n}{n!} \hat{D}^n \begin{pmatrix} D^{-1}Q & -D^{-1}Q \\ 0 & D^{-1}Q^\dagger \end{pmatrix} - \sum_{n=1}^{\infty} \frac{t_m^n}{n!} (n-1) \hat{D}^n \begin{pmatrix} 0 & D^{-2}QQ^\dagger \\ 0 & 0 \end{pmatrix} \right\|_2 \\ &= \left\| I + (e^{\hat{D}t_m} - I) \begin{pmatrix} D^{-1}Q & -D^{-1}Q \\ 0 & D^{-1}Q^\dagger \end{pmatrix} + \left[\sum_{n=1}^{\infty} \frac{t_m^n}{n!} \hat{D}^n - \sum_{n=1}^{\infty} \frac{nt_m^n}{n!} \hat{D}^n \right] \hat{D}^{-1} \hat{B} \right\|_2 \\ &= \left\| I + (e^{\hat{D}t_m} - I) \hat{D}^1 \hat{A} + \left[e^{\hat{D}t_m} - I - \sum_{n=1}^{\infty} \frac{t_m^{n-1}}{(n-1)!} \hat{D}^{n-1} \hat{D} t_m \right] \hat{D}^{-1} \hat{B} \right\|_2 \\ &= \left\| I + (e^{\hat{D}t_m} - I) \hat{D}^1 \hat{A} + \left[(e^{\hat{D}t_m} - I) - e^{\hat{D}t_m} \hat{D} t_m \right] \hat{D}^{-1} \hat{B} \right\|_2 \\ &= \left\| I + (e^{\hat{D}t_m} - I) \hat{D}^{-1} \hat{A} + ([I - \hat{D} t_m] e^{\hat{D}t_m} - I) \hat{D}^{-1} \hat{B} \right\|_2. \quad (162)\end{aligned}$$

Finally, since D is diagonal with negative entries that grow in magnitude with l , we can neglect the matrix exponentials and obtain

$$\begin{aligned}\gamma &\sim \left\| I - \hat{D}^{-1}\hat{A} - \hat{D}^{-1}\hat{B} \right\|_2 \sim \left\| \hat{D}^{-1}(\hat{A} + \hat{B}) \right\|_2 \\ &\sim \frac{1}{s} \left\| \begin{pmatrix} Q & -Q + D^{-1}QQ^\dagger \\ 0 & Q^\dagger \end{pmatrix} \right\|_2,\end{aligned}\tag{163}$$

where we used $D \sim sI$. From this expression, which is (146) given earlier in Section 5.3, we obtain – as explained there – the lower bound for the large l limit

$$\gamma \gtrsim K_{EQ}^2.\tag{164}$$

REFERENCES

- [1] ANDERSSON, P., BERGGREN, M., and HENNINGSON, D. S., “Optimal disturbances and bypass transition in boundary layers,” *Phys. Fluids*, vol. 11, p. 134, 1999.
- [2] ARANSON, I., LEVINE, H., and TSIMERING, L., “Controlling spatiotemporal chaos,” *Phys. Rev. Lett.*, vol. 72, p. 2561, 1994.
- [3] ARANSON, I. S. and KRAMER, L., “The world of the complex Ginzburg-Landau equation,” *Rev. Mod. Phys.*, vol. 74, p. 99, 2002.
- [4] ARMAOU, A. and CHRISTOFIDES, P. D., “Feedback control of the Kuramoto-Sivashinsky equation,” *Physica D*, vol. 137, p. 49, 2000.
- [5] ARMAOU, A. and CHRISTOFIDES, P. D., “Global stabilization of the Kuramoto-Sivashinsky equation via distributed output feedback control,” *Systems and Control Letters*, vol. 39, p. 283, 2000.
- [6] AUERBACH, D., “Controlling extended systems of chaotic elements,” *Phys. Rev. Lett.*, vol. 72, p. 1184, 1994.
- [7] AUERBACH, D., GREBOGI, C., OTT, E., and YORKE, J. A., “Controlling chaos in high dimensional systems,” *Phys. Rev. Lett.*, vol. 69, p. 3479, 1992.
- [8] BAGGETT, J., DRISCOLL, T., and TREFETHEN, L., “A mostly linear model of transition to turbulence,” *Phys. Fluids*, vol. 7, p. 833, 1995.
- [9] BAGGETT, J. and TREFETHEN, L., “Low-dimensional models of subcritical transition to turbulence,” *Phys. Fluids*, vol. 9, p. 1043, 1997.
- [10] BAMIEH, B. and DAHLEH, M., “Energy amplification in channel flows with stochastic excitation,” *Phys. Fluids*, vol. 13, p. 3258, 2001.
- [11] BAMIEH, B., PAGANINI, F., and DAHLEH, M., “Distributed control of spatially invariant systems,” *IEEE Trans. Aut. Cont.*, vol. 47, p. 1092, 2002.
- [12] BATTOGTOKH, D. and MIKHAILOV, A., “Controlling turbulence in the complex Ginzburg-Landau equation,” *Physica D*, vol. 90, p. 84, 1996.
- [13] BATTOGTOKH, D., PREUSSER, A., and MIKHAILOV, A., “Controlling turbulence in the complex Ginzburg-Landau equation II: Two-dimensional systems,” *Physica D*, vol. 106, p. 327, 1997.
- [14] BERTOZZI, A. L. and BRENNER, M. P., “Linear stability and transient growth in driven contact lines,” *Phys. Fluids*, vol. 9, p. 530, 1997.
- [15] BERTRAM, M. and MIKHAILOV, A., “Pattern formation in a surface chemical reaction with global delayed feedback,” *Phys. Rev. E*, vol. 63, p. 0661021, 2001.

- [16] BEWLEY, T., “Flow control: New challenges for a new renaissance,” *Prog. Aerospace Sci.*, vol. 37, p. 21, 2001.
- [17] BEWLEY, T. and LIU, S., “Optimal and robust control and estimation of linear paths to transition,” *J. Fluid Mech.*, vol. 365, p. 305, 1998.
- [18] BLEICH, M. E., HOCHHEISER, D., MOLONEY, J. V., and SOCOLAR, J. E. S., “Controlling extended systems with spatially filtered, time-delayed feedback,” *Phys. Rev. E*, vol. 55, p. 2119, 1997.
- [19] BLEICH, M. E. and SOCOLAR, J. E. S., “Controlling spatiotemporal dynamics with time-delay feedback,” *Phys. Rev. E*, vol. 54, p. R17, 1996.
- [20] BOCCALETTI, S., GREBOGI, C., LAI, Y. C., MANCINI, H., and MAZA, D., “The control of chaos: Theory and applications,” *Phys. Reports*, vol. 329, p. 103, 2000.
- [21] BOYD, S. P. and BARRATT, C. H., *Linear Controller Design - Limits of Performance*. New Jersey: Prentice-Hall, 1991.
- [22] BRAIMAN, Y. and GOLDBIRSH, I., “Taming chaotic dynamics with weak periodic perturbations,” *Phys. Rev. Lett.*, vol. 66, p. 2545, 1991.
- [23] BREEN, B. J., *Computational Nonlinear Dynamics: Monostable Stochastic Resonance and a bursting Neuron Model*. PhD thesis, Georgia Institute of Technology, 2003.
- [24] BROSA, U. and GROSSMANN, S., “Minimum description of the onset of pipe turbulence,” *Eur. Phys. J. B*, vol. 9, p. 343, 1999.
- [25] BUTLER, K. M. and FARRELL, B. F., “Three-dimensional optimal perturbations in viscous shear flow,” *Phys. Fluids A*, vol. 4, p. 1637, 1992.
- [26] CAMARGO, S. J., TIPPETT, M. K., and CALDAS, I. L., “Nonmodal energetics of electromagnetic drift waves,” *Physics of Plasmas*, vol. 7, p. 2849, 2000.
- [27] CHAGELISHVILI, G. D., CHANISHVILI, R. G., HRISTOV, T. S., and LOMINADZE, J. G., “A turbulence model in unbounded smooth shear flows: The weak turbulence approach,” *J. Exp. Th. Phys.*, vol. 94, p. 434, 2002.
- [28] CHANDRASEKHAR, S., *Hydrodynamic and Hydromagnetic Stability*. Oxford: Clarendon Press, 1961.
- [29] CHAPMAN, S. J., “Subcritical transition in channel flows,” *J. Fluid Mech.*, vol. 451, p. 35, 2002.
- [30] CHEN, C. T., *Linear System Theory and Design*. New York: CBS College Publishing, 1984.
- [31] CHRISTOFIDES, P., *Nonlinear and Robust Control of PDE Systems: Methods and Applications to Transport-Reaction Processes*. Boston: Birkhäuser, 2001.
- [32] CRAWFORD, J. D., “Introduction to bifurcation theory,” *Rev. Mod. Phys.*, vol. 63, p. 991, 1991.

- [33] CROSS, M. C. and HOHENBERG, P. C., "Pattern formation outside of equilibrium," *Rev. Mod. Phys.*, vol. 65, p. 851, 1993.
- [34] DORATO, P., ABDALLAH, C. T., and CERONE, V., *Linear Quadratic Control*. Melbourne: Krieger Publishing Company, 2000.
- [35] DOYLE, J. C., GLOVER, K., KHARGONEKAR, P. P., and FRANCIS, B. A., "State-space solutions to standard H_2 and H_∞ problems," *IEEE Trans. Aut. Cont.*, vol. 34, p. 831, 1989.
- [36] DUTTON, K., THOMPSON, S., and BARRACLOUGH, B., *The Art of Control Engineering*. Boston: Addison-Wesley, 1997.
- [37] ECKHARDT, B. and MERSMANN, A., "Transition to turbulence in a shear flow," *Phys. Rev. E*, vol. 60, p. 509, 1999.
- [38] EGOLF, D. A. and SOCOLAR, J. E. S., "Failure of linear control in noisy coupled map lattices," *Phys. Rev. E*, vol. 57, p. 5721, 1998.
- [39] EMBREE, M. and TREFETHEN, L. N., "Pseudospectra Gateway," <http://www.comlab.ox.ac.uk/pseudospectra>, 2004.
- [40] FARRELL, B. F. and IOANNOU, P. J., "Optimal excitation of perturbations in viscous shear flow," *Phys. Fluids*, vol. 31, p. 2093, 1988.
- [41] FARRELL, B. F. and IOANNOU, P. J., "Stochastic forcing of the linearized Navier-Stokes equations," *Phys. Fluids A*, vol. 5, p. 2600, 1993.
- [42] FARRELL, B. F. and IOANNOU, P. J., "Generalized stability theory, part I: Autonomous operators," *J. Atmospheric Sci.*, vol. 53, p. 2025, 1996.
- [43] FARRELL, B. F. and IOANNOU, P. J., "Turbulence suppression by active control," *Phys. Fluids*, vol. 8, p. 1257, 1996.
- [44] FARRELL, B. F. and IOANNOU, P. J., "Perturbation growth and structure in time-dependent flows," *J. Atmospheric Sci.*, vol. 56, p. 3622, 1999.
- [45] FEDOTOV, S., "Non-normal and stochastic amplification of magnetic energy in the turbulent dynamo: Subcritical case," *Phys. Rev. E*, vol. 68, p. 067301, 2003.
- [46] FEDOTOV, S., BAHSKIRTSEVA, I., and RYASHKO, L., "Stochastic analysis of a non-normal dynamical system mimicking a laminar-to-turbulent subcritical transition," *Phys. Rev. E*, vol. 66, p. 066310, 2002.
- [47] FI, "Variance maintained by stochastic forcing of non-normal dynamical systems associated with linearly stable shear flows," *prl*, vol. 72, p. 1188, 1994.
- [48] FRANCESCHINI, G., BOSE, S., and SCHÖLL, E., "Control of chaotic spatiotemporal spiking by time-delay autosynchronization," *Phys. Rev. E*, vol. 60, p. 5426, 1999.
- [49] FRONZONI, L. and GIOCONDO, M., "Controlling chaos with parametric perturbations," *Int. J. of Bif. and Chaos*, vol. 8, p. 1693, 1998.

- [50] GANG, H., JINGHUA, X., JIJUA, G., XIANGMING, L., YUGUI, Y., and HU, B., “Analytical study of spatiotemporal chaos control by applying local injections,” *Phys. Rev. E*, vol. 62, p. R3043, 2000.
- [51] GANG, H. and KAIFEN, H., “Controlling chaos in systems described by partial differential equations,” *Phys. Rev. Lett.*, vol. 71, p. 3794, 1993.
- [52] GANG, H. and ZHILIN, Q., “Controlling spatiotemporal chaos in coupled map lattice systems,” *Phys. Rev. Lett.*, vol. 72, p. 68, 1994.
- [53] GARNIER, N., GRIGORIEV, R. O., and SCHATZ, M. F., “Optical manipulation of microscale fluid flow,” *Phys. Rev. Lett.*, vol. 91, p. 054501, 2004.
- [54] GEBHARDT, T. and GROSSMANN, S., “Chaos transition despite linear stability,” *Phys. Rev. E*, vol. 50, p. 3705, 1994.
- [55] GOHBERG, I. C. and KREIN, M. G., *Introduction to the Theory of Linear Non-selfadjoint Operators*. Providence: American Mathematical Society, 1969.
- [56] GOLUB, G. H. and VAN LOAN, C. F., *Matrix Computations*. Baltimore: The John Hopkins University Press, 1996.
- [57] GREEN, M. and LIMEBEER, D. J. N., *Linear Robust Control*. New Jersey: Prentice-Hall, 1995.
- [58] GRIGORIEV, R. O., “Control of spatially extended chaotic systems,” in *Handbook of Chaos Control* (SCHUSTER, H. G., ed.), New Jersey: Wiley-VCH, 1998.
- [59] GRIGORIEV, R. O., “Symmetry and control: spatially extended chaotic systems,” *Physica D*, vol. 140, p. 171, 2000.
- [60] GRIGORIEV, R. O., “Control of evaporatively driven instabilities of thin liquid films,” *Phys. Fluids*, vol. 14, p. 1895, 2002.
- [61] GRIGORIEV, R. O., “Contact line instability and pattern selection in thermally driven liquid films,” *Phys. Fluids*, vol. 15, p. 1363, 2003.
- [62] GRIGORIEV, R. O. and CROSS, M. C., “Controlling physical systems with symmetries,” *Phys. Rev. E*, vol. 57, p. 1550, 1998.
- [63] GRIGORIEV, R. O., CROSS, M. C., and SCHUSTER, H. G., “Pinning control of spatiotemporal chaos,” *Phys. Rev. Lett.*, vol. 79, p. 2795, 1997.
- [64] GRIGORIEV, R. O. and HANDEL, A., “Localized control in a pattern forming system,” *submitted to Physica D*.
- [65] GRIGORIEV, R. O. and HANDEL, A., “Spectral theory for the failure of linear control in a nonlinear stochastic system,” *Phys. Rev. E*, vol. 66, p. R065301, 2002.
- [66] GRIGORIEV, R. O., LALL, S. G., and DULLERUD, G. E., “Localized optimal control of spatiotemporal chaos,” in *Proc. NOLTA*, 1997.
- [67] GROSSMANN, S., “The onset of shear flow turbulence,” *Rev. Mod. Phys.*, vol. 72, p. 603, 2000.

- [68] HALL, G. M. and GAUTHIER, D. J., “Experimental control of cardiac muscle alternans,” *Phys. Rev. Lett.*, vol. 88, p. 1981021, 2002.
- [69] HAYES, S., GREBOGI, C., OTT, E., and MARK, A., “Experimental control of chaos for communication,” *Phys. Rev. Lett.*, vol. 73, p. 1781, 1994.
- [70] HELLER, J., *Catch-22*. New York: Simon and Schuster, 1961.
- [71] HIGHAM, D. J., “An algorithmic introduction to numerical simulation of stochastic differential equations,” *SIAM Review*, vol. 43, p. 525, 2001.
- [72] HOF, B., JUEL, A., and MULLIN, T., “Scaling of the turbulence transition threshold in a pipe,” *Phys. Rev. Lett.*, vol. 91, p. 2445021, 2003.
- [73] HÖGBERG, M., BEWLEY, T., and HENNINGSON, D. S., “Linear feedback control and estimation of transition in a plane channel flow,” *J. Fluid Mech.*, vol. 481, p. 149, 2003.
- [74] HORN, R. A. and JOHNSON, C. R., *Matrix Analysis*. Cambridge: Cambridge University Press, 1985.
- [75] HOWLE, L. E., “Active control of Rayleigh-Bénard convection,” *Phys. Fluids*, vol. 9, p. 1861, 1997.
- [76] HUNT, E. R., “Stabilizing high-period orbits in a chaotic system: The diode resonator,” *Phys. Rev. Lett.*, vol. 67, p. 1953, 1991.
- [77] JOHN, J. K. and AMRITKAR, R. E., “Synchronization of unstable orbits using adaptive control,” *Phys. Rev. E*, vol. 49, p. 4843, 1994.
- [78] JOSEPH, D. D., *Stability of Fluid Motions, Vol. I and II*. Berlin: Springer, 1976.
- [79] JOSHI, S. S., SPEYER, J. L., and KIM, J., “A systems theory approach to the feedback stabilization of infinitesimal and finite-amplitude disturbances in plane Poiseuille flow,” *J. Fluid Mech.*, vol. 332, p. 157, 1997.
- [80] JOVANOVIĆ, M. R. and BAMIEH, B., “Componentwise energy amplification in channel flows,” *J. Fluid Mech.* - *to be published*.
- [81] JOVANOVIĆ, M. R. and BAMIEH, B., “Unstable modes versus non-normal modes in supercritical channel flows,” *J. Fluid Mech.* - *to be published*.
- [82] KITTEL, A., PARISI, J., and PYRAGAS, K., “Delayed feedback control of chaos by self-adapted delay time,” *Phys. Lett. A*, vol. 198, p. 433, 1995.
- [83] KOLODNER, P. and FLÄTGEN, G., “Spatial-feedback control of dispersive chaos in binary-fluid convection,” *Phys. Rev. E*, vol. 61, p. 2519, 2000.
- [84] LASIECKA, I. and TRIGGIANI, R., *Control Theory for Partial Differential Equations: Continuous and Approximation Theories*. Cambridge: Cambridge University Press, 2000.
- [85] LAUGA, E. and BEWLEY, T. R., “Performance of a linear robust control strategy on a nonlinear model of spatially-developing flows,” *J. Fluid Mech.* - *to be published*.

- [86] LAUGA, E. and BEWLEY, T. R., "Modern control of linear global instability in a cylinder wake model," *Int. J. of Heat and Fluid Flow*, vol. 23, p. 671, 2002.
- [87] LAUGA, E. and BEWLEY, T., "The decay of stabilizability with Reynolds number in a linear model of spatially developing flow," *Proc. R. Soc. London A*, vol. 459, p. 2077, 2003.
- [88] LI, Q. S. and JI, L., "Control of Turing pattern formation by delayed feedback," *Phys. Rev. E*, vol. 69, p. 046205, 2004.
- [89] LIMA, R. and PETTINI, M., "Suppression of chaos by resonant parametric perturbations," *Phys. Rev. A*, vol. 41, p. 726, 1990.
- [90] LUMLEY, J. and BLOSSEY, P., "Control of turbulence," *Annu. Rev. Fluid Mech.*, vol. 30, p. 311, 1998.
- [91] LÜTHJE, O., WOLFF, S., and PFISTER, G., "Control of chaotic Taylor-Couette flow with time-delayed feedback," *Phys. Rev. Lett.*, vol. 86, p. 1745, 2001.
- [92] MANNEVILLE, P., *Dissipative Structures and Weak Turbulence*. San Diego: Academic Press, Inc., 1990.
- [93] MESEGUER, Á. and TREFETHEN, L. N., "Linearized pipe flow to Reynolds number 10,000,000," *J. Comp. Phys.*, vol. 186, p. 178, 2003.
- [94] MOLER, C. and LOAN, C. V., "Nineteen dubious ways to compute the exponential of a matrix," *SIAM Review*, vol. 20, p. 801, 1978.
- [95] MONTAGNE, R. and COLET, P., "Nonlinear diffusion control of spatiotemporal chaos in the complex Ginzburg-Landau equation," *Phys. Rev. E*, vol. 56, p. 4017, 1997.
- [96] MORRIS, K., *Introduction to Feedback Control*. San Diego: Harcourt Academic Press, 2001.
- [97] OR, A. C., CORTELEZZI, L., and SPEYER, J. L., "Robust feedback control of Rayleigh-Bénard convection," *J. Fluid Mech.*, vol. 437, p. 175, 2001.
- [98] OTT, E., GREBOGI, C., and YORKE, J. A., "Controlling chaos," *Phys. Rev. Lett.*, vol. 64, p. 1196, 1990.
- [99] PAREKH, N., PARTHASARATHY, S., and SINHA, S., "Global and local control of spatiotemporal chaos in coupled map lattices," *Phys. Rev. Lett.*, vol. 81, p. 1401, 1998.
- [100] PAREKH, N. and SINHA, S., "Controlling dynamics in spatially extended systems," *Phys. Rev. E*, vol. 65, p. 036227, 2002.
- [101] PETERSEN, I. R., UGRINOVSKII, V. A., and SAVKIN, A. V., *Robust Control Design Using H^∞ Methods*. London: Springer, 2000.
- [102] PIKOVSKY, A., ROSENBLUM, M., and KURTHS, J., *Synchronization - A universal concept in nonlinear sciences*. Cambridge: Cambridge University Press, 2001.
- [103] PLASS, A., *View from a Bouncy Castle*. London: Fount Paperbacks, 1991.

- [104] PYRAGAS, K., “Continuous control of chaos by self-controlling feedback,” *Phys. Lett. A*, vol. 170, p. 421, 1992.
- [105] PYRAGAS, K., “Control of chaos via extended delay feedback,” *Phys. Lett. A*, vol. 206, p. 323, 1995.
- [106] PYRAGAS, K., “Control of chaos via an unstable delayed feedback controller,” *Phys. Rev. Lett.*, vol. 86, p. 2265, 2001.
- [107] REDDY, S. C., SCHMID, P. J., and HENNINGSON, D. S., “Pseudospectra of the Orr-Sommerfeld operator,” *SIAM J. on Appl. Math.*, vol. 53, p. 15, 1993.
- [108] REDDY, S. C. and TREFETHEN, L. N., “Pseudospectra of the convection-diffusion operator,” *SIAM J. Appl. Math.*, vol. 54, p. 1634, 1994.
- [109] REMPFER, D., “Low-dimensional modeling and numerical simulation of transition in simple shear flows,” *Annu. Rev. Fluid Mech.*, vol. 35, p. 229, 2003.
- [110] SCHMID, P. J., “Linear stability theory and bypass transition in shear flows,” *Physics of Plasmas*, vol. 7, p. 1788, 2000.
- [111] SCHMID, P. and HENNINGSON, D., *Stability and Transition in Shear Flows*. New York: Springer, 2001.
- [112] SOCOLAR, J. E. S. and GAUTHIER, D. J., “Analysis and comparison of multiple-delay schemes for controlling unstable fixed points of discrete maps,” *Phys. Rev. E*, vol. 57, p. 6589, 1998.
- [113] SOCOLAR, J. E. S., SUKOW, D. W., and GAUTHIER, D. J., “Stabilizing unstable periodic orbits in fast dynamical systems,” *Phys. Rev. E*, vol. 50, p. 3245, 1994.
- [114] SREENIVASAN, K., “Fluid turbulence,” *Rev. Mod. Phys.*, vol. 71, p. S383, 1999.
- [115] TANG, J. and BAU, H. H., “Stabilization of the no-motion state in Rayleigh-Bénard convection through use of feedback control,” *Phys. Rev. Lett.*, vol. 70, p. 1795, 1993.
- [116] TREFETHEN, L. N., “Pseudospectra of linear operators,” *SIAM Rev.*, vol. 39, p. 383, 1997.
- [117] TREFETHEN, L. N., TREFETHEN, A. E., REDDY, S. C., and DRISCOLL, T. A., “Hydrodynamic stability without eigenvalues,” *Science*, vol. 261, p. 578, 1993.
- [118] WALEFFE, F., “On a self-sustaining process in shear flows,” *Phys. Fluids*, vol. 9, p. 883, 1997.
- [119] XIAO, J., HU, G., YANG, J., and GAO, J., “Controlling turbulence in the complex Ginzburg-Landau equation,” *Phys. Rev. Lett.*, vol. 81, p. 5552, 1998.
- [120] ZHANG, H., HU, B., HU, G., OUYANG, Q., and KURTHS, J., “Turbulence control by developing a spiral wave with a periodic signal injection in the complex Ginzburg-Landau equation,” *Phys. Rev. E*, vol. 66, p. 046303, 2002.